Fracture mechanics of concrete : Nordic seminar held at Division of Building Materials, November 6,1986

Hillerborg, Arne

1986

DIVISION OF BUILDING MATERIALS
LUND INSTITUTE OF TECHNOLOGY

FRACTURE MECHANICS OF CONCRETE

Nordic seminar held at Division of Building Materials, November 6, 1986

REPORT TVBM-3025
LUND, SWEDEN, 1986

CODEN: LUTVDG/(TVBM-3025)/1-155/(1986)

FRACTURE MECHANICS OF CONCRETE

Nordic seminar held at Division of Building Materials, November 6, 1986

ISSN 0348-7911

CONTENT

Preface

Fracture mechanics of concrete has aroused much interest in many universities within the Nordic countries. Therefore a need was felt to arrange a seminar in order to exchange information on the work which is going on. The seminar was arranged as a mini-seminar, i.e. a one day seminar with participation mainly restricted to active researchers in the field.

At the seminar a number of papers were presented and discussed. These papers are presented in this report. The papers are presented in an informal way. No reviewing has been performed, and no attempt has been made to unify the presentation or typing. Some papers may appear more or less unchanged in other publications.

I would like to thank the participants of the seminar for their contributions to the discussions at the seminar and for their contributions to this publication.

Lund, March 1987

Arne Hillerborg

LIST OF PARTICIPANTS

From Denmark

Harder, N. A.	Inst. f. Bygningsteknik, AUC, Sohngårdsholms-vej 57, DK 9000 Aalborg.
Holkmann Olsen, Nicholaus	ABK, DTH, Bygning 118, DK-2800 Lyngby.
Stang, Henrik	" " " "

From Finland

Lanu, Matti	Technical Research Centre of Finland, Kemistintie 3, SF-02150 Espoo

From Norway

Aasved Hansen, Einar	SINTEF-FCB/Inst. f. betongkonstr., NTH, N 7034 Trondheim-NTH.
Bergan, Björn	" " " " "

From Sweden

Gylltoft, Kent	Statens Provningsanstalt, Byggnadsteknik, Box 857, S-501 15 Borås.
Daerga, Per Anders	Konstruktionsteknik, Tekn. Högsk. i Luleå, S-951 87 Luleå.
Elfgren, Lennart	" " " " "
Ohlsson, Ulf	" " " " "
Grzybowski, Miroslaw	Inst. f. brobyggnad, KTH, S-100 44 Stockholm
Norberg, Jan	" " " " "
Dahlblom, Ola	Byggnadsmekanik, LTH, Box 118, S-221 00 Lund
Gustafsson, Per Johan	" " " " "
Petersson, Hans	" " " " "
Saaby-Ottosen, Niels	" " " " "
Hassanzadeh,Manoucehr	Byggnadsmaterial, LTH, Box 118, S-221 00 Lund
Hillerborg, Arne	" " " " "
Zhou, Fanping	" " " " "

FINITE ELEMENT ANALYSIS OF MIXED MODE FRACTURE USING A DISCRETE CRACK APPROACH

by

Ulf Ohlsson Kent Gylltoft

Division of Structural Engineering, University of Luleå, S-951 87, Sweden

PREFACE

This report presents an experimental and numerical study of the fracture of a notched unreinforced concrete beam. The work has been carried out at the Division of Structural Engineering, Luleå University of Technology under the direction of Professor Lennart Elfgren. The tests were planned by Kent Gylltoft in 1984 when he was an assistant professor in Luleå. The tests were carried out by Leif Hedlund and Ulf Ohlsson. Ulf Ohlsson also carried out the numerical analysis and wrote this report. The work has been supported by The Swedish Council for Building Research (BFR 830900-3).

1. INTRODUCTION

A crack in a structure can propagate in different ways. To facilitate the analysis three basic modes have been named, see Fig. 1.1. A lot of work has been carried out to study mode I, the opening mode, see for example [1], [2], [3]. The other two modes sliding and tearing have so far only been studied in a few tests.

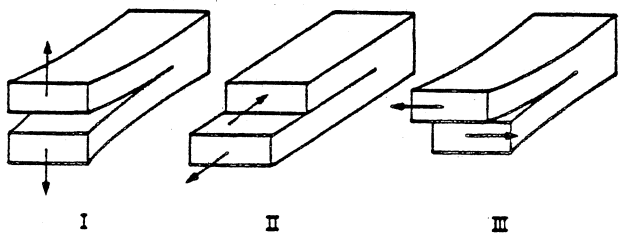

Fig. 1.1 Basic modes of crack extension:
I, opening mode; II, sliding mode; III, tearing mode [3]

In this paper a study of a mixed mode fracture is presented. Experimental and analytical results are compared for a beam according to Fig. 1.2. Here both mode I and II occur.

The first experiments on the beam in Fig. 1.2 were carried out by Arrea and Ingraffea in 1982 [4]. They subjected the beams to cyclic loading. After each loading cycle the crack growth was inspected. One conclusion Arrea and Ingraffea drew from their tests was that the fracture mechanism was a mode I opening (tensile) fracture.

Another type of beam that has been tested is the double notched beam in Fig. 1.3. Four different sizes of the beam were tested by Bazant and Pfeiffer in 1985 [5]. Compared to the beam in Fig. 1.2 the loading points were here located more close to the notch. The fracture mechanism was said to be a mode II sliding (shear) fracture.

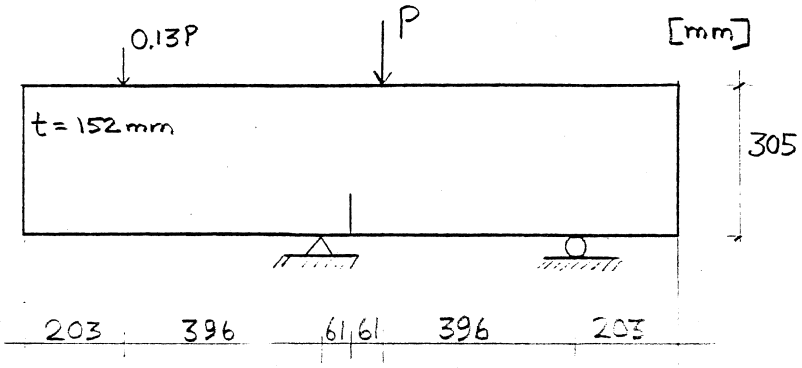

Fig. 1.2 Tested beam of Arrea and Ingraffea

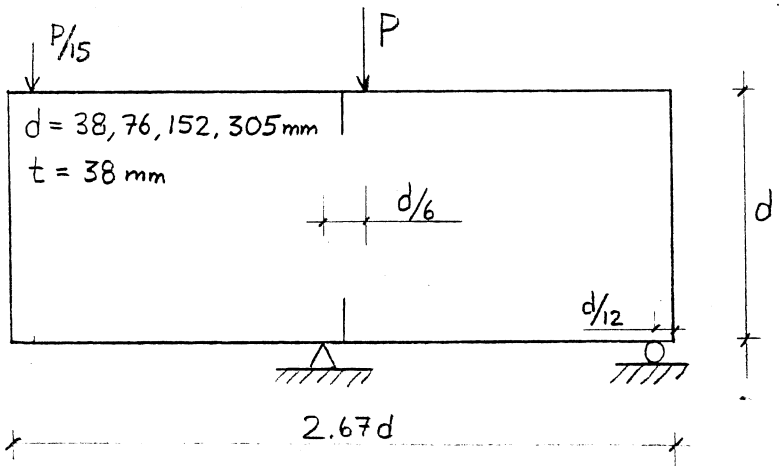

Fig. 1.3 Tested beam of Bazant

Several investigators have modelled the beams in Figs. 1.2 and 1.3 with the finite element method using both discrete and smeared fracture models.

Arrea and Ingraffea, 1982 [4], used a discrete fracture model, based on linear fracture mechanics with different mixed-mode fracture initiation theories. Crack trajectories observed in the tests were reproduced with the finite element analysis.

Glemberg, 1984 [6], modelled the beam in Fig. 1.2 using a smeared fracture model. The calculated load-displacement curves are in agreement with the experimentally obtained curves, but the calculated crack trajectory does not match the laboratory tests.

Rots, 1985 [7], modelled the beam in Fig. 1.3 with a smeared fracture model. He succeeded in reproducing the experimental crack trajectories.

Oldenburg, 1985 [8], also used a smeared fracture model for the beam in Fig. 1.2. But his model also included the possibility of plastic deformations in compression. He succeeded in matching the calculated load-displacement curves and the crack trajectories with the experimental results.

De Borst, 1986 [9], analyzed the beam in Fig. 1.2 using a smeared fracture model. The load-increment is determined from the condition of constant increase of Crack Mouth Sliding Displacement, CMSD, at every step. He obtained a very good correlation between the experimental and the calculated load-displacement curves, but the crack trajectories did not match the experimental ones.

2. EXPERIMENTAL STUDY

2.1 Test specimen

Four concrete beams were cast for the experiments. They were cast in plywood forms and in two different batches. Steel plates, thickness 3 mm, were fixed in the bottom of the forms to make the notches. Six concrete cubes, 150 x 150 x 150 mm^3, were also cast in each batch.

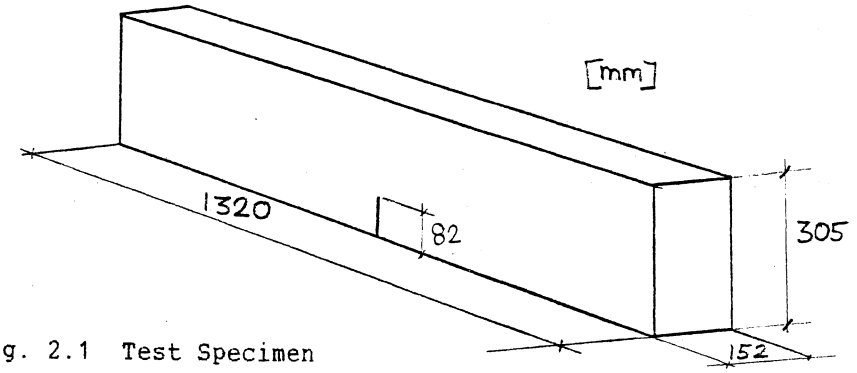

Fig. 2.1 Test Specimen

After the casting the beams were covered with plastic film and kept wet. The forms were removed after three days and the beams were then moved and cured in water until the day of testing.

The concrete mix had the following proportions: cement 10.6 %, fine aggregate 41.9 %, coarse aggregate (crushed stone, maximum size 16 mm) 39.9 % and water 7.6 %. The cement used was Cementa Std Slite. The water/cement ratio was 0.72.

Results from the cube tests are summarized in Table 1. The mean values of the tensile and compression strengths in batch 2 were f_{ct} = 3.0 MPa and f_{cc} = 35.4 MPa.

Table 2.1 Cube tests

	Cube No.	Age days	Density ϱ kg/m^3 x 1000	Splitting strength, f_{ct} MPa	Compression strength, f_{cc} MPa
Batch 2	1	68	2.39	3.0	33.9
	2	68	2.39	3.1	35.4
	3	68	2.38	3.2	36.1
	4	68	2.39	3.1	35.2
	5	68	2.38	2.8	35.7
	6	68	2.40	2.9	36.0

2.2 Test set-up

A servohydraulic testing equipment with a capacity of 270 kN was used in the tests. The test set-up is shown in Fig. 2.2 and 2.3. The deflection of the beam, at the loadpoint C, was measured with two Linear Variable Differential Transformers, LVDT, attached to a steel frame. The Crack Mouth Displacement, CMD, was measured with an extensiometer, see Fig. 2.4.

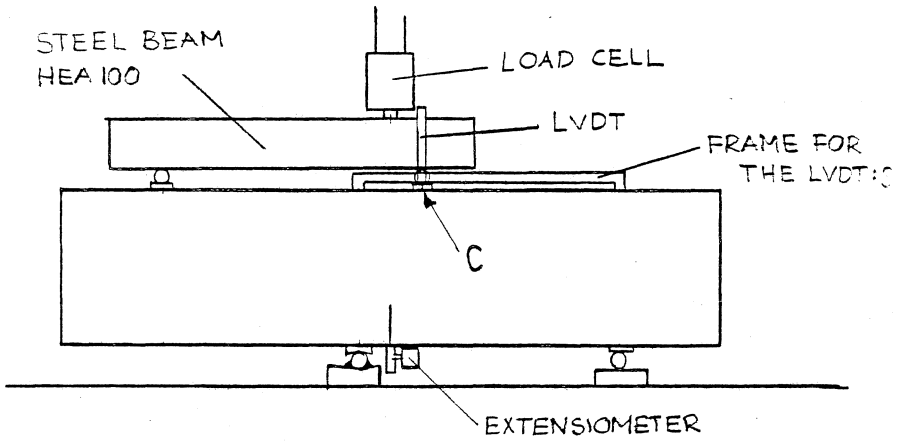

Fig. 2.2 Test set-up

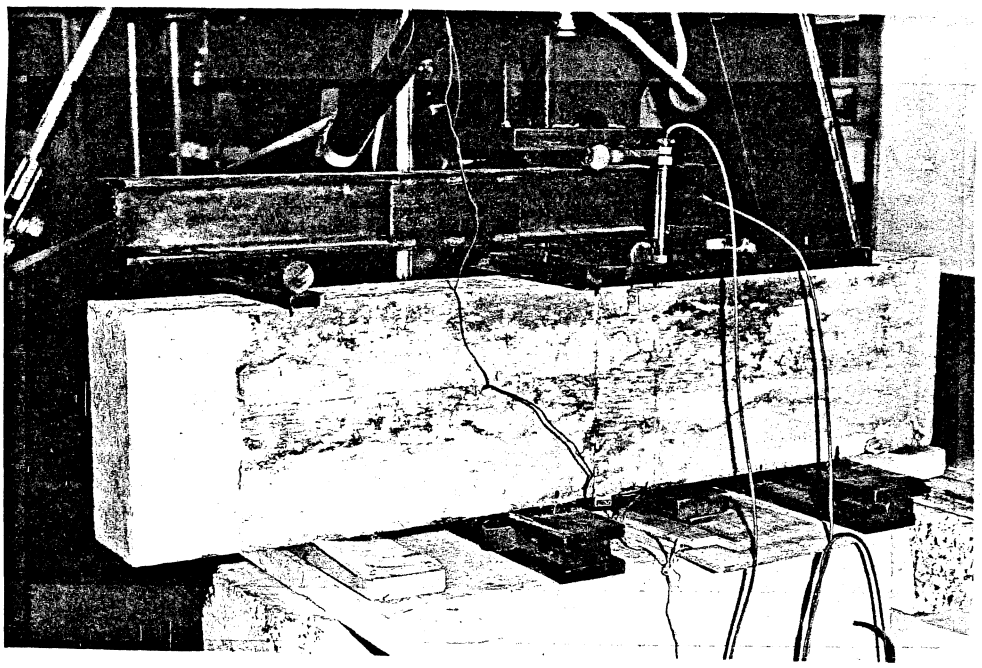

Fig. 2.3 Test set-up

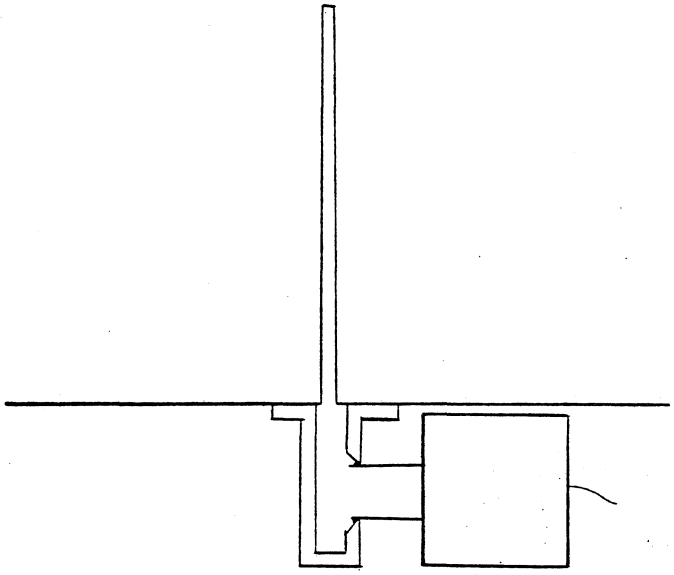

Fig. 2.4 Extensiometer

The CMD measured in the tests includes the crack opening as well as the crack sliding. The ratio between the Crack Mouth Displacement, CMD, and the Crack Mouth Sliding Displacement, CMSD, is 1.3 at peak-load according to the FEM-calculations.

The load was measured with a load cell with a range of $\pm$ 500 kN. The loading of the beam was strain-controlled, with the extensiometer at the crack tip as the feedback source to the hydraulic cylinder. The loading velocity was equal to an increase in CMD of 0.08 μm/s.

Test data was collected on two xy-recorders, plotting load versus CMD and load versus deflection.

2.3 Test results

Test results from two beam tests are presented in this report. The two beams were cast in the second batch. Test results from the beams cast in the first batch are not presented due to difficulties in controlling the load during the tests.

Fig. 2.5 shows the load versus CMD and Fig. 2.6 the load versus deformation curves of the tested beams. Only one load-deflection curve is shown, due to a transducer fault.

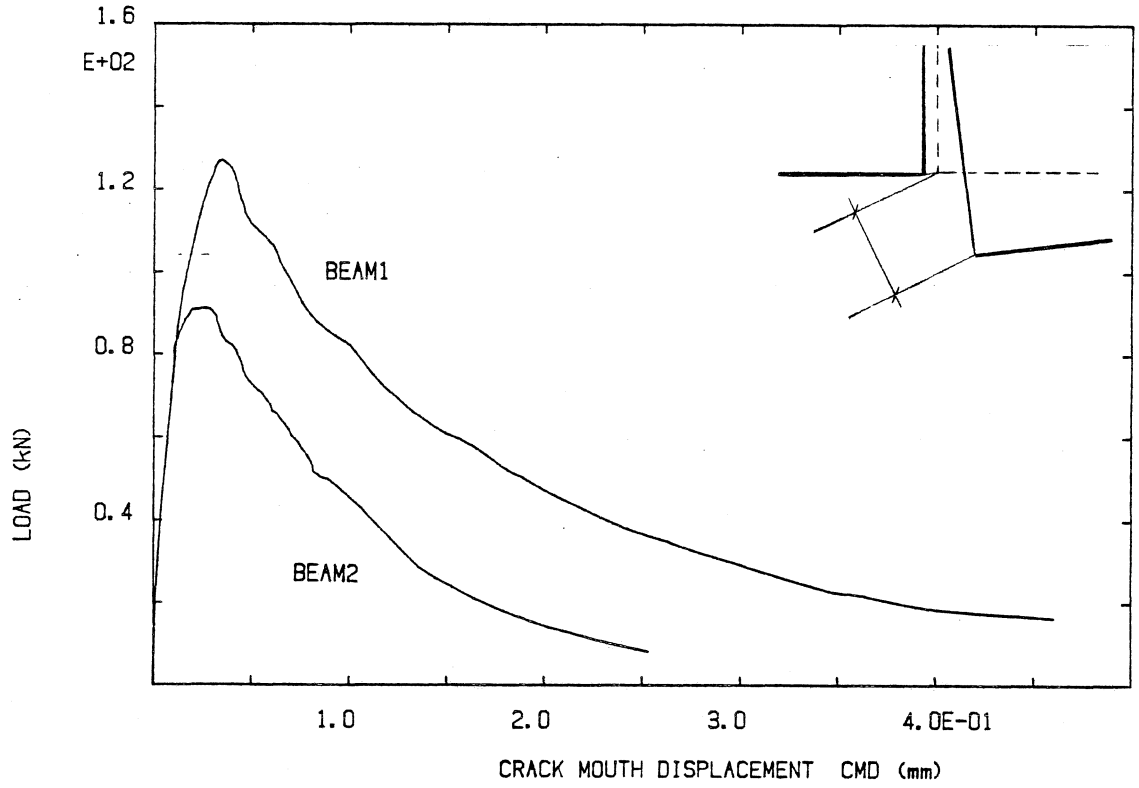

Fig. 2.5 Experimental load-CMD curves

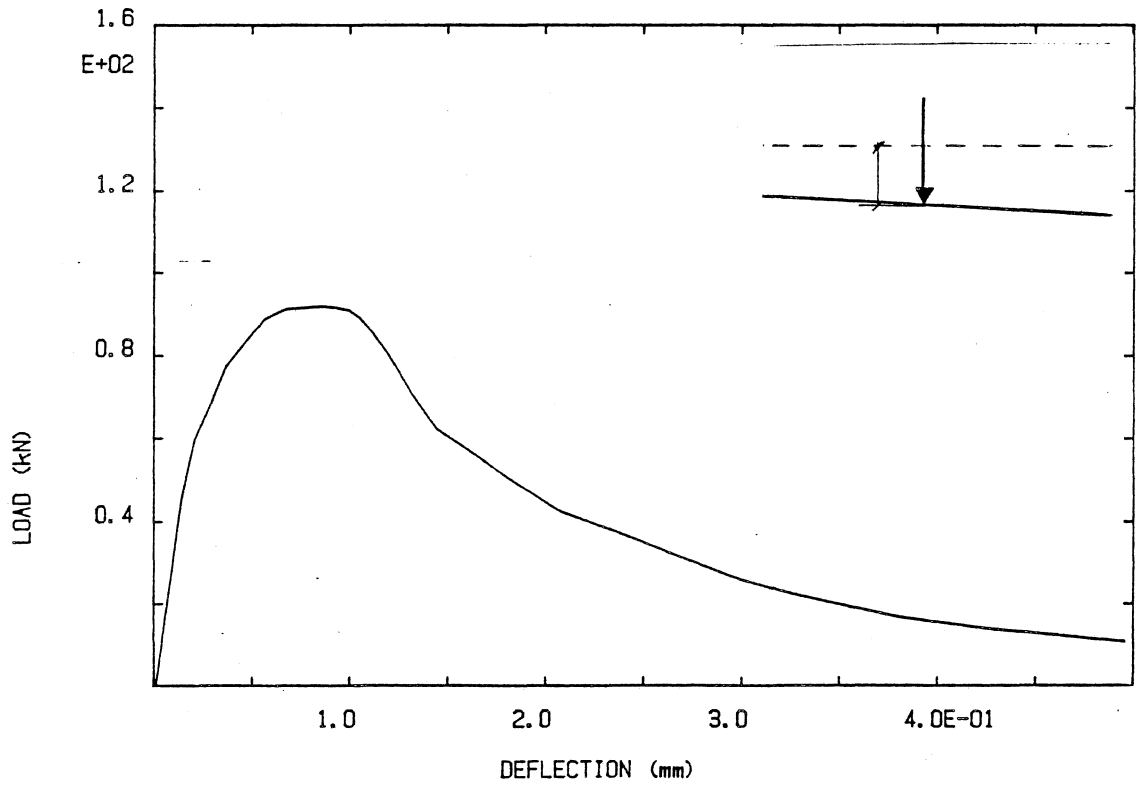

Fig. 2.6 Experimental load-deflection curve

The experiments were run in a very stable manner and could be controlled until the dead-weight of the beam broke it into pieces.

The crack trajectories are presented in Fig. 2.7. They are curved and in accordance with the tests of Ingraffea [4].

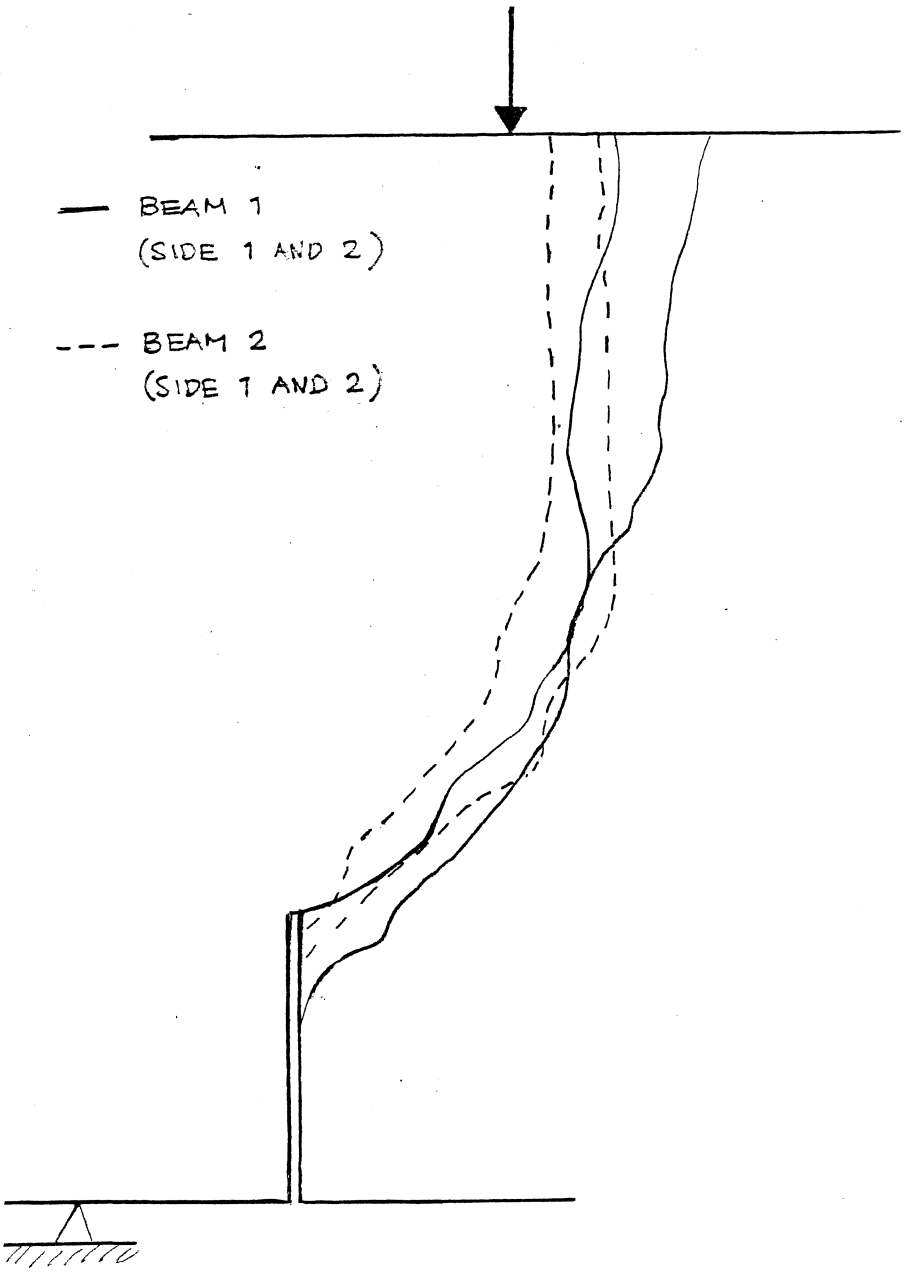

Fig. 2.7 Experimental crack trajectories

Figs. 2.8-2.11 show the tested beams after failure.

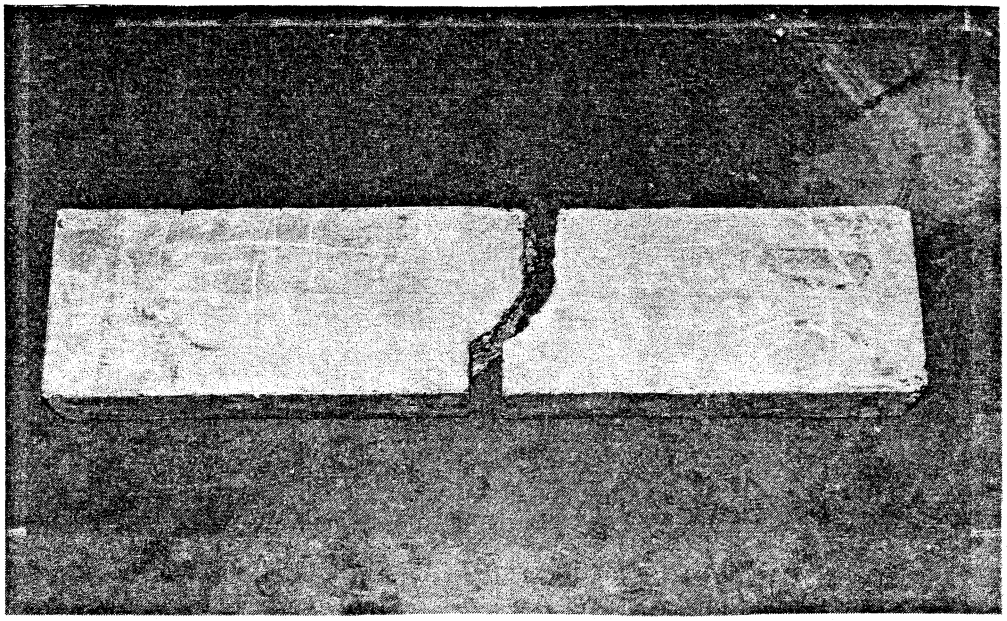

Fig. 2.8 Beam 1 after testing

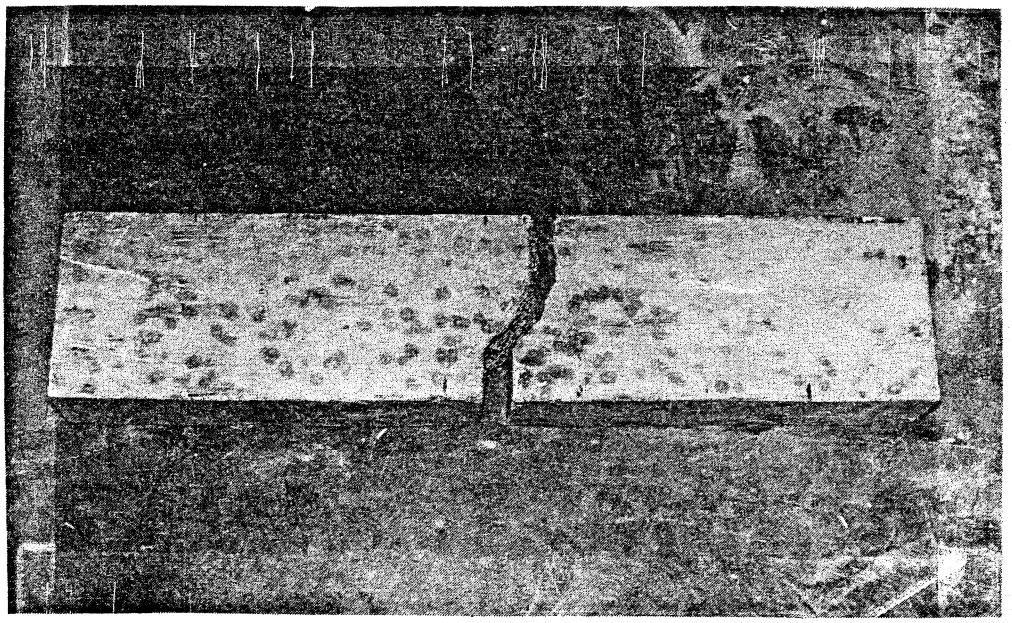

Fig. 2.9 Beam 2 after testing

Fig. 2.10 Crack surface of beam 1

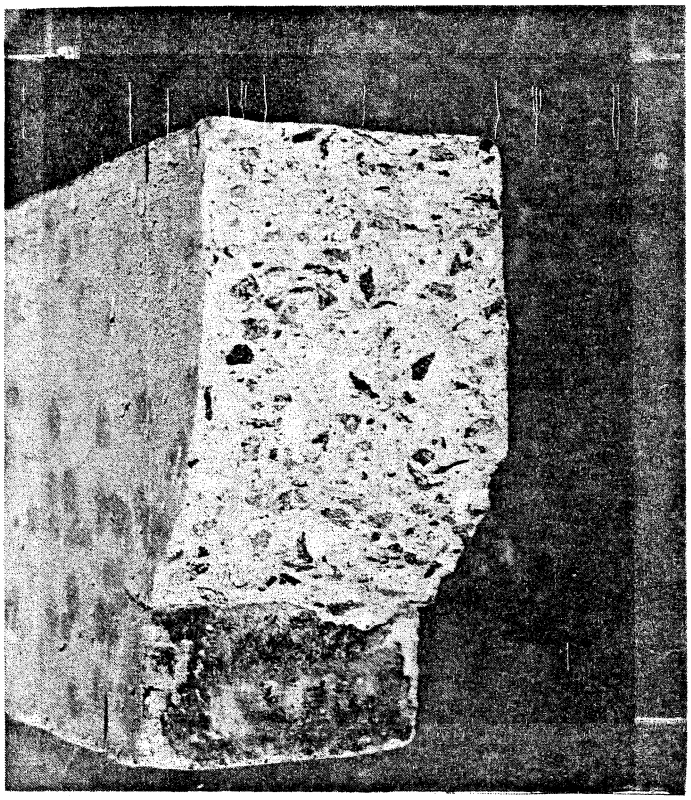

Fig. 2.11 Crack surface of beam 2

3. NUMERICAL STUDY

3.1 Finite element model

The adopted material model is based on nonlinear fracture mechanics. The element mesh is shown in Fig. 3.1.

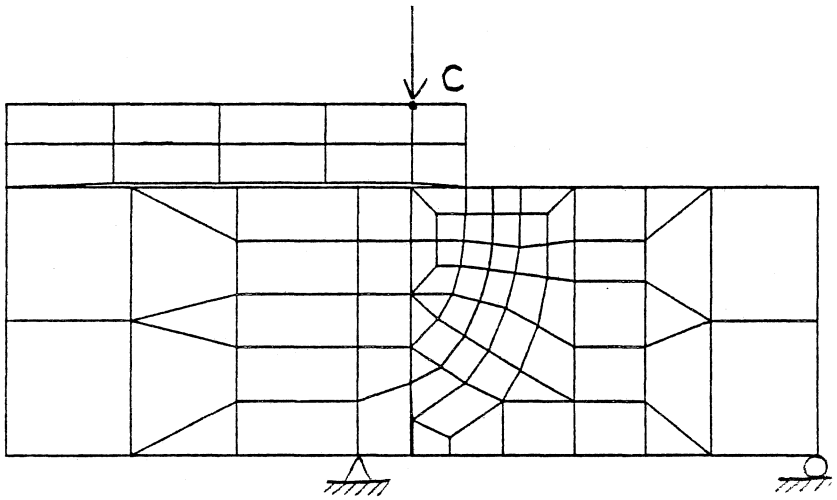

(a)

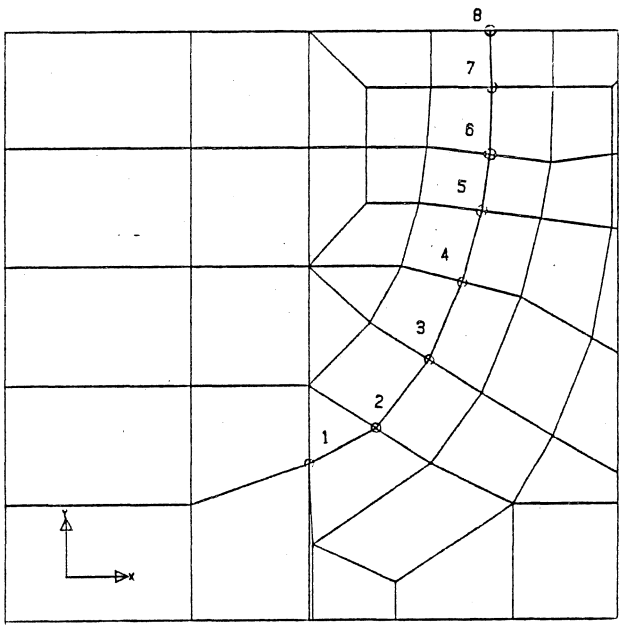

(b)

Fig. 3.1 a) Finite element model of the beam
b) Linkage elements

Plane, linear elastic three- and four-node elements together with two-node linkage elements were used.

A fracture zone, with the same trajectory as the crack in the tests, was modelled with the linkage elements.

The linkage element can be visualized like in Fig. 3.2. It has non-linear material properties. The 1-direction is normal to and the 2-direction, the shear-direction, is parallel to the fracture zone. The material properties are different in the two directions. Fig. 3.3 describes the constitutive relations for the linkage element. There is also an interaction between the stresses in the 1- and 2-direction, so that when the peak stress is reached in the tension-direction, the fracture stressline 2 in the shear-direction is lowered, Fig. 3.4.

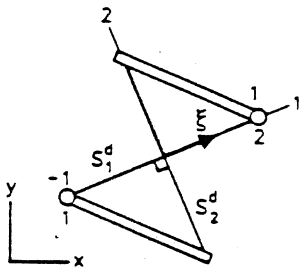

Fig. 3.2 Linkage element [3]

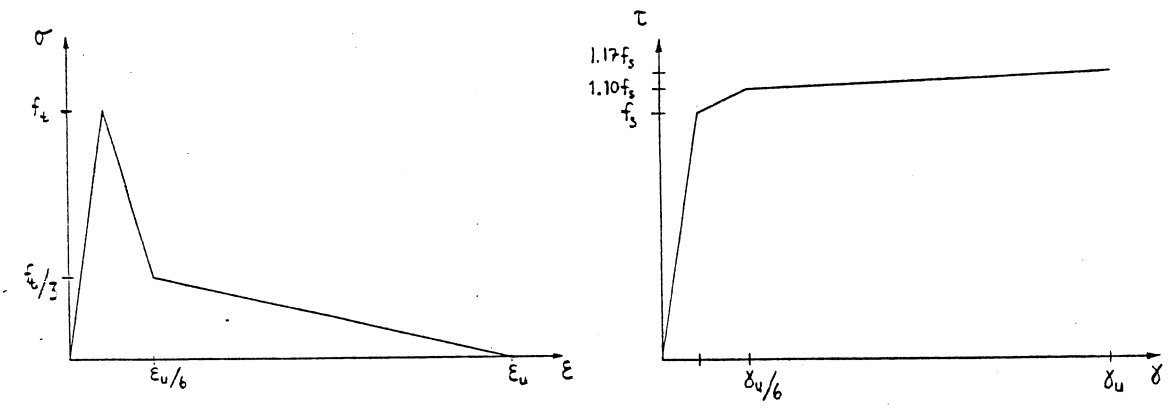

Fig. 3.3 Constitutive relations for the fracture zone

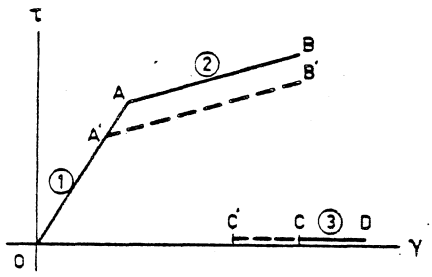

Fig. 3.4 Lowering of the fracture stressline 2 in the shear-direction [3]

The linkage element has been developed by Kent Gylltoft and is further described in [3]. The linkage element is implemented in a special version of the finite element program FEMP [10].

The following material parameters were used:

E = 30 GPa
f_t = 3.0 MPa
f_s = 3.0 MPa
f_s = 5.0 MPa (upper part of the beam where high compressive stresses are present)
ε_u = 20
G_f = 150 N/m

The width of the fracture zone was 10^{-5} m. The loading of the beam was performed by stepwise moving the point C in Fig. 3.1 downwards.

3.2 Results from the finite element calculations

The numerically obtained curve of load versus CMSD is shown in Fig. 3.5. The solution is stable up to peak load, but the softening part is unstable and gives numerical problems.

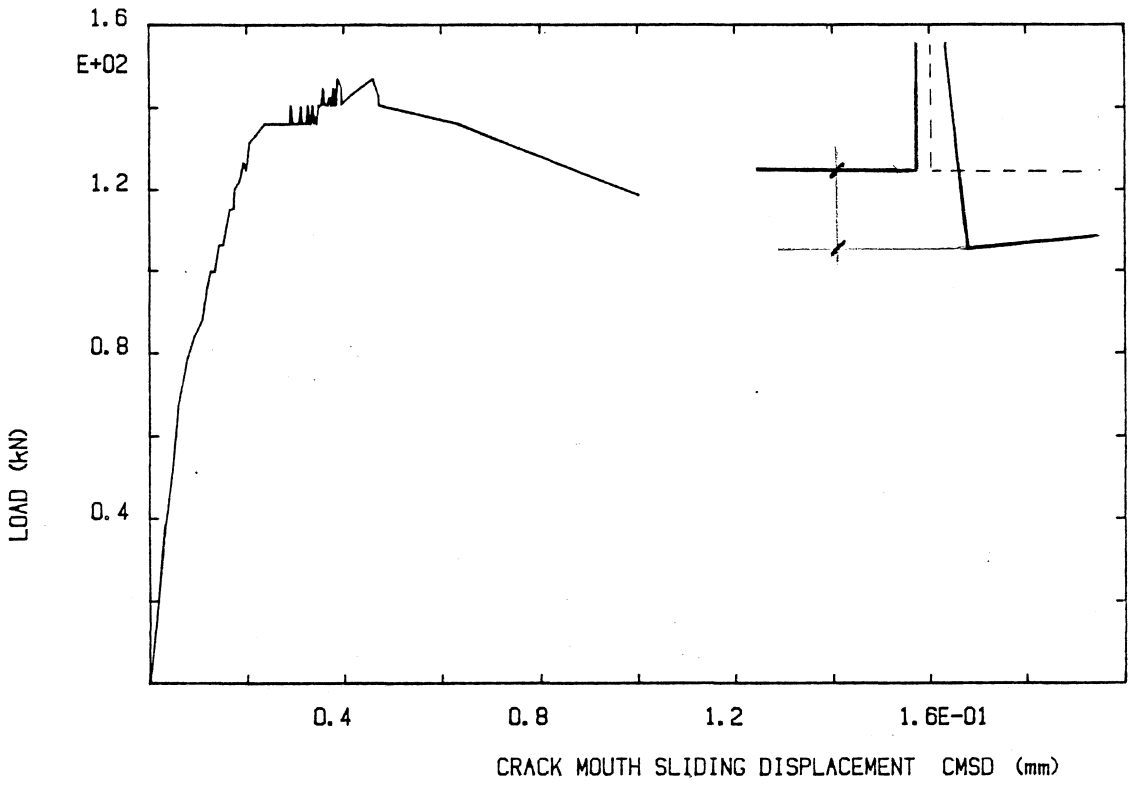

Fig. 3.5 Load versus CMSD curve from the finite element analysis

The curve of load versus CMD from the FEM-calculation is in Fig. 3.6 compared to the test results from beam 1. There is a good correlation in the prepeak part of the curves and the peakload differs only 15 %, but the model gives a too ductile post-peak behaviour.

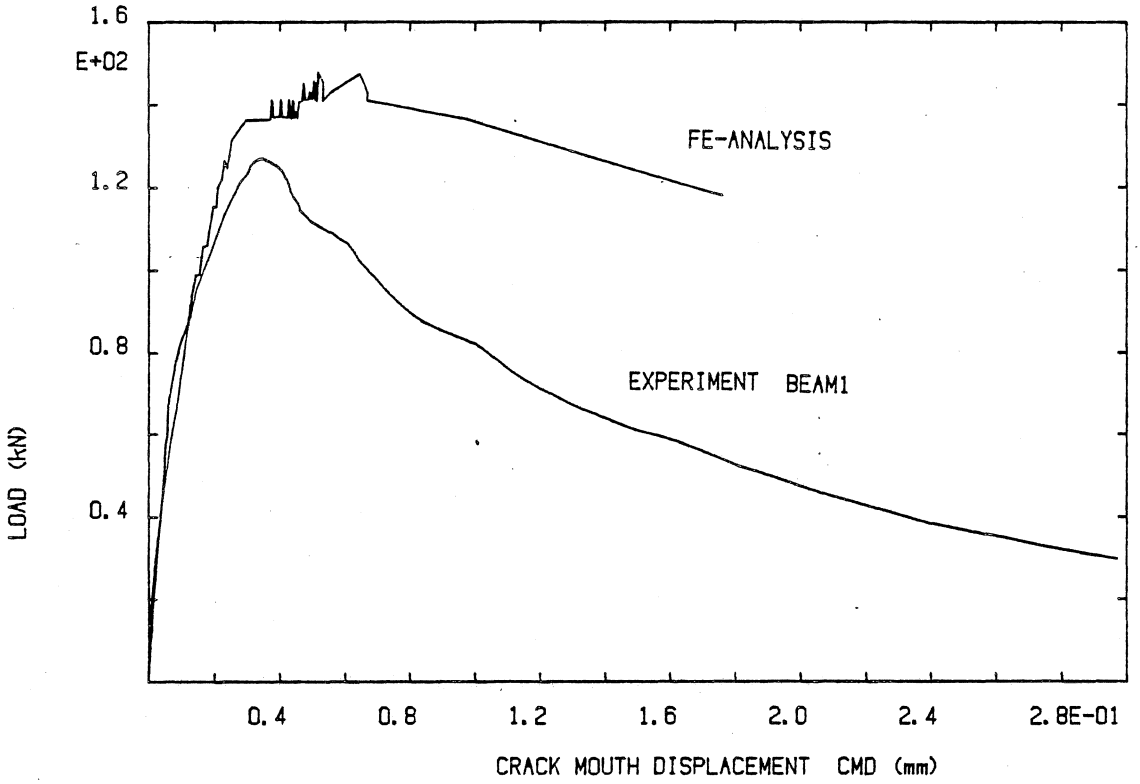

Fig. 3.6 Load versus CMD curve from the finite element analysis

We shall now look at the stresses in the fracture zone at different load levels. The location of the linkage elements is shown in Fig 3.1b and in Fig. 3.7 the tensile stresses in the elements 1 to 5 are shown as a function of the CMSD.

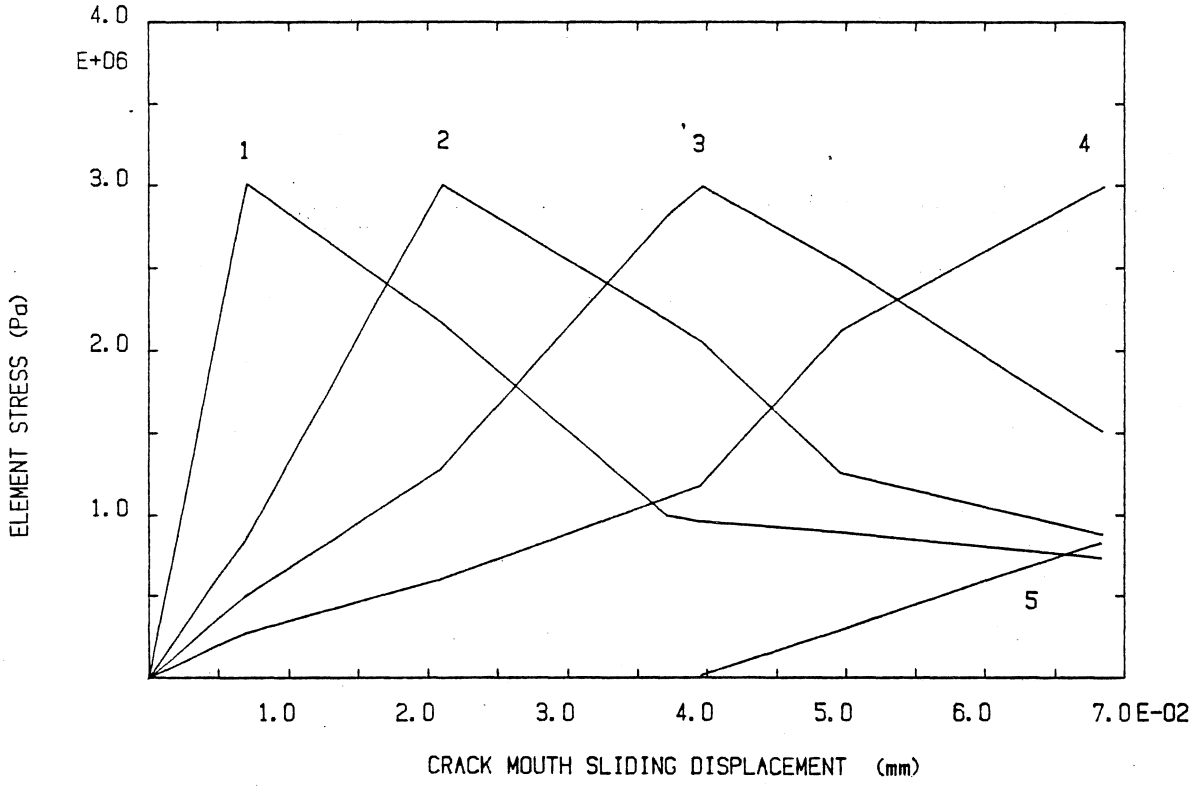

Fig. 3.7 Tensile stresses in elements 1 to 5

The figure shows that the crack in the FEM-model developes as a tensile crack. After peak load for CMSD = 0.07 mm element number 4 has reached the maximum stress 3 MPa. The stress in element 1 has decreased to 0.8 MPa.

The elements 6-8 are subjected to large compressive stresses together with shear stresses. The shear strength is therefore raised to 5 MPa for the three elements. Fig. 3.6 shows the shear stresses in the elements. No fracture occurs in these elements during the calculation.

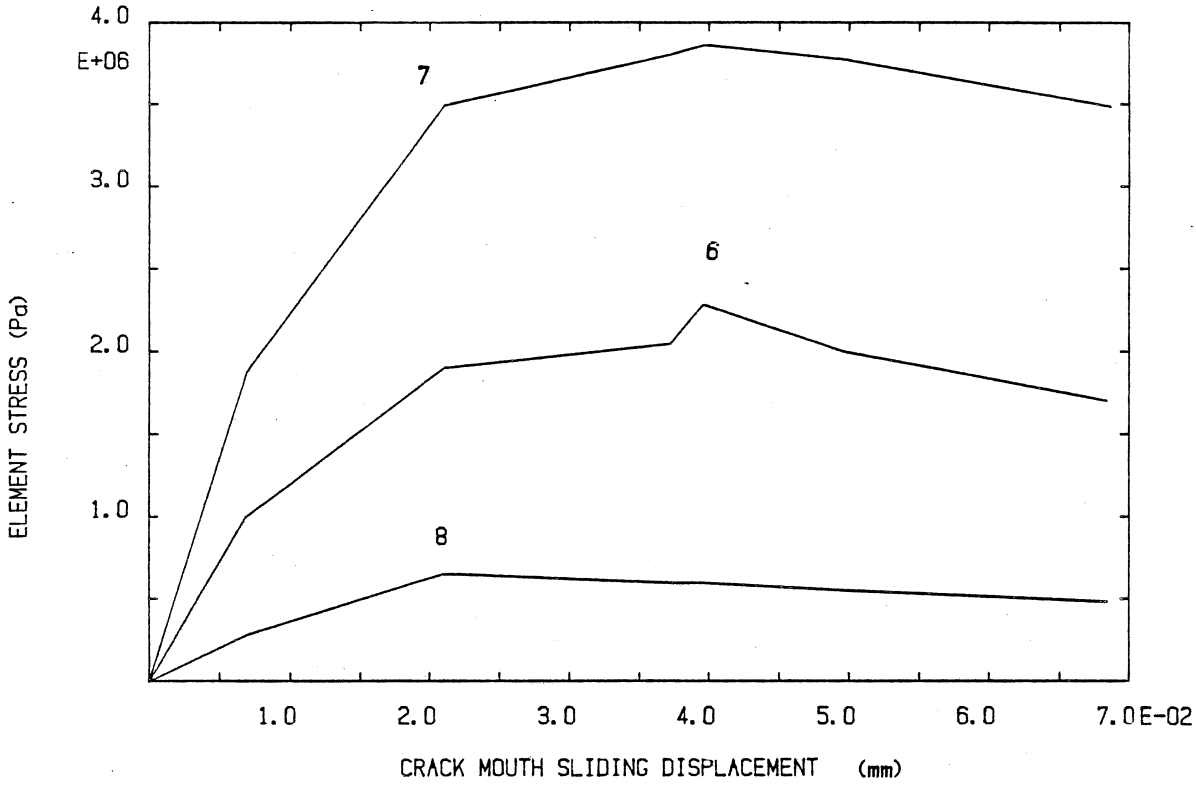

Fig. 3.8 Shear stresses in element 6 to 8

Plots of deflections and principal stresses at three different load levels are shown in Appendix 1.

4. DISCUSSION

The numerical study shows that the fracture of the beam can be modelled as a tensile fracture. The model gives a good prediction of the peak load and the crack growth at different load levels can be studied.

When the peak load is passed, the model gives a too ductile solution and it soon runs into numerical problems. What can then be improved, to get a better result?

A finer element mesh will probably give smoother load-deflection curves. The crack is now modelled with only 8 linkage elements.

The chances of getting a more stable post-peak curve had probably been greater if the loading was performed by giving desplacement control to the nodes on the top of the concrete beam, instead of a prescribed displacement at the loading point of the steel beam. The steel beam cannot be modelled infinitely stiff, and if the steel beam is weak compared to the concrete beam the solution after peakload will never converge.

Fig. 4.1 shows the experimental load deflection curve on the second beam at the loadpoint C in Fig. 4.2. The deflection was measured with two LVDT:s attached to a steel frame placed on top of the beam. The load deflection curve therefore shows the deflection related to a line between point A and B in Fig. 4.2.

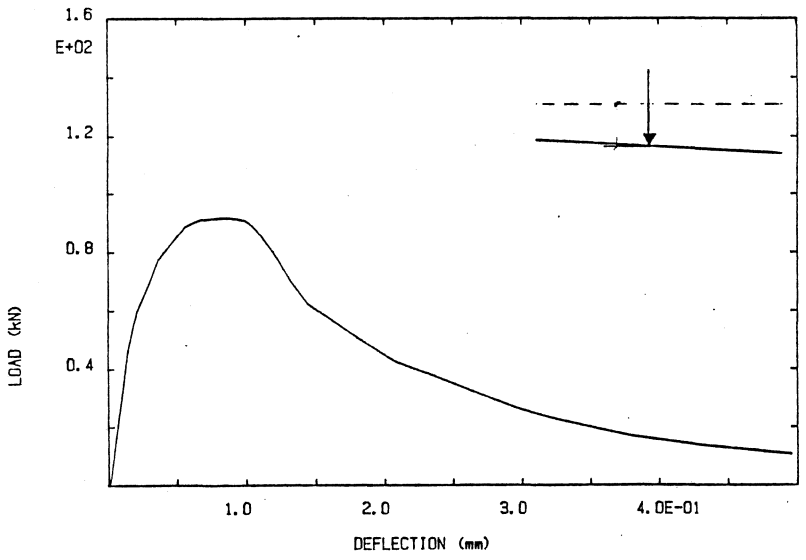

Fig. 4.1 Experimental load deflection curve

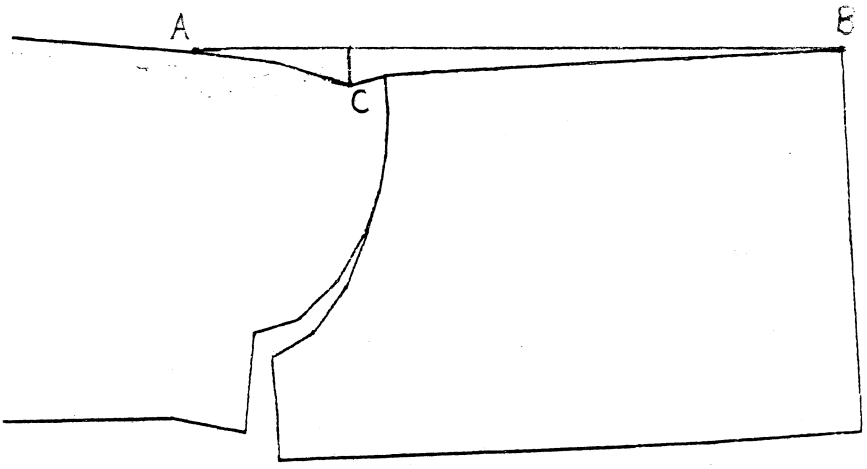

Fig. 4.2 Definition of deflection

What is then the real deflection of the beam? If we look at the numerical study of the beam and calculate the downward movement of point A and B at the peakload of beam 2, point A has moved downwards a distance of 0.026 mm and point B a distance of 0.006 mm. When the load after peakload decreases again, point A and B will start moving upwards. The real load-displacement curve will then be like in Fig. 4.3.

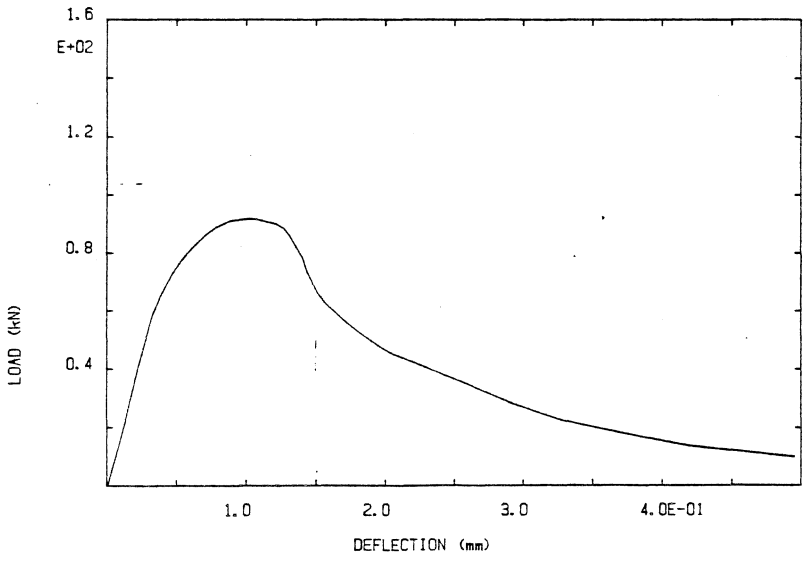

Fig. 4.3 Modified load deflection curve

The post-peak part is now much steeper. This shows that even if the loading was performed by giving displacement control to the nodes on the concrete beam, it would be difficult or impossible to get the right post-peak solution.

APPENDIX 1

This appendix shows plots of the displacements and the principal stresses at three different load levels in the FEM-calculation.

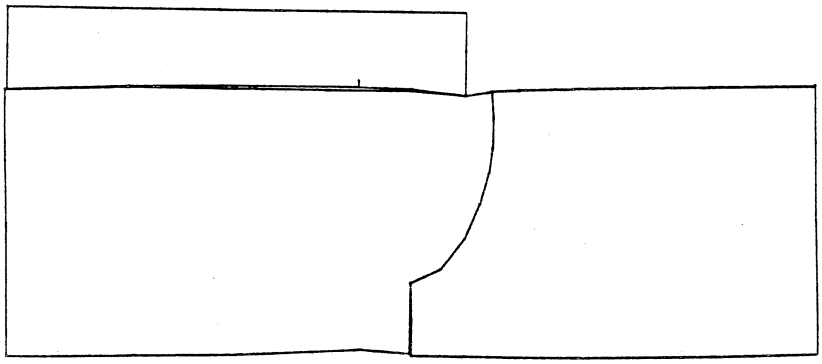

Fig. A 1.1 Displacements P=72 kN

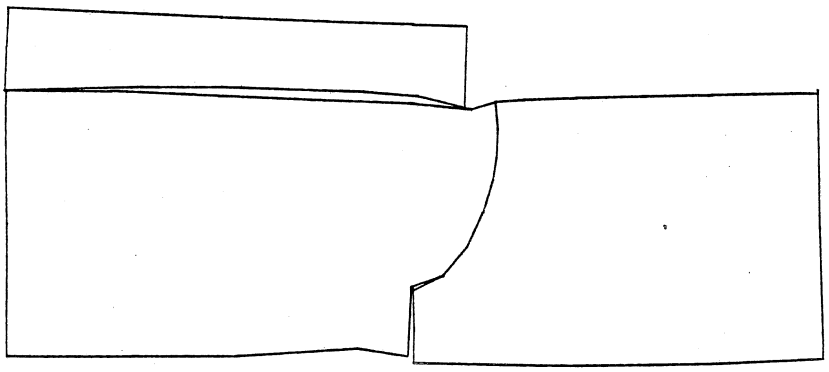

Fig. A 1.2 Displacements P=132 kN

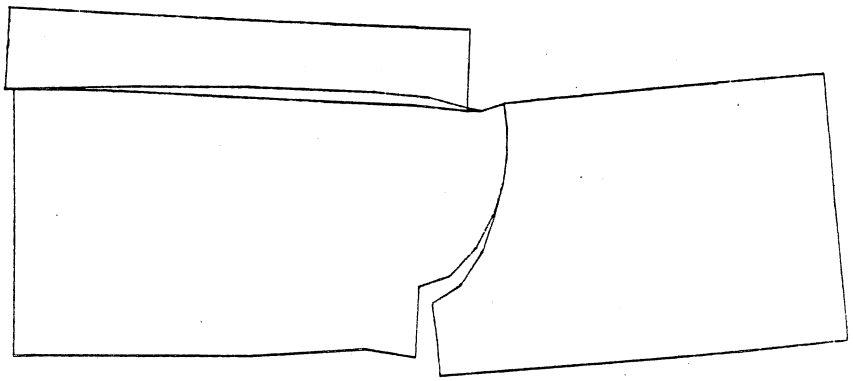

Fig. A 1.3 Displacements P=137 kN (AFTER PEAKLOAD)

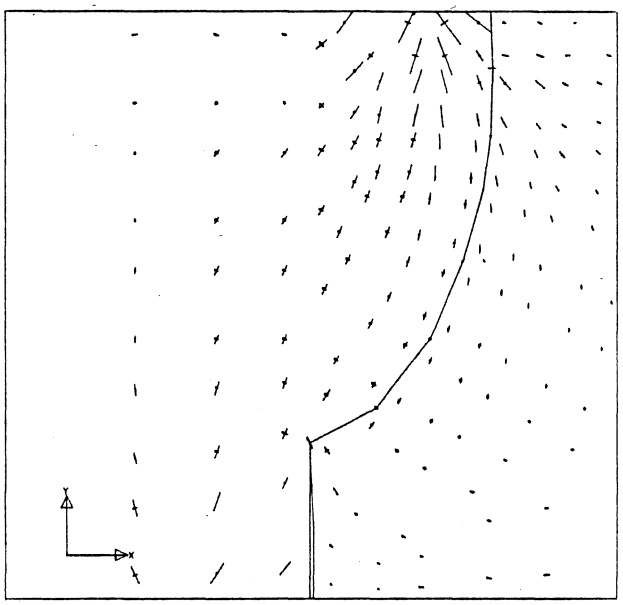

P=72 kN

Fig. A 1.4 Principal stresses

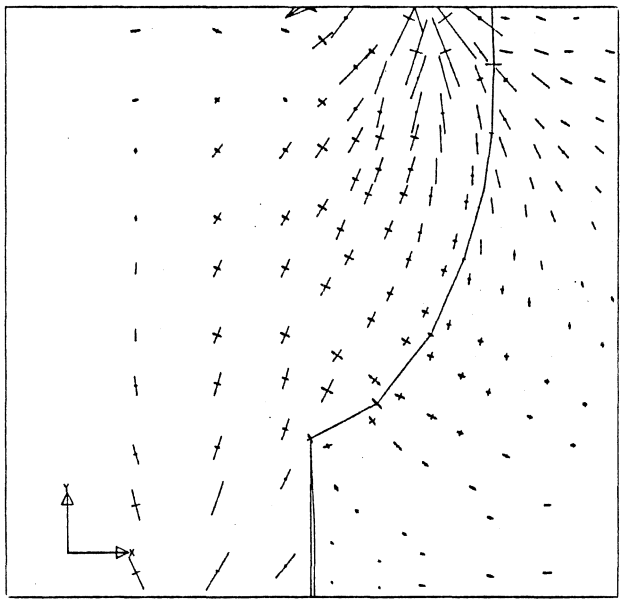

P=132 kN

Fig. A 1.5 Principal stresses

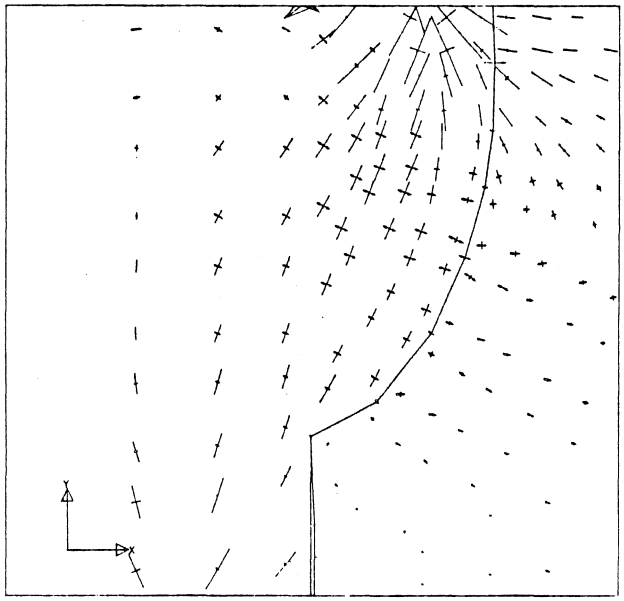

P=137 kN (AFTER PEAKLOAD)

Fig. A 1.6 Principal stresses

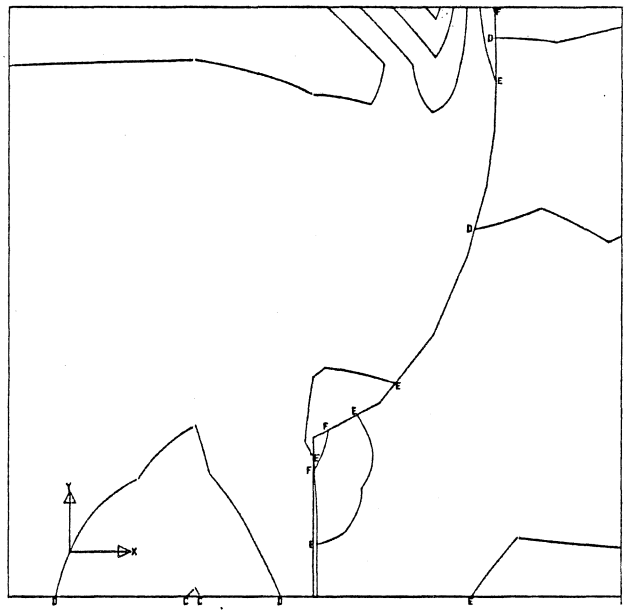

P=72 kN

Fig. A 1.7 Principal stresses

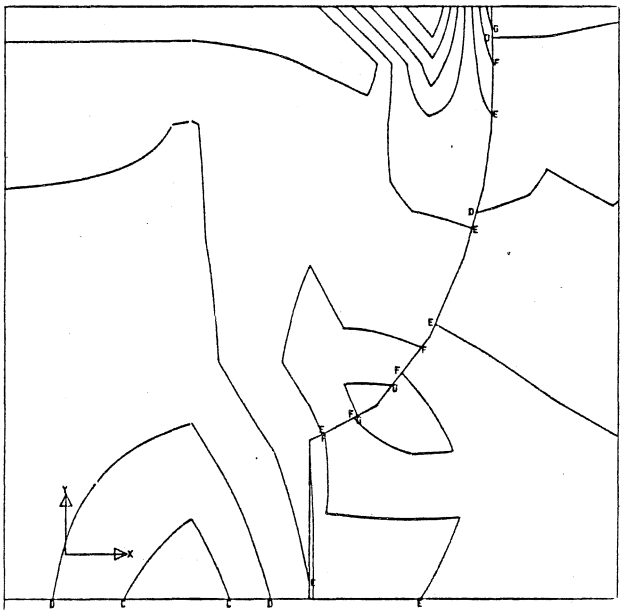

P=132 kN

Fig. A 1.8 Principal stresses

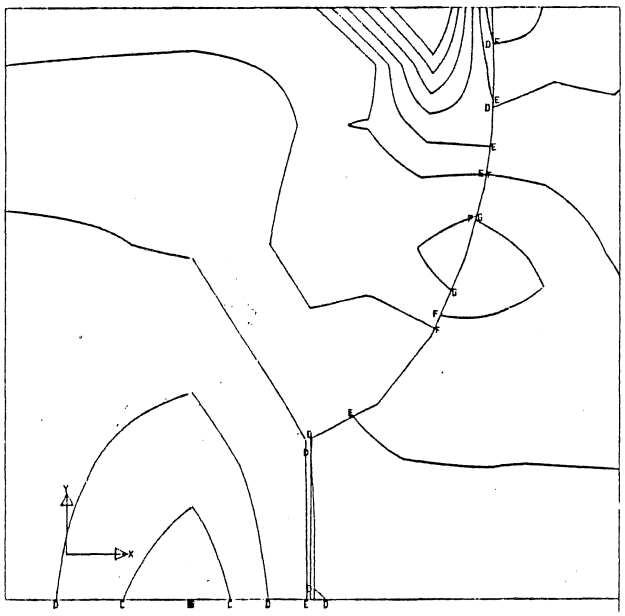

P=137 kN (AFTER PEAKLOAD)

Fig. A 1.9 Principal stresses

REFERENCES

[1] Wittman, F.H. Ed. 1985. Fracture mechanics of concrete, Elsevier, Netherlands.

[2] Wittman, F.H. Ed. 1985. Proc. of International Conference on Fracture Mechanics of Concrete, Elsevier Science Publ., Amsterdam, Netherlands.

[3] Gylltoft, K. 1983. Fracture Mechanics models for fatigue in concrete structures. Doctoral Thesis 1983:25D, Division of Structural Engineering, Luleå University of Technology, Luleå.

[4] Arrea, M. and Ingraffea, A.R. 1982. Mixed-mode crack propagation in mortar and concrete. Report No. 81-13, Department of Structural Engineering, Cornell University, New York.

[5] Bazant, Z.P., Pfeiffer, P.A. Shear fracture of concrete. Materials and structures, Vol. 19, No 110, pp 111-121.

[6] Glemberg, R. 1984. Dynamic analysis of concrete structures. Publication 84:1, Department of Structural Mechanics, Chalmers University of Technology, Göteborg.

[7] Rots, J.G. 1985. Strain-softening analysis of concrete fracture specimens. Proc. Int. Conf. on Fracture Mechanics of Concrete (Ed. F.H. Wittman), Elsevier Science Publ., Amsterdam, Netherlands.

[8] Oldenburg, M. 1985. Finite element analysis of tensile fracturing structures. Licentiate Thesis 1985:010L, Division of Computer Aided Analysis and Design, Luleå University of Technology, Luleå.

[9] De Borst, R. 1986. Non-linear analysis of frictional materials. Dissertation, Delft University of Technology, Delft, Netherlands.

[10] Nilsson, L. and Oldenburg, M. 1983. FEMP - An interactive graphic finite element program for small and large computer systems. Technical Report 1983:07T, Luleå University of Technology, Luleå.

SMEARED CRACK ANALYSIS OF CONCRETE USING A NONLINEAR FRACTURE MODEL

by

Ola Dahlblom and Niels Saabye Ottosen
Division of Structural Mechanics, Lund Institute of Technology
Box 118, S-221 00 LUND, Sweden

SUMMARY

The smeared crack approach is adopted and to circumvent the problem of lack of objectivity, this smeared approach is based on a reinterpretation of the fictitious crack model of Hillerborg et al. This reinterpretation is based on the introduction of the essential quantity, the socalled equivalent length, which is a purely geometrical quantity determined entirely by the size and form of the element region of interest. Following the same concept, it turns out to be possible to obtain an objective description of the shear stiffness along the crack plane, which depends on the size and form of the element region in question and the elongation across the infinitely thin crack zone.

The theory is implemented in a finite element program and results obtained for the response of a concrete tension specimen support the appealing features of the proposed approach.

INTRODUCTION

Modelling of cracks in concrete can, in principle, be accomplished by two different approaches: a discrete and a smeared approach.

The discrete approach, Ngo and Scordelis [1] and Nilson [2], is physically appealing as it reflects the localized nature of cracking, but its numerical implementation is hampered by the need for letting the cracks follow the element boundaries which, in turn, requires the introduction of additional nodal points. Alternatively, the cracks can be allowed to develop in arbitrary directions and thereby intersecting the elements, but this approach requires a redefinition of the original mesh arrangement. Obviously, this redefinition complicates the approach significantly even though automatic procedures for the redefinition of the mesh have been developed, Ingreffea and Saouma [3].

Computationally, the smeared approach is much simpler, as possible strain and displacement discontinuities introduced by the cracking are ignored and attention is given only to the changing ability to transfer stresses across the crack plane. Consequently, only the constitutive model expressed in terms of stresses and strains needs to be modified by the appearance of cracks. This modification is performed in a smeared manner over the element region of interest and it therefore leads to a very convenient numerical scheme, originally proposed by Rashid [4].

However, this original smeared concept exhibits an essential shortcoming, as demonstrated by Bazant and Cedolin [5]. For a completely brittle behaviour together with a simple strength criterion to detect the initiation and propagation of cracks, the loading that results in propagation of cracks in a structure loaded in tension, depends entirely on the mesh size. This socalled lack of objectivity also implies that the total energy dissipated by the cracks approaches zero, when the elements become infinitely small.

Significant improvements of the modelling of cracks were provided by the crack band model of Bazant and Oh [6] and by the fictitious crack model of Hillerborg et al. [7]. Whereas the crack band model describes the bilinear behaviour of a crack by three parameters (tensile strength σ_t, fracture energy G_c, and size of process zone w_c) all considered to be material parameters, the fictitious crack model is a two-parameter model (σ_t, G_c).

Moreover, whereas the crack band model of Bazant and Oh [6] is essentially a smeared approach, the fictitious crack model of Hillerborg et al. [7] is originally a discrete approach. Nilsson and Oldenburg [8,9] pioneered the idea of making a smeared version of the fictitious crack model without, however, being able to obtain entirely satisfactory results, Oldenburg [9]. Also the later composite fracture model of Willam [10] bears similarities with this work. Pursuing this concept and following the lines of [11], the fictitious crack model has been reformulated in [12] so that it can be applied in a smeared manner. This reinterpretation of the fictitious crack model leaves its predictions entirely unchanged, but in order to obtain a smeared interpretation it becomes necessary to introduce a socalled equivalent length. This implies that also the smeared version of the fictitious crack model becomes a three-parameter model, but it turns out that the equivalent length is a purely geometrical quantity determined entirely by the form and size of the element region of interest, whereas the corresponding quantity in the crack band model of Bazant and Oh [6], the size of the process zone w_c, is claimed to be a material property.

In the present paper, the smeared version of the

fictitious crack model [12] is presented. Finally, some results for tensile test specimens are presented.

FICTITIOUS CRACK MODEL

The fictitious crack model of Hillerborg et al. [7] takes as its basis the experimentally observed fact that cracking is a discrete phenomenon and that cracking is not completely brittle, but rather is characterized by a softening effect caused by cohesive stresses in the microcracked region. For a concrete bar loaded in tension into its post-peak region, the fictitious crack model describes cracking as elastic unloading along the entire length of the bar and an additional elongation occurring in an infinitely thin cracked zone. It is of interest that the fictitious crack model does not rely upon a relation between stresses and strains as the behaviour of the infinitely thin cracked zone is described by a constitutive relation expressed in terms of stress and elongation. This description was originally suggested using experimental evidence, only, but it is of interest that its acceptance can be based on purely thermodynamical arguments, [11].

Following the discussion above, the fictitious crack model describes the post-peak behaviour of the uniform and homogeneous concrete tension bar of length L as illustrated in Fig. 1, where, for simplicity, a linear relation between stress σ and crack elongation w is adopted.

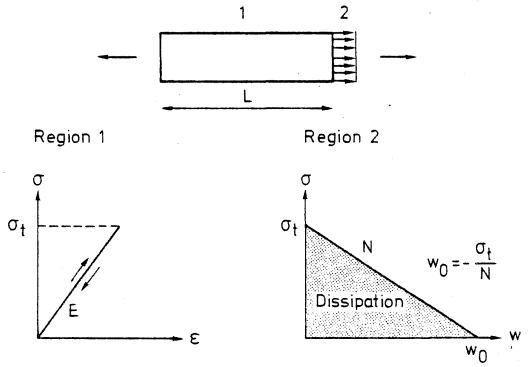

Fig. 1 - Fictitious crack model of Hillerborg et al. [7]

The resulting elongation, u, for the entire bar becomes

$$u = L\frac{\sigma}{E} + \frac{1}{N}(\sigma - \sigma_t) \qquad (1)$$

where E = Young's modulus, σ_t = tensile strength, and N is the slope of the σ-w curve. Tension and elongation are considered positive quantities. The total energy dissipated, D_t, when the stress eventually has dropped to zero is related to the area

under the σ-w curve of Fig. 1, i.e.

$$D_t = \frac{1}{2}\sigma_t w_0 A = G_c A; \qquad \text{i.e. } G_c = \frac{1}{2}\sigma_t w_0 \tag{2}$$

where A is the cross sectional area of the bar and G_c denotes the critical fracture energy. Observing that $w_0 = -\sigma_t/N$, cf. Fig. 1, we obtain from Eq. 2

$$N = -\frac{\sigma_t^2}{2G_c} \tag{3}$$

Moreover, defining the quantity λ by

$$\lambda = \frac{2G_c E}{\sigma_t^2} \tag{4}$$

we obtain

$$N = -\frac{E}{\lambda} \tag{5}$$

It should be observed that λ, the socalled characteristic length, is a material parameter having the dimension of length.

DEFINITION OF EQUIVALENT LENGTH

The previous equations can be reinterpreted in the spirit of a smeared crack approach by introducing an equivalent strain ϵ^*, uniformly distributed on the bar length, i.e. $\epsilon^* = u/L$. From Eqs. 1 and 5 we obtain

$$\epsilon^* = \frac{\sigma}{E}\left(1 - \frac{\lambda}{L}\right) + \frac{\sigma_t}{E}\frac{\lambda}{L} \tag{6}$$

The tangential stiffness modulus, E_T, then becomes

$$\frac{d\sigma}{d\epsilon^*} = E_T = \frac{E}{1 - \frac{\lambda}{L}} \tag{7}$$

As the bar is assumed to be subjected to an increasing elongation, E_T must be negative, providing the following restriction

$$L < \lambda \tag{8}$$

Equations 6 and 7 clearly show that the post-peak behaviour not only depends on the material parameters E and λ, but also becomes size-dependent through the appearance of the term L. This effect is illustrated in Fig. 2 and in accordance with experimental evidence, it appears that the longer the bar, the more brittle the response. However, it is of importance to realize, that irrespective of the length L, the description of the post-peak behaviour given through Eq. 6, implies that the correct total energy = AG_c will always be dissipated when the stress eventually has dropped to zero.

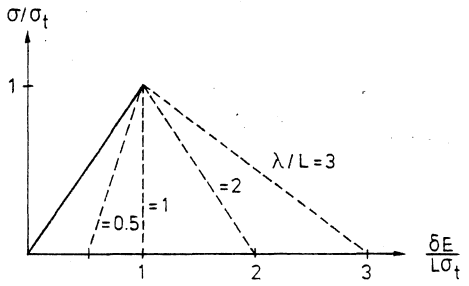

Fig. 2 - Behaviour of bar for different λ/L-ratios

Starting from the original discrete approach of the fictitious crack model, we have arrived at an alternative description given by Eqs. 6 and 7, which provides exactly the same predictions. It appears, however, that Eqs. 6 and 7 yield a constitutive relation expressed in terms of stress and strain. This means that Eqs. 6 and 7 can be used in a smeared crack approach. It is important, however, that to achieve this formulation, we have introduced a length L into the constitutive relation.

For the onedimensional case considered, this length L is simply the length of the bar considered. If more onedimensional finite elements were used to model the bar, we must for the element, which exhibits cracking, use the constitutive relation Eq. 6, where L now should be the length of that element. Consequently, we are led to introduce a socalled equivalent length, L_{eq}, into the constitutive relation Eq. 6. For the onedimensional elements considered, this equivalent length is simply the length of the cracked element normal to the crack plane. This observation suggests the following definition of the equivalent length applicable to all elements: the equivalent length, L_{eq}, of a finite element is the maximum length of the element region of interest in the direction normal to crack plane. This definition is illustrated in Fig. 3 for the 3-node triangle and the 8-node isoparametric element with 2×2 Gauss point integration.

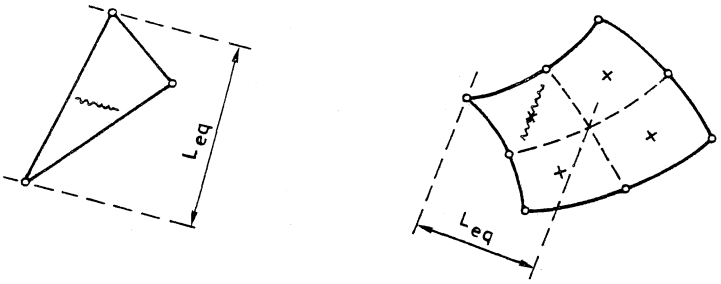

Fig. 3 - Definition of equivalent length L_{eq}

Note that for the 3-node triangle, the element region of interest is obviously the total element region, whereas for the 8-node element, the element region of interest is the region related to the Gauss point in question. The above definition of equivalent length applies for three-dimensional elements as well.

SMEARED CONSTITUTIVE EQUATIONS - PLANE STRESS

Having established the definition of equivalent length for arbitrary finite elements with arbitrary crack directions, we shall now generalize the smeared constitutive relations discussed above.

For simplicity we shall assume linear elastic behaviour and cracking under plane stress conditions (consideration to plastic effects and other stress states is straight forward). Assume that a crack plane develops normal to the x-axis.

In accordance with the experimental evidence that no necking effects are related to the crack development, the displacements in the infinitely thin cracked zone are assumed to be purely elongational, i.e. no Poisson effect is present. Therefore, the strain in the y-direction is determined by the usual Hooke's law. In the x-direction, σ_x results in a strain component given by Eq. 6, whereas σ_y provides a strain component in the x-direction equal to the usual elastic contribution. The above observations lead to

$$\begin{bmatrix}\sigma_x\\ \sigma_y\\ \tau_{xy}\end{bmatrix} = \frac{E}{1-\nu^2-\frac{\lambda}{L_{eq}}}\begin{bmatrix}1 & \nu & 0\\ \nu & 1-\lambda/L_{eq} & 0\\ 0 & 0 & \frac{1-\nu^2-\lambda/L_{eq}}{E}G_{ef}\end{bmatrix}\begin{bmatrix}\epsilon_x\\ \epsilon_y\\ \gamma_{xy}\end{bmatrix} - \frac{\frac{\lambda}{L_{eq}}\sigma_t}{1-\nu^2-\frac{\lambda}{L_{eq}}}\begin{bmatrix}1\\ \nu\\ 0\end{bmatrix} \tag{9}$$

From Eq. 9, we have the relation $\tau_{xy} = G_{ef}\gamma_{xy}$, where G_{ef} = effective shear modulus. The determination of G_{ef} is a subject of much controvercy, see for instance [13]. Its inclusion makes it possible to simulate shear stiffness along the crack plane, i.e. aggregate interlock. Usually, one writes $G_{ef} = \alpha G$, where G = elastic shear modulus and α = shear retention factor ($0 \leq \alpha \leq 1$). Often, the α-factor is simply given a constant value, typically α = 0.1-0.4, and many numerical experiments have been performed in order to evaluate the effect of different α-values.

In reality, the α-value must be a function of crack width, relative displacement tangential to the crack plane and of the nature of the crack surface. Also, the α-value is expected to decrease with increasing crack width so that for small widths, α is close to unity and for large widths, α is close to zero. Moreover, just like the tangential slope of the softening branch, E_T, the α-factor must also depend on the size of the finite element in question in order that the total shear behaviour of a concrete specimen does not depend on the number of elements.

The objectives above can be achieved in a manner completely analogous with the derivation of Eq. 6 by assuming the relative displacement tangential to the crack plane, w_s, related to the infinitely thin cracked zone to be determined by

$$w_s = \frac{w}{G_s}\tau_{xy} \tag{10}$$

where the constant G_s = slip modulus. In the finite element outside the infinitely thin cracked zone, the usual elastic shear relation $\tau_{xy} = G\gamma_{xy}$ is assumed to hold. The assumptions above imply that

$$G_{ef} = \frac{G}{1 + \frac{G}{G_s}\frac{w}{L_{eq}}} \tag{11}$$

where w as before denotes the crack elongation normal to the crack plane and where L_{eq} is the equivalent length of the finite element region in question. The simple relation, Eq. 10, provides close agreement with the experimental results of Paulay and Loeber [14] when G_s = 3.8 MPa.

Eq. 9 is written in a total form, but for numerical purposes the corresponding incremental formulation might be advantageous. Noting that G_{ef} is not a constant, but depends on

w, which is given by $w = (\sigma_x - \sigma_t)/N$, cf. Fig. 1, we obtain from Eqs. 9 and 11 after some algebra

$$\begin{bmatrix} d\sigma_x \\ d\sigma_y \\ d\tau_{xy} \end{bmatrix} = \frac{E}{1-\nu^2-\frac{\lambda}{L_{eq}}} \begin{bmatrix} 1 & \nu & 0 \\ \nu & 1-\lambda/L_{eq} & 0 \\ \frac{G_{ef}^2 \lambda \gamma_{xy}}{G_s L_{eq} E} & \frac{G_{ef}^2 \lambda \nu_{xy}}{G_s L_{eq} E} & \frac{1-\nu^2-\lambda/L_{eq}}{E} G_{ef} \end{bmatrix} \begin{bmatrix} d\epsilon_x \\ d\epsilon_y \\ d\gamma_{xy} \end{bmatrix} \tag{12}$$

It is of interest that whereas Eq. 9 is symmetric, Eq. 12 is not. Moreover, Eq. 12 clearly shows that the incremental shear stress is coupled not only to the incremental shear strain, but also to the incremental normal strains.

FINITE ELEMENT RESULTS

The theory proposed above has been implemented into a finite element program and some results for the behaviour of the concrete tension specimen shown in Fig. 4 will be given below. Due to symmetry, only one quarter of the specimen will be considered. The dimensions of the specimen are taken from the experimental investigation of Petersson [15].

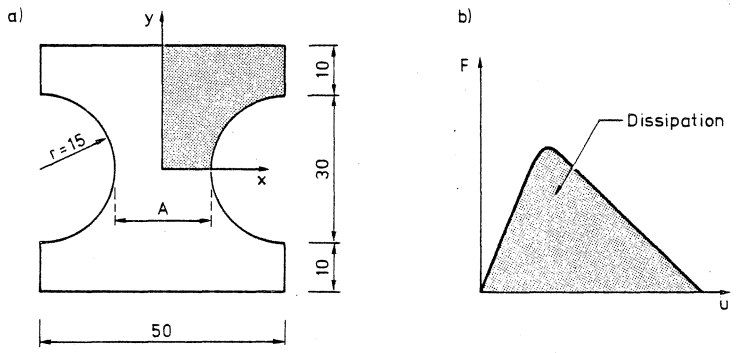

Fig. 4 - a) concrete specimen of Petersson [15], dimensions are in mm, A = cross sectional area; b) calculated total force - total elongation diagram shown in principle

The finite element solution scheme follows a tangential approach and the following material parameters all representative for concrete were adopted: $E = 2.1 \cdot 10^4$ MPa, $\nu = 0.2$, $\sigma_t = 3.3$ MPa, $G_c = 130$ N/m, $G_s = 3.8$ MPa.

By prescribing equal, increasing displacements along the upper and lower surface of the specimen, the specimen is loaded into the post-peak region until it has disintegrated

completely. In reality, cf. Petersson [15], this disintegration corresponds to the development of a single crack having the area A, as shown in Fig. 4a).

The purpose of the calculations is not to compare results with experimental evidence, but rather to document that the suggested smeared approach is objective in the sense that for decreasing finite element size the total energy dissipated due to cracking approaches the correct value. By definition, the correct total dissipated energy is AG_c, where G_c is the prescribed fracture energy = 130 N/m. From the calculation results, we can construct the total force-total elongation diagram as shown in principle in Fig. 4b). The calculated dissipated energy is obtained from the area under this curve and by dividing by the cross sectional area A, we can determine the calculated fracture energy $G_{c,cal}$. For decreasing sizes of the finite elements, $G_{c,cal}$ should converge towards the exact value G_c, if the suggested smeared approach should be objective.

Using a 3-node triangular element and a 4-node isoparametric element, the finite element mesh of different models is shown in Fig. 5. The crack pattern, when the specimen has disintegrated completely, is also shown.

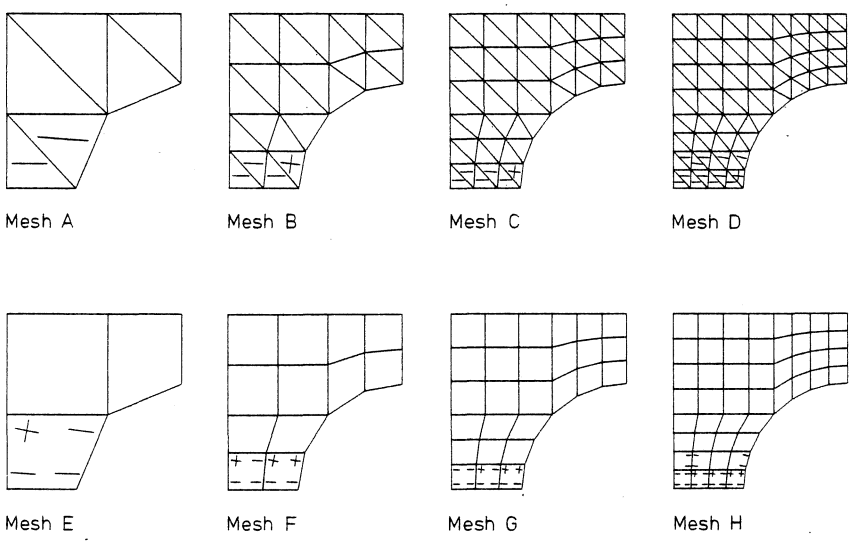

Fig. 5 - Finite element meshes and crack patterns

Because the stresses and strains in the constant strain element are evaluated here simply at the centroid of the elements, the calculated crack direction might differ from the true horizontal direction. This implies that shearing along the

crack plane will contribute to the load bearing capacity. It is of interest that even for the tension specimen considered, this mobilization of the shear stiffness might be quite considerable.

To illustrate this, mesh C of Fig. 5 was used in combination with the usual simplified assumption for the shear stiffness along the crack plane, i.e. $G_{ef} = \alpha G$, where α is considered to be a constant. For typical α-values = 0.01, 0.1, and 0.4 the obtained force-elongation diagram is shown in Fig. 6. It appears that even for this simple tension specimen is an accurate description of the variation of the shear modulus, G_{ef}, very essential. Consequently, in all the remaining calculations, the consistent approach proposed by Eq. 11 was applied.

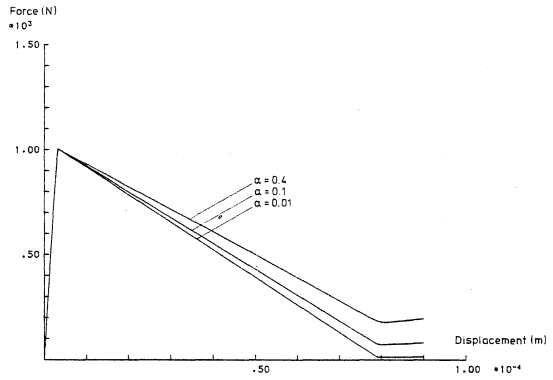

Fig. 6 - Force-displacement curves for mesh C of Fig. 5 with $G_{ef} = \alpha G$, where α is considered to be a constant

The resulting force-displacement curves for the meshes shown in Fig. 5 are shown in Fig. 7 and the significant improvement compared with Fig. 6 is obvious.

The resulting calculated fracture energy, $G_{c,cal}$, is shown in Fig. 8 as function of the number of degrees of freedom. It appears that the calculated fracture energy converges very closely to the exact value, G_c, documenting that the adopted smeared approach is objective. Moreover, we observe a dramatic improvement of the results as compared with the corresponding results of Oldenburg [9].

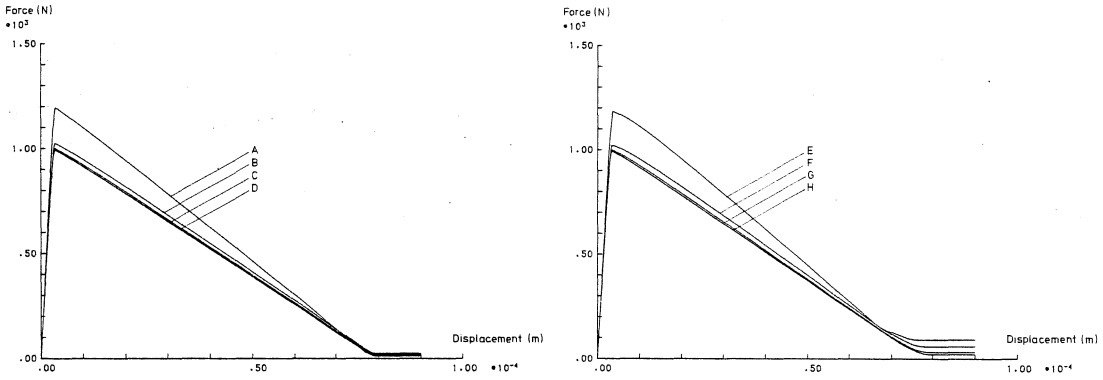

Fig. 7 - Force-displacement curves for the meshes shown in Fig. 5

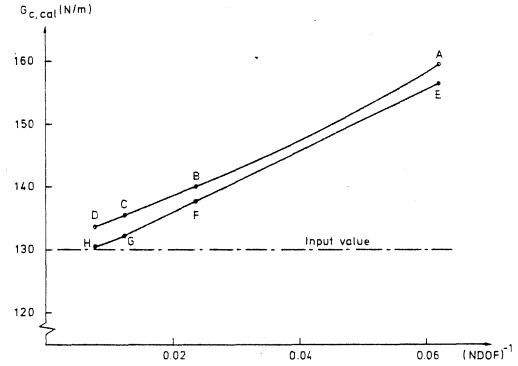

Fig. 8 - Calculated fracture energy for the meshes of Fig. 5 as function of number of degrees of freedom (DOF)

The results shown above cannot be claimed to be of complete generality, as the cracks mainly are parallel to one of the element boundaries. In a general finite element analysis, cracks will have arbitrary directions with the element boundaries.

To investigate this aspect, the highly distorted meshes shown in Fig. 9 were adopted. The crack pattern when the specimen has disintegrated completely is also shown.

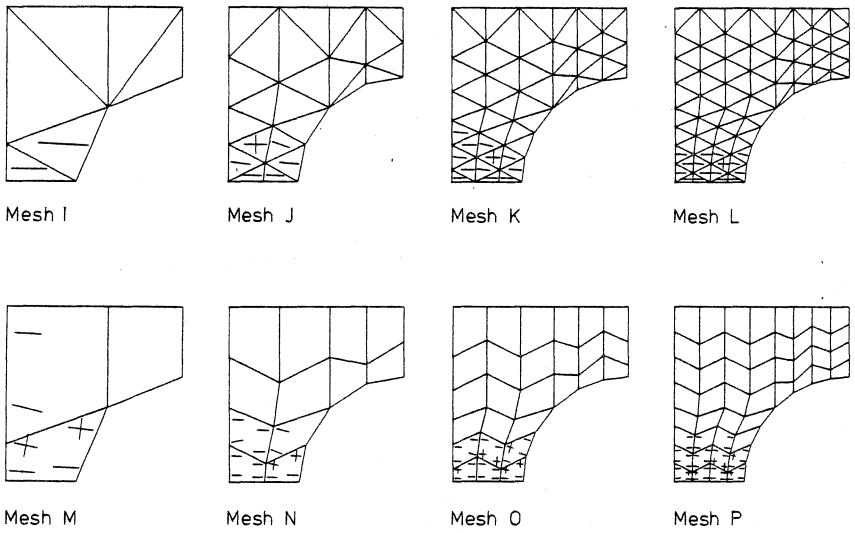

Fig. 9 - Highly distorted finite element meshes and crack patterns

The resulting force-displacement curves are shown in Fig. 10. It is apparent that due to the low order of the triangular element, the distorted meshes have difficulties with reflecting the correct deformation mode. Even though the response shown in Fig. 10 is inferior compared with the results shown in Fig. 7, it is of interest that a smooth convergence occurs. In calculating the fracture energies of Fig. 11, the tail of the force-displacement curves have been replaced by straight lines as shown in Fig. 10.

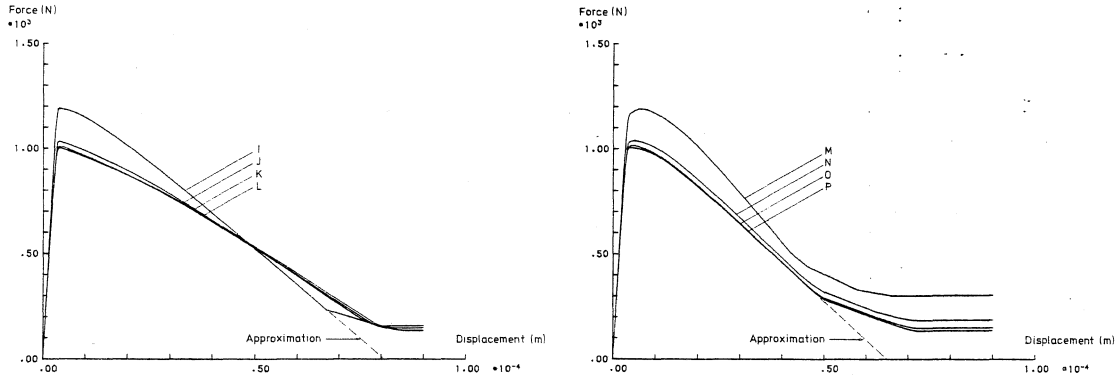

Fig. 10 - Force-displacement curves for the distorted meshes of Fig. 9.

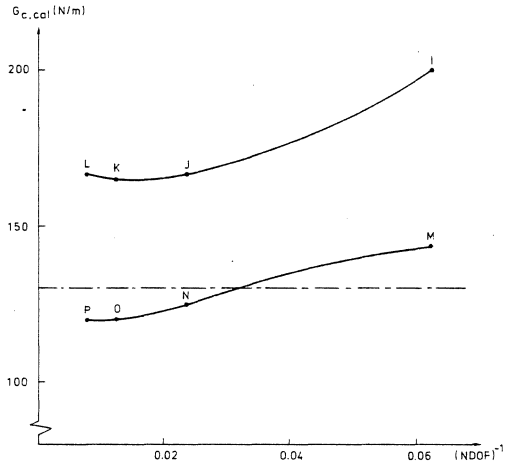

Fig. 11 - Calculated fracture energies for the distorted meshes of Fig. 9 as function of number of degrees of freedom (DOF)

The obtained results demonstrate that the presently used smeared approach is objective. For distorted meshes of triangular elements the estimation of the fracture energy is, however, a bit high. This is a result of the inability of the element type to model the inhomogeneous strain distribution correctly, when highly distorted meshes are used. It may be concluded that elements of low order is unfavourable in connection with smeared crack analysis. This is also supported by results obtained with eight-node isoparametric elements.

CONCLUSIONS

The fictitious crack model of Hillerborg et al. [7] is originally formulated as a discrete model. In recognition of the essential numerical drawbacks related to such an approach, we have made a reinterpretation of the fictitious crack model in the spirit of a smeared approach. The key to this reinterpretation is the introduction of the socalled equivalent length being a purely geometrical quantity determined entirely by the size and form of the element region of interest. The introduction of the equivalent length implies that irrespective of the size of the finite element, the dissipated fracture energy remains, in principle, the same. Following the same concept, it turns out to be possible to obtain an objective description of the shear stiffness along the crack plane, which depends on the size and form of the element region in question through the equivalent length and which also depends on the elongation across the infinitely thin crack zone.

Through finite element calculations of a tension concrete specimen, the theory was demonstrated to be objective even for highly distorted meshes. However, the results obtained with distorted element meshes indicate that a low order of the element shape functions is unfavourable in connection with smeared crack analysis.

REFERENCES

[1] Ngo, D., and Scordelis, A.C., 'Finite Element Analysis of Reinforced Concrete Beams', Journal of the American Concrete Institute, Vol. 64, No. 3, March 1967, 152-163.

[2] Nilson, A.H., 'Nonlinear Analysis of Reinforced Concrete by the Finite Element Method', Journal of the American Concrete Institute, Vol. 65, No. 9, Sept. 1968, 757-766.

[3] Ingreffea, A.R., and Saouma, V., 'Numerical Modelling of Discrete Crack Propagation in Reinforced and Plain Concrete', in Fracture Mechanics of Concrete: Structural Application and Numerical Calculation. Ed. by G.C. Sih and A. DiTommaso, Martinus Nijhoff Publ., Dordrecht, 1985, 171-225.

[4] Rashid, Y.R., 'Ultimate Strength Analysis of Reinforced Concrete Pressure Vessels', Nuclear Engineering and Design, Vol. 7, No. 4, April 1968, 334-344.

[5] Bazant, Z.P., and Cedolin, L., 'Blunt Crack Band Propagation in Finite Element Analysis', Journal of the Engineering Mechanics Division, ASCE, Vol. 105, No. EM2, April 1979, 297-315.

[6] Bazant, Z.P., and Oh, B.H., 'Crack Band Theory for Fracture of Concrete', Materials and Structures, RILEM, Vol. 16, 1983, 155-177.

[7] Hillerborg, A., Modeer, M., and Petersson, P-E., 'Analysis of Crack Formation and Crack Growth in Concrete by Means of Fracture Mechanics and Finite Elements', Cement and Concrete Research, Vol. 6, 1976, 773-782.

[8] Nilsson, L., and Oldenburg, M., 'Nonlinear Wave Propagation in Plastic Fracturing Materials - A Constitutive Modelling and Finite Element Analysis', IUTAM Symposium: Nonlinear Deformation Waves, Tallin 1982, Springer, Berlin, 1982, 209-217.

[9] Oldenburg, M., 'Finite Element Analysis of Tensile Fracturing Structures', Licentiate Thesis 1985: 010L, Div. of Comp. Aided Anal. and Des., Luleå University, Sweden, 1985.

[10] Willam, K.J., ' Experimental and Computational Aspects of Concrete Fracture', Computer Aided Analysis and Design of Concrete Structures, Pineridge Press, Swansea, UK, 1984, 33-70.

[11] Ottosen, N.S., 'Thermodynamical Consequences of Strain Softening in Tension', to be published in Journal of Engineering Mechanics, ASCE, 1986.

[12] Ottosen, N.S. and Dahlblom, O.: Smeared crack analysis using a nonlinear fracture model for concrete, Numerical Methods for Non-Linear Problems, Vol. 3, Edited by C. Taylor, D.R.J. Owen, E. Hinton and F.B. Damjanic, Pineridge Press, pp. 363-376, 1986.

[13] Finite Element Analysis of Reinforced Concrete, ASCE, New York, 1982.

[14] Paulay, T., and Loeber, P.J., 'Shear Transfer by Aggregate Interlock', Shear in Reinforced Concrete, Vol. 1, Special Publ. SP-42, ACI, Detroit, Michigan, 1974.

[15] Petersson, P-E., 'Crack Growth and Development of Fracture Zones in Plain Concrete and Similar Materials', Report TVBM-1006, Div. of Building Materials, Lund Institute of Technology, Sweden, 1981.

A DESCRIPTION OF CONCRETE AND FRC MATERIALS BY MEANS OF COMPOSITE MATERIAL THEORY AND CONTINUUM DAMAGE MECHANICS

by

H. Stang

Department of Structural Engineering
Technical University of Denmark

Paper presented at Nordiskt Miniseminarium
"Betongens Brottmekanik"
LTH, Lund den 6. november 1986.

INTRODUCTION

In terms of constitutive equations materials such as rock, concrete, and other cement based composite materials are characterized by the fact that they exhibit a socalled strain softening behavior prior to failure.

Though there is still a great deal of discussion on the validity of stress/strain curves which include strain softening, see e.g. [1], it is generally agreed on that failure of rock and cement based composite materials is always governed by the nucleation and growth of microvoids or microcracks [2]. It is also agreed on that it is this damage evolution that is responsible for the nonlinearity of the stress strain curves for the above mentioned materials. Damage evolution is also responsible for the development of a so-called process zone ahead of tension cracks in rock and concrete.

In the calculation of e.g. concrete structures loaded in tension or bending damage evolution has been accounted for in a number of different ways. As two extremes one might mention the fracture mechanical approach where the process zone has been included as a fictitious crack [3] - [6], and the continuum approach, see e.g. [7] - [11], where the damage evolution is included via a stress-strain curve with strain softening.

Further information on the treatment of strain softening and crack development can be found via the detailed bibliography in [9].

Though the correct approach to damage modelling in concrete structures is not gennerally agreed on, it is evident that a continuum approach is very suitable in describing damage evolution in fibre reinforced (cement based) materials, since we are dealing here with a highly homogenized kind of damage, and it is possible to define and experimentally examine a well defined set of damage modes, e.g. matrix cracking, fibre cracking, fibre/matrix debonding, and so on [16].

In this paper the continuum approach to damage modelling will be investigated. We will not deal with the structural level, but with the microscopic level. Thus to be precise, we will investigate the possibility of deriving phenomenological constitutive equations which can be used in a continuum approach to e.g. concrete. The

tools that will be used are the so-called continuum damage mechanics theory (CDM), see e.g. [12] - [16], and composite material theory (CMT), see e.g. [17] - [19]. CDM-theories constitute a group of theories which derives local constitutive equations in the continuum mechanics sense from three definitions or laws/assumptions:

1) A definition of internal variables which describe the damage modes in question.
2) Constitutive equations involving the influence of the internal damage variables on the overall material behavior.
3) Evolution equations which describe the damage evolution as function of the applied load.

By applying composite material theory the first and the second problem of the CDM-approach has been solved in one step, as we shall see in the following. Furthermore, due to the rather general CMT's which are available, it is possible to a) model damage with a 3D model, b) model the effect of anisotropic damage, and c) model the effect of damage geometry (e.g. spheres contra microcracks, given a damage evolution law).

Finally, it should be mentioned that the results from 3D-composite material theory can be reduced to 2D or 1D models, as it will be shown in the case of the derivation of the constitutive equation for a unidirectional fibre reinforced composite material.

COMPOSITE MATERIAL THEORY FOR MATERIALS WITH VOIDS OR CRACKS

First we will summarize some of the basic results of elastic CMT. These results are general, i.e. they apply to any composite material whether it contains infinitely stiff inclusions or voids or cracks. The results are due mainly to Hill [20].

The starting point for a 3D-composite material analysis is usually a so-called representative volume element, RVE, with total volume V (including voids) and surface $\delta(V)$ (which does not include internal surfaces on voids and/or cracks). On the structural level a RVE can be thought of as a material point, however, on the microscopic level the RVE is an element containing many inhomogenities.

In the following it is assumed that all phases (matrix and inclusions) are linear elastic and small strain elasticity is used throughout the analysis.

In order to investigate the behavior of the RVE two kinds of boundary conditions are prescribed. Either

$$\sigma_{ij}\, n_j = \Sigma_{ij}\, n_j \quad \text{on} \quad \delta(V), \tag{1}$$

where σ_{ij} is the microscopic stress field, n_i is the outward unit normal to $\delta(V)$ and Σ_{ij} is a stress tensor which is constant in space.

Or

$$u_i = E_{ij}\, x_j \quad \text{on} \quad \delta(V), \tag{2}$$

where u_i are the microscopic displacements, E_{ij} is a strain tensor constant in space, and x_i are the coordinates.

The tensors Σ_{ij} and E_{ij} are called the macroscopically homogeneous stress and strain, respectively, since they represent the homogeneous fields which would be introduced if eq. (1) and (2) were prescribed on a <u>homogeneous</u> volume element.

Denoting by an overbar the volume average of the stress and strain field:

$$\bar{\sigma}_{ij} = \frac{1}{V} \int_V \sigma_{ij}\, dV\ , \tag{3}$$

$$\bar{\varepsilon}_{ij} = \frac{1}{V} \int_V \varepsilon_{ij}\, dV\ , \tag{4}$$

it follows from the divergens theorem that

$$\bar{\sigma}_{ij} = \Sigma_{ij} \quad \text{given (1)}, \tag{5}$$

and

$$\bar{\varepsilon}_{ij} = E_{ij} \quad \text{given (2)}. \tag{6}$$

Furthermore, it follows from the principle of virtual work that the volume average of strain energy density, $\bar{W}$, is given by

$$\bar{W} = \frac{1}{V} \int \frac{1}{2} \sigma_{ij} \varepsilon_{ij} \, dV = \frac{1}{2} \bar{\sigma}_{ij} \bar{\varepsilon}_{ij} \, , \tag{7}$$

given the boundary conditions (1) or (2).

Next we define the free energy density ψ for the RVE as

$$\psi = \bar{W} - \frac{1}{V} \int_{\delta(V)_p} u_i \sigma_{ij} n_j \, dA, \tag{8}$$

where $\delta(V)_p$ denotes the part of $\delta(V)$ where the stress is prescribed. It is readily shown, using the divergens theorem once more, that

$$\psi = -\frac{1}{2} \bar{\sigma}_{ij} \bar{\varepsilon}_{ij} \qquad \text{given (1)}, \tag{9}$$

$$\psi = \frac{1}{2} \bar{\sigma}_{ij} \bar{\varepsilon}_{ij} \qquad \text{given (2)}. \tag{10}$$

The stiffness and compliance of the composite material are in general defined by

$$\left.\begin{aligned} \bar{\sigma}_{ij} &= L_{ijkl} \bar{\varepsilon}_{kl} \\ \bar{\varepsilon}_{ij} &= M_{ijkl} \bar{\sigma}_{kl} \end{aligned}\right\} \quad \text{given (1) or (2)} \qquad \begin{matrix} (11) \\ (12) \end{matrix}$$

where $L_{ijkl} = M^{-1}_{ijkl}$.

We will not go into details about the determination of L_{ijkl} or M_{ijkl} just mention that there exists a whole class of solutions which are based on eq. (5) and (6) and on the solution for an ellipsoidal inclusion embedded in an infinite matrix. Non-dilute concentrations of ellipsoidal voids or cracks can e.g. be dealt with using Levin's method, [21] and [22].

The solution for the compliance, obtained by using Levin's method, can in general be written as

$$M_{ijkl} = M^m_{ijkl} + \beta \, H_{ijmn} \, M^m_{mnkl} \, , \tag{13}$$

where superscript 'm' refers to the matrix material, and β is a scalar which describes the crack density or the volume concentration of the voids, and where H_{ijkl} is a fourth order tensor. We will consider three cases here:

(i) Aligned, penny-shaped cracks: Here β is given by

$$\beta = \frac{4\pi}{3} n a^3 \tag{14}$$

where n is the number of cracks per volume and a is the crack radius. The tensor H_{ijkl} is transversely isotropic. The explicit expression is given in Appendix 1.

(ii) Randomly distributed penny-shaped cracks: Here β is again given by eq. (14), but H_{ijkl} is now isotropic. An expression is given in Appendix 2.

(iii) Spherical voids: Here β is given by

$$\beta = \frac{c}{1-c} \tag{15}$$

where c denotes the volume concentration of the voids. The H-tensor is again isotropic and an expression is given in Appendix 3.

Note, finally, that with the composite material compliance given by eq. (13), the corresponding stiffness is given by

$$L_{ijkl} = L_{ijmn} R_{mnkl} , \tag{16}$$

with

$$R^{-1}_{ijkl} = I_{ijkl} + \beta H_{ijkl} , \tag{17}$$

where I_{ijkl} denotes the fourth order identity tensor.

A completely different approach to the determination of composite material stiffness and compliance is the composite material element approach. In this approach the stiffness/compliance of a single inhomogenity surrounded by a suitable amount of matrix material is determined by subjecting this material element to appropriate bound-

ary conditions. Finally, the stiffness/compliance of the composite material element is equated with the stiffness/compliance of the composite material as a whole.

Using this approach the 1D axial compliance of a fibre reinforced composite material containing unidirectional infinitely long fibres and transverse matrix cracks along with fibre/matrix debonding has been determined. The solution can be written as ($\bar{\varepsilon}$, M, and $\bar{\sigma}$ denoting scarlars):

$$\bar{\varepsilon} = M\,\bar{\sigma} \ , \tag{18}$$

with

$$M = 2\left(1 + \frac{b}{t}\right)\frac{nt}{E^f}\left\{\left(\frac{\ell}{t}\ \frac{\tanh\lambda\ell}{\lambda\ell} + \frac{E^f}{E^m}\ \frac{\ell}{b}\right)\frac{bE^m}{tE^f + bE^m} + \frac{d}{t}\right\}, \tag{19}$$

where b denotes matrix thickness, t fibre thickness, ℓ length of non-debonded interface, and d length of debonded interface. See also fig. 1. E^f and E^m denote Young's modulus for the fibres and the matrix respectively, and n denotes the number of transverse cracks per length of the fibre. Given n and d where

$$d \leq \frac{1}{2n} \ , \tag{20}$$

we have

$$\ell = \frac{1}{2n} - d \ , \tag{21}$$

and $\lambda\ell$ is determined according to

$$(\lambda\ell)^2 = \frac{3}{2}\frac{\ell^2}{tb}\frac{tE^f + bE^m}{bE^f(1+\nu^m) + tE^m(1+\nu^f)} \ . \tag{22}$$

Here ν^m and ν^f denotes Poisson's ratio for the matrix and the fibres, respectively. The ratio b/t describes the volume concentration of the fibres since

$$\frac{t}{b+t} = c^f \ . \tag{23}$$

Once M has been determined, the stiffness of the composite material can be determined from

$$L = \frac{1}{M} \quad . \tag{24}$$

The solution (19) has been derived by means of a shear lag type of analysis. The derivation is outlined in Appendix 4.

Note, finally, that eq. (18) is the one-dimensional equivalent to eq. (12). It is clear that there exist one-dimensional equivalents to eqs. (1) - (11) as well.

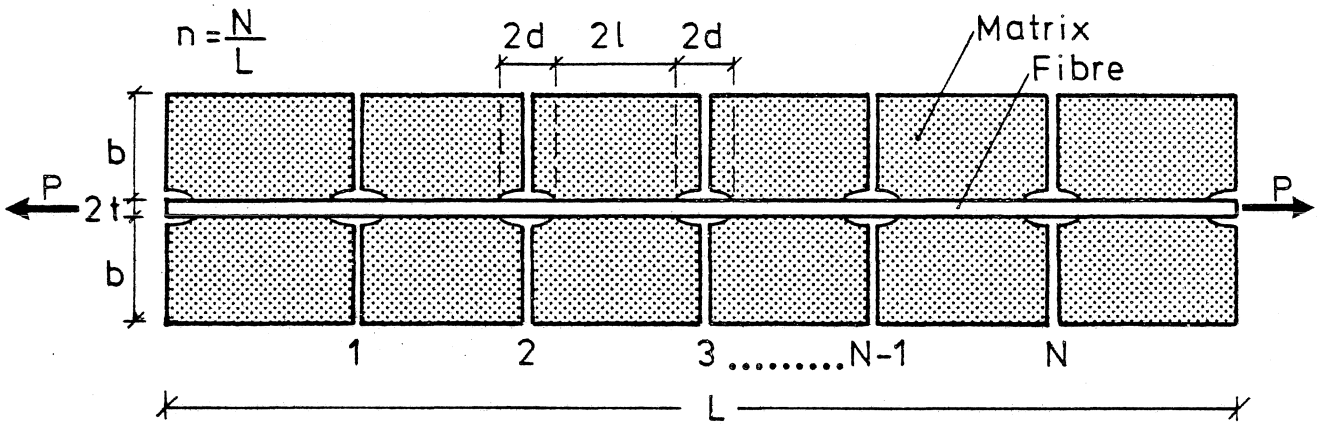

Fig. 1. The composite material element representing the fibre reinforced material with matrix cracks and fibre/matrix debonding.

THE CDM - APPROACH

In the previous section some expressions for the determination of the stiffness and compliance of different materials with voids or cracks are given, along with an expression for the free energy density related to the volume element under consideration. The expression for the free energy density depends on the type of boundary conditions prescribed to the RVE.

In terms of damage description the 3D - material with voids or cracks are described by a non-dimensional damage parameter β which can be split into two non-dimensional damage parameters α_1, α_2. In the case of penny-shaped cracks we would get

$$\beta = \alpha_1 \alpha_2 \ , \tag{25}$$

and in the case of spherical voids we would get

$$\beta = \frac{\alpha_1 \alpha_2}{1 - \alpha_1 \alpha_2} \ , \qquad \alpha_1 \alpha_2 < 1 \ , \tag{26}$$

where in both cases

$$\alpha_1 = (k)^3 n \ , \tag{27}$$

$$\alpha_2 = \frac{4\pi}{3} \left(\frac{a}{k}\right)^3 \ , \tag{28}$$

where k is a characteristic length and a denotes the radius of either crack or void.

The damage of the fibre reinforced material was described by two damage parameters, n, number of cracks per length, and d, length of the debonded fibre/matrix zone. Dimensionless versions of these parameters are easily introduced by writing

$$\alpha_1 = \frac{d}{t} \ , \tag{29}$$

$$\alpha_2 = n \cdot t \ . \tag{30}$$

(See eq. (19)).

Assuming that α_1 and α_2 are independent internal variables, a thermodynamic force A_γ can be defined as

$$A_\gamma = - \frac{\partial \psi}{\partial \alpha_\gamma} \ , \qquad \gamma = 1, 2 \ . \tag{31}$$

This thermodynamic force can be interpreted as a 2D energy release rate.

With the 3D composite material theory the damage force can be written as

$$A_\gamma = \frac{1}{2} \frac{\partial \beta}{\partial \alpha_\gamma} \Sigma_{ij} H_{ijmn} M^m_{mnkl} \Sigma_{kl} \ , \qquad \gamma = 1, 2 \ , \tag{32}$$

given the boundary condition (1), or as

$$A_\gamma = -\frac{1}{2} E_{ij} L_{ijmn} \left(\frac{\partial R}{\partial \alpha_\gamma}\right)_{mnkl} E_{kl} , \qquad \gamma = 1, 2 , \tag{33}$$

given the boundary condition (2).

Similar expressions can be given for A_γ in the case of the one-dimensional description of the fibre reinforced composite material:

$$A_\gamma = \frac{1}{2} \Sigma^2 \frac{\partial M}{\partial \alpha_\gamma} , \tag{34}$$

when a macroscopic stress Σ is prescribed, or

$$A_\gamma = -\frac{1}{2} E^2 \frac{\partial L}{\partial \alpha_\gamma} , \tag{35}$$

when a macroscopic strain E is prescribed.

The last step in the CDM-approach is to define a damage evolution law. We chose here the simplest possible, the socalled brittle law.

For a given (admissible) damage state, α_γ, admissible strain or stress states are defined by a constant positive scalar function f, such that

$$f(A_\gamma) \leq 1. \tag{36}$$

Furthermore, we assume that damage growth follows an evolution law which can be written as

$$d\alpha_\gamma = (0, 0) \quad \text{when} \quad f(A_\gamma) < 1 \tag{37a}$$

$$d\alpha_\gamma = (0, 0) \quad \text{when} \left\{ \begin{array}{l} f(A_\gamma) = 1 \\ \dfrac{\partial f}{\partial E_{ij}} dE_{ij} \leq 0 \quad \text{or} \quad \dfrac{\partial f}{\partial \Sigma_{ij}} d\Sigma_{ij} \leq 0 \end{array} \right. \tag{37b}$$

$$d\alpha_\gamma = \delta \frac{\partial f}{\partial A_\gamma} \quad \text{when} \left\{ \begin{array}{l} f(A_\gamma) = 1 \\ \dfrac{\partial f}{\partial E_{ij}} dE_{ij} > 0 \quad \text{or} \quad \dfrac{\partial f}{\partial \Sigma_{ij}} d\Sigma_{ij} > 0 \end{array} \right. \tag{37c}$$

depending on the boundary conditions. In eq. (37c) δ is given by

$$\delta = \left(\frac{\partial f}{\partial \alpha_\gamma}\,\frac{\partial f}{\partial A_\gamma}\right)^{-1}\left(-\frac{\partial f}{\partial \Sigma_{ij}}\,d\Sigma_{ij}\right), \tag{38a}$$

$$\delta = \left(\frac{\partial f}{\partial \alpha_\gamma}\,\frac{\partial f}{\partial A_\gamma}\right)^{-1}\left(-\frac{\partial f}{\partial E_{ij}}\,dE_{ij}\right), \tag{38b}$$

depending on the prescribed boundary condition. Strictly speaking eqs. (37) and (38) apply to the 3D case. In our 1D case the last term on the right hand side is simplified since the indices i,j vanish.

We are now, in principle, ready to model any stress - strain history and investigate the influence of damage description and evolution laws. We can e.g. start with some initial damage state (α_1, α_2) (which might be (0, 0)), and then strain the RVE. At some point in the load history we will reach $f = 1$ and the damage evolution will start. Additional straining will result in damage evolution such that $f \equiv 1$ according to eq. (38b). The direction (in the $\alpha_1\ \alpha_2$ - plane) in which the damage takes place depends on the initial damage state and the f-function according to eq. (37c).

Results are most easily obtained by using a numerical scheme which models the load history by means of incremental steps. Note in this connection that if the damage evolution results in a descending stress-strain curve, then the load history must be described in terms of strain and not stress, in other words δ must be positive.

SOME EXAMPLES

To illustrate the method described above, we have prescribed a uniaxial tensile strain field to a RVE containing spherical voids, randomly distributed, penny-shaped cracks, or penny-shaped cracks aligned so that the crack surfaces are perpendicular to the strain field.

As f-function we have chosen a "super ellipsoid"

$$f(A_\gamma) = \left(\frac{A_1}{A_{1\,crit}}\right)^3 + \left(\frac{A_2}{A_{2\,crit}}\right)^3, \tag{39}$$

where A_1^{crit}, A_2^{crit} are constants. Writing $\left(A_1^{crit}, A_2^{crit}\right)$ as

$$\left(A_1^{crit}, A_2^{crit}\right) = A^{crit}(1, g) = A^{crit}\,\vec{g}\ , \qquad (40)$$

we can say that A^{crit} describes the overall critical energy level and g (or $\vec{g}$) describes the difference in the energy levels related to the two damage modes. Following this line of thinking, we can think of the f-function as a description of the interaction of the damage modes.

In fig. 2 to fig. 4 we have outlined the influence of the initial damage vector given the damage description and the f-function; furthermore, the influence of the f-function given the damage description and the initial damage and, finally, the influence of the damage description given the f-function and the initial damage.

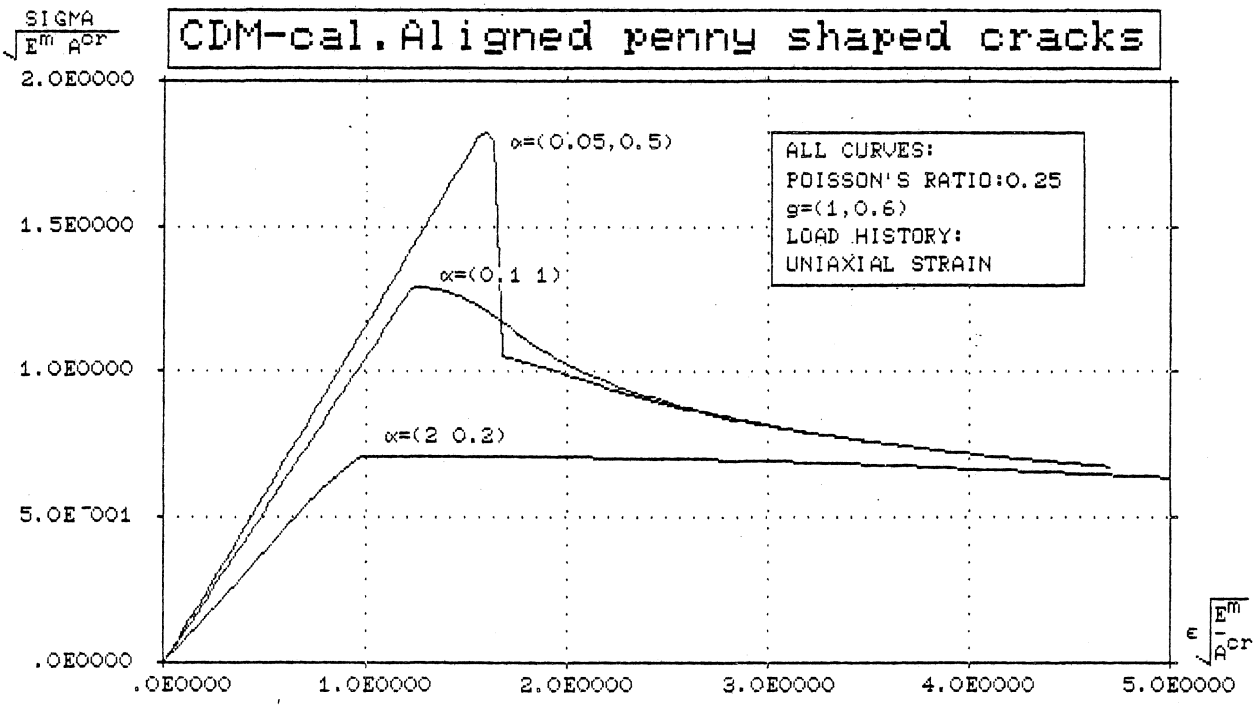

Fig. 2. CDM - calculation of material containing aligned penny-shaped cracks. Effect of initial damage.

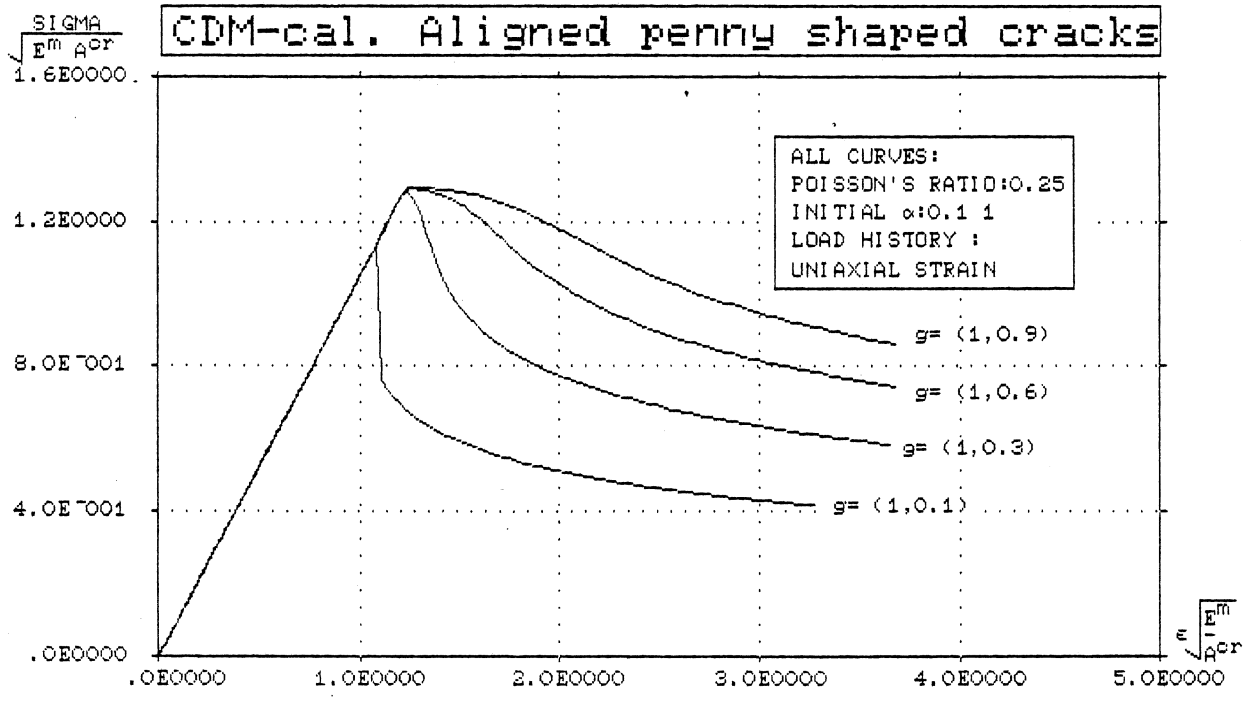

Fig. 3. CDM - calculation of material containing aligned penny-shaped cracks. Effect of f-function (in terms of g).

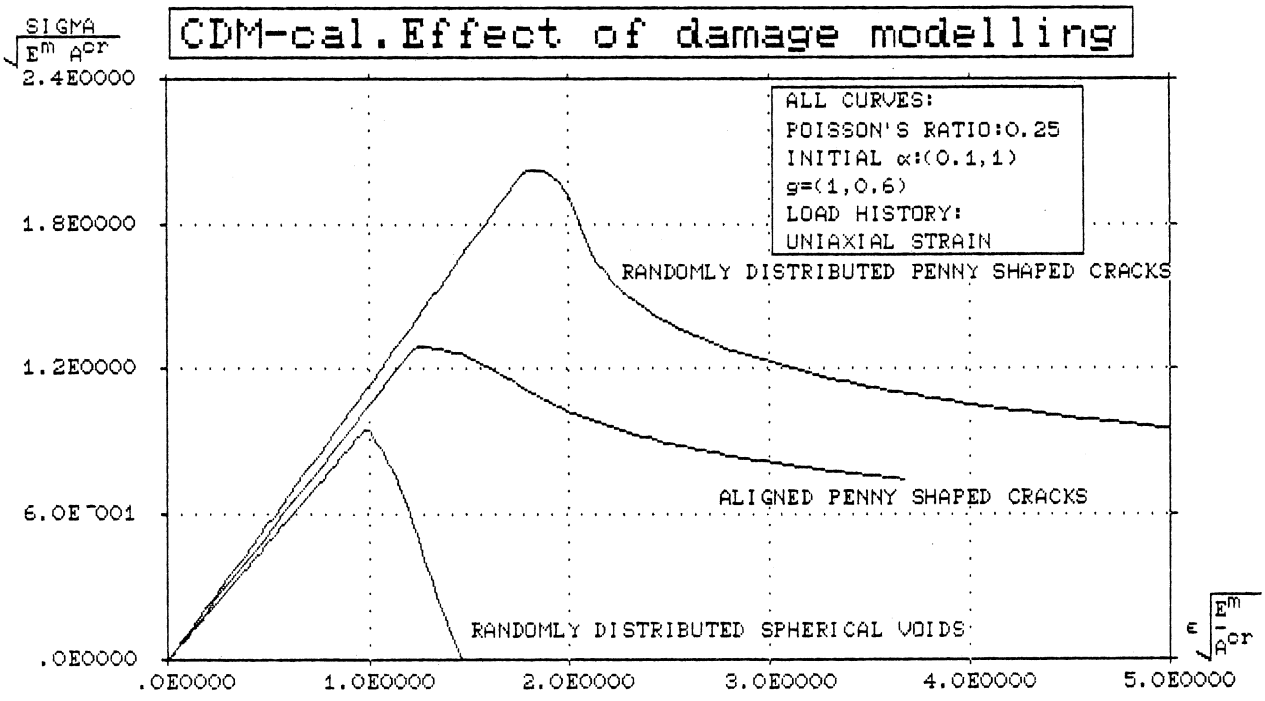

Fig. 4. CDM - calculation of material containing damage modelled by spheres, or aligned or randomly distributed penny-shaped cracks.

In fig. 5 we have shown some experimental results for strain softening in tension by Balavadze (shown in [24]) and Hughes and Chapman [25]. We can see that some of the theoretical curves resemble the experimental ones a great deal, however, the validity of such a comparison depends heavily on the degree of homogenity of the stress/strain fields in the test specimens.

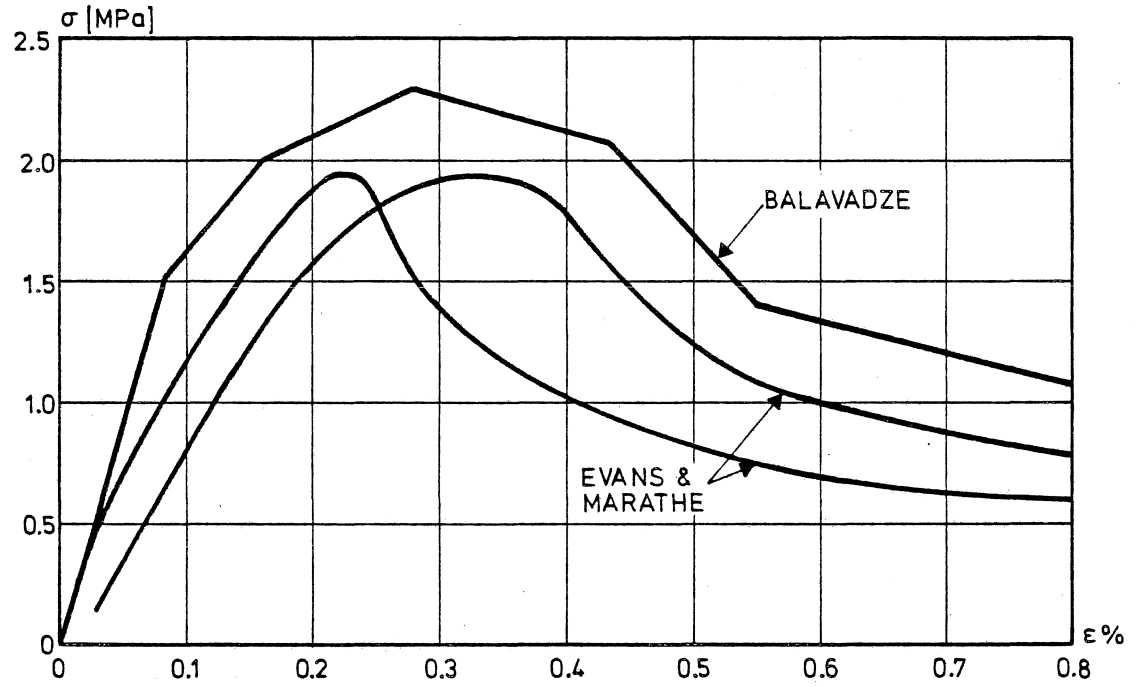

Fig. 5. Experimental results for concrete in tension.

We have also shown some theoretical stress/strain curves for the fibre reinforced composite material, see fig. 6. In this case we have used

$$f = \left(\frac{A_1}{A_1^{crit}}\right)^2 + \left(\frac{A_2}{A_2^{crit}}\right)^2 , \tag{41}$$

with

$$\left(A_1^{crit}, A_2^{crit}\right) = A^{crit}(1, \infty) \quad , \tag{42}$$

thus we have eliminated the fibre debonding damage mode.

The material parameters used in fig. 6 correspond to a polypropylene fibre reinforced cement matrix. Some experimental results for such a material consisting of infinitely long uniaxial pp-fibres in a cement matrix subjected to uniaxial tension is also shown in fig. 6 and we observe a nice agreement. Note in this connection that the only curve fitting parameters that we used are A^{crit} and the initial damage state, and note also that all the theoretical curves have been determined using the same value for A^{crit}.

Finally, it should be noted that the experiments clearly showed that the damage in the test specimens was homogeneous. It was not possible to detect any visible cracks even at 1.5% strain, thus it is reasonable to assume that the nonlinear effects are due to microcrack nucleation as assumed in the theoretical model.

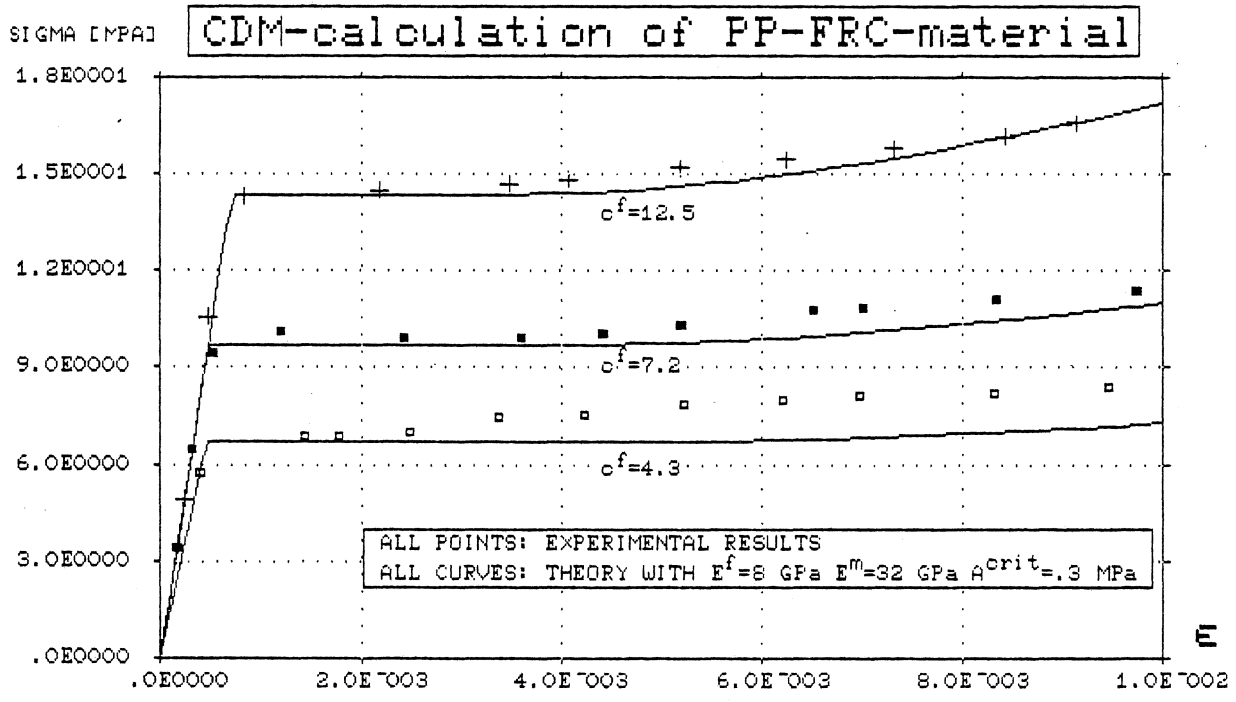

Fig. 6. FRC - material, CDM - curves and experimental results.

REFERENCES

[1] H.E. Read and G.A. Hegemier. Strain softening of rock, soil and concrete - A review article. Mech. of Mater., 3, 271-294, (1984).

[2] S. Ziegeldorf. Phenomenological aspects of the fracture of concrete. In Fracture Mechanics of Concrete, ed. F.H. Wittmann. Elsevier Science Publishers, Amsterdam, pp. 31-41, (1983).

[3] A. Hillerborg, M. Modéer, and P.-E. Petersson. Analysis of crack formation and crack growth by means of fracture mechanics and finite elements. Cement and Concrete Research, 6, 773-781, (1976).

[4] A. Hillerborg. Analysis of fracture by means of the fictitious crack model, particularly for fibre reinforced concrete. The Int. J. Cement Comp., 2, 177-184, (1980).

[5] P.-E. Petersson. Crack growth and development of fracture zones in plain concrete and similar materials. Division of Building Materials, Lund Institute of Technology. Report TVBM-1006. (1981).

[6] P.J. Gustafsson. Fracture mechanics studies of non-yielding materials like concrete: Modelling of Tensile Fracture and Applied Strength Analysis. Division of Building Materials, Lund Institute of Technology. Report TVBM-1007. (1985).

[7] Z.P. Bažant and B.H. Oh. Rock fracture via strain-softening finite elements. J. Eng. Mech., 110. 1015-1035. (1984).

[8] Z.P. Bažant and B.H. Oh. Microplane model for progressive fracture of concrete and rock. J. Eng. Mech., 111, 559-582. (1985).

[9] Z.P. Bažant. Mechanics of distributed cracking. Appl. Mech. Rev., 39, 675-705. (1986).

[10] L.S. Costin. A microcrak model for the deformation and failure of brittle rock. J. Geophys. Res., 88, 9485-. (1983).

[11] L.S. Costin. Damage mechanics in the post-failure regime. Mech. of Mater., 4, 149-160. (1985).

[12] D. Krajcinovic. Constitutive Equations for Damaging Materials. J. Appl. Mech., 50, 335-360. (1983).

[13] D. Krajcinovic. Continuum Damage Mechanics. Appl. Mech. Rev., 37, 1-6. (1984).

[14] D. Krajcinovic. Continuous Damage Mechanics Revisited: Basic Concepts and Definitions. J. Appl. Mech., 52, 829-834. (1985).

[15] J.J. Marigo. Modelling of brittle and fatigue damage for elastic material by growth of microvoids. Eng. Frac. Mech., 21, 861-875. (1985).

[16] F. Sidorff. Damage mechanics and its application to composite materials. In Mechanical characterization of load bearing fibre composite laminates, eds. A.H. Cardon and G. Verchery. Elsevier Applied Science Publishers. pp. 21-35. (1985).

[17] Z. Hashin. Analysis of Composite Materials. - A Survey. J. Appl. Mech., 50, 481-505. (1983)

[18] L.J. Walpole. Elastic behavior of composite materials: Theoretical foundations. Adv. Appl. Mech., 21, 169-242. (1981).

[19] R.M. Christensen. Mechanics of Composite Materials. A Wiley-Interscience Publication, John Wiley and Sons. (1979).

[20] R. Hill. Elastic properties of reinforced solids: Some theoretical principles. J. Mech. Phys. Solids, 11, 357-372. (1963).

[21] V.M. Levin. Determination of effective elastic moduli of composite materials. Dokl. Akad. Nauk SSSR, 220, 1042-1045, (1975). (Sov. Phys. Dokl., 20. 147-148, 1975).

[22] H. Stang. Strength of composite materials with small cracks in the matrix. Accepted for publication in Int. J. Solids Struc. (1986).

[23] R. Hill. Continuum micro-mechanics of elastoplastic polycrystals. J. Mech. Phys. Solids, 13, 89-101. (1965).

[24] J. Kasperkiewicz. Fracture and crack propagation energy in plain concrete. Heron, 31, 5-14. (1986).

[25] B.P. Hughes and G.P. Chapman. The complete stress-strain curve for concrete in direct tension. RILEM Bulletin, No. 30, 95-97. (1966).

APPENDIX 1

In the case of unidirectional penny-shaped cracks the H-tensor is transversely isotropic and given by the following expression:

$$H_{ijkl} = \frac{4}{\pi}\left[\frac{(1-\nu^m)^2}{(1-2\nu^m)} D^2_{ijkl} + \frac{(1-\nu^m)}{(2-\nu^m)} D^4_{ijkl} + \frac{(1-\nu^m)\nu^m}{(1-2\nu^m)} D^5_{ijkl}\right], \tag{A.1.1}$$

where ν^m denotes Poisson's ratio for the matrix material and where D^2_{ijkl}, D^4_{ijkl}, and D^5_{ijkl} are three of the six transversely isotropic elementary tensors given by Walpole, see e.g. [18]. (Denoted E^2_{ijkl}, E^4_{ijkl}, and E^5_{ijkl} by Walpole).

APPENDIX 2

In the case of randomly distributed penny-shaped cracks the H-tensor is isotropic and given by the following expression:

$$H_{ijkl} = \frac{4}{3\pi} \frac{(1-(\nu^m)^2)}{(1-2\nu^m)} J_{ijkl} + \frac{8}{15\pi} \frac{(1-\nu^o)(5-\nu^o)}{(2-\nu^o)} K_{ijkl}, \tag{A.2.1}$$

where ν^m denotes Poisson's ratio for the matrix material and

where J_{ijkl} and K_{ijkl} are the two isotropic elementary tensors given by Hill [23].

APPENDIX 3

In the case of isotropically dispersed spherical voids the H-tensor is isotropic and given by:

$$H_{ijkl} = \frac{3}{2} \frac{(1 - \nu^m)}{(1 - 2\nu^m)} J_{ijkl} + 15 \frac{(1 - \nu^m)}{(7 - 5\nu^m)} K_{ijkl} , \qquad (A.3.1)$$

where ν^m is Poisson's ratio for the matrix material and J_{ijkl} and K_{ijkl} are the isotropic elementary tensors mentioned in Appendix 2.

APPENDIX 4

First the compliance of the single composite material element shown in fig. 7 will be determined.

The behavior of the element is described by the following equations:

$$\frac{p^m_{,x}}{2} - \tau^i = 0 , \qquad (A.4.1)$$

$$\frac{p^f_{,x}}{2} + \tau^i = 0 , \qquad (A.4.2)$$

$$\frac{p^m}{2b} = E^m \varepsilon^m_x , \qquad (A.4.3)$$

$$\frac{p^f}{2t} = E^f \varepsilon^f_x , \qquad (A.4.4)$$

$$\tau^i = \varphi(u^m - u^f) , \qquad (A.4.5)$$

$$\varepsilon^m_x = u^m_{,x} , \qquad (A.4.6)$$

$$\varepsilon^f_y = u^f_{,x} , \qquad (A.4.7)$$

where

$$\frac{P^f}{2} = \int_o^t \sigma_x \, dy \ , \tag{A.4.8}$$

$$\frac{P^m}{2} = \int_t^b \sigma_x \, dy \ , \tag{A.4.9}$$

and where superscripts m, f, and i refer to the matrix, the fibre and the interface, respectively.

The factor φ is determined by assuming a 2. order variation in the y-direction in the axial displacements u, and by identifying u^m and u^f with the following mean values of the displacement field:

$$u^f = \frac{1}{t}\int_o^t u \, dy \ , \tag{A.4.10}$$

$$u^m = \frac{1}{b}\int_t^b u \, dy \ . \tag{A.4.11}$$

Furthermore, the boundary conditions $\tau_{y=0} = 0$, $\tau_{y=t} = \tau^i$ and $\tau_{y=b+t} = 0$ are fulfilled.
We get

$$\varphi = \frac{3G^m \, G^f}{b\,G^f + t\,G^m} \ . \tag{A.4.12}$$

Now we can solve for u^f, and using the boundary conditions $P^m(\ell) = 0$, $P^f(\ell) = P$, $u^m(0) = 0$, $u^f(0) = 0$, along wiht the condition $P^m + P^f = P$, we get

$$u^f(x) = P\left\{ \frac{\tanh(\lambda x)}{E^f \, 2t \, \lambda} + \frac{x}{E^m \, 2b} \right\} \frac{E^m b}{E^f t + E^m b} \ , \tag{A.4.13}$$

where λ is given in eq. (22).

Thus the compliance, c for the single element is given by

$$c(\ell) = \frac{2u^f(\ell)}{P} \ . \tag{A.4.14}$$

The compliance, C, for the multicracked element shown in fig. 1 can then be written as

$$C = N \left\{ c(\ell) + \frac{d}{E^f t} \right\}_{\ell = \frac{1}{2n} - d} , \qquad (A.4.15)$$

where N is the total number of cracks (elements) and where $n = N/L$. Thus the stiffness of the multicracked composite material element is given by

$$L = M^{-1} , \qquad (A.4.16)$$

where

$$M = 2(b + t)n \left\{ c(\ell) + \frac{d}{E^f t} \right\}_{\ell = \frac{1}{2n} - d} . \qquad (A.4.17)$$

The solution is valid for

$$d < \frac{1}{2n} . \qquad (A.4.18)$$

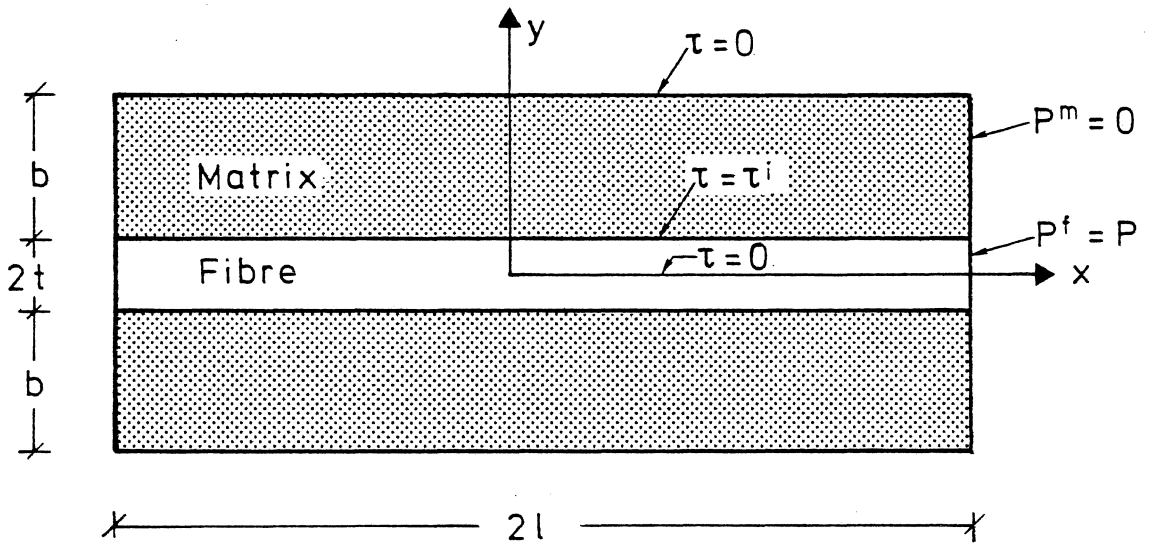

Fig. 7. The basic composite material element.

FRACTURE MECHANICS AND DIMENSIONAL ANALYSIS FOR CONCRETE STRUCTURES

N. A. Harder
Institute of Building Technology and Structural Engineering
University of Aalborg
Denmark

SUMMARY
It is shown how some results obtained by dimensional analysis can be used to check a new fracture mechanical theory »the fictitious crack model» and to determine an optimal linear σ-w relation to be applied in this theory.

INTRODUCTION

It is well known that a small-scale model of a concrete beam is comparatively stronger than a similar full-scale beam. In [2] Hillerborg, using a new fracture mechanical model »the fictitious crack model», has shown in a qualitative way, why it must be so. In the present paper the same aspect is discussed in a more quantitative way applying dimensional analysis.

Among other things, the role of the brittleness modulus is explained in a new way. I.e. one of the model laws from dimensional analysis says that the model must have the same brittleness modulus as the prototype. As this, however, cannot be achieved, it is shown how to find a correction factor to the model law giving the ultimate load of the prototype determined from a small-scale model test. At last it is shown how the result from this dimensional analysis can be used to determine an optimal linear σ-w relation to be used in the fictitious crack method.

FRACTURE-MECHANICAL RELATIONS

In the present paper use will be made of some relations from linear fracture mechanics [6] summarized as follows.

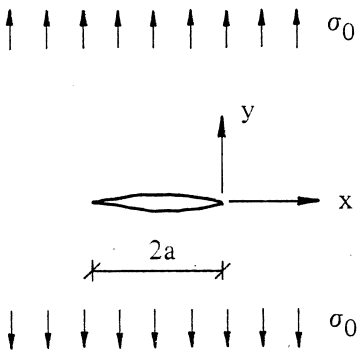

Figure 1.

The simplest problem dealt with in linear fracture mechanics is that illustrated in figure 1 showing a crack of length 2a in a medium under uniform tension σ_0.

The condition for the crack to be stable is

$$\sigma_0 < \sigma_c = \frac{\sqrt{EG_c}}{\sqrt{\pi a}}$$

For other stress-fields than uniform tension the inequality can be written

$$\sigma_0 < \sigma_c = \frac{\sqrt{EG_c}}{\theta\sqrt{a}} \tag{1}$$

As an approximation $\theta = 2$ can be used in general for small cracks, but for long cracks θ may be much greater [3]. E is the modulus of elasticity and G_c is the potential energy release per created one-sided new crack area for $\sigma_0 = \sigma_c$. In linear fracture mechanics G_c is the same as the fracture energy, G_F being the energy dissipation per created one-sided new crack area. G_F is assumed to be a material property. σ_c is the critical value of σ_0.

The condition that the crack will be stable up to the stress $\sigma_0 = \sigma_u$, σ_u being the ultimate tensile stress, is

$$\sigma_u < \sigma_c = \frac{\sqrt{EG_F}}{\theta\sqrt{a}} \tag{2}$$

or

$$a < a_c = \frac{EG_F}{\theta^2\sigma_u^2} = \frac{\ell_c}{\theta^2} \tag{3}$$

$$\ell_c = \frac{EG_F}{\sigma_u^2} \tag{4}$$

where a_c is the critical crack length and ℓ_c is called the characteristic length of the material. ℓ_c can be used instead of G_F as a fracture mechanical material property.

In general, one speaks of a ductile fracture (assuming σ_u is a yield stress) if $a < a_c$, and a brittle fracture, i.e. crack-instability, if $a_c < a$. (3) can also be written

$$B = \frac{a}{\ell_c} < B_c = \frac{1}{\theta^2}$$

where B is the brittleness modulus for a material with small internal cracks as in figure 1. B_c is called the critical brittleness modulus. For $B < B_c$ the fracture is ductile. For $B_c < B$ the fracture is brittle, and for $B = B_c$ the fracture is brittle and ductile at the same time.

THE BRITTLENESS MODULUS

The brittleness modulus for a structural element is defined as

$$B = \frac{\ell}{\ell_c}$$

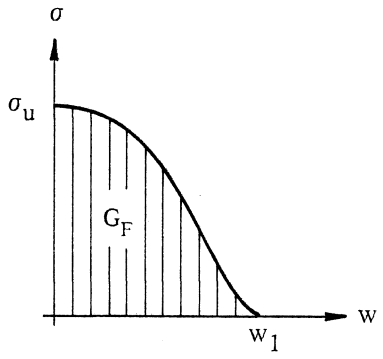

Figure 2.

where ℓ is a typical length. All similar elements have the same critical brittleness modulus B_c which can be determined by putting the ultimate load at yielding equal to the ultimate load at crack instability [6].

THE FICTITIOUS CRACK MODEL

In this model it is assumed that yielding does not take place beyond a very narrow zone called the fracture zone or the fictitious crack. In the fracture zone the constitutive relation between the tensile stress σ and the opening w of the fictitious crack is defined by a σ-w relation as shown in figure 2, [2].

Hence, the area under the σ-w curve is the fracture energy G_F. In a way this provides a connection between the linear fracture mechanics and the fictitious crack model.

DIMENSIONAL ANALYSIS

Consider a linear elastic body with or without initial cracks and under a process of deformation. The loads consist of constant loads p, q, r multiplied by a load factor γ, ranging from zero to γ_u at ultimate load. γ_u can be written as a function

$$\gamma_u = \gamma_u(p, q, r, u, \ell, a, \ell_c, E, \nu, \sigma_u)$$

Taking force (F) and length (L) as fundamental dimensions, the dimensions of the parameters being the arguments of the function are as follows:

- p a concentrated force: F
- q a line force: $F \cdot L^{-1}$
- r a surface force: $F \cdot L^{-2}$
- u a prescribed displacement: L
- ℓ a typical length: L
- a length of a crack at the surface of the body or half the length of an internal crack: L
- ℓ_c characteristic length of the material: L
- ν Poissons ratio: Dimensionless
- σ_u ultimate stress: $F \cdot L^{-2}$

It is assumed that the material is linear elastic up to the ultimate stress σ_u, i.e. yielding does not occur. But when a tensile stress σ at a point reaches σ_u, then a new crack starts at this point. Taking p and ℓ as fundamental parameters, the following complete set of dimensionless parameters called π-products [1] is obtained.

$$\pi_\gamma = \gamma \qquad \text{(A)}$$

$$\pi_q = q \cdot \ell \cdot p^{-1} \qquad \text{(B)}$$

$$\pi_r = r \cdot \ell^2 \cdot p^{-1} \qquad \text{(C)}$$

$$\pi_u = u \cdot \ell^{-1} \qquad \text{(D)}$$

$$\pi_a = a \cdot \ell^{-1} \qquad \text{(E)}$$

$$\pi_{\ell_c} = \ell_c \cdot \ell^{-1} \qquad \text{(F)}$$

$$\pi_E = E \cdot \ell^2 \cdot p^{-1} \qquad \text{(G)}$$

$$\pi_\nu = \nu \qquad \text{(H)}$$

$$\pi_{\sigma_u} = \sigma_u \cdot \ell^2 \cdot p^{-1} \qquad \text{(I)}$$

The set of π-products is said to be complete, because the parameters are independent, i.e. no single π-product can be expressed by a product of the other π-products. For the unknown parameter γ_u the following π-product can be formed

$$\pi_{\gamma_u} = \gamma_u \qquad \text{(K)}$$

If all the π-products in the model (index M) are taken as being equal to those of the prototype (index P) the following MODEL LAWS for complete similarity are obtained.

$$\frac{\gamma_P}{\gamma_M} = 1 \qquad \text{(a)}$$

$$\frac{q_P}{q_M} = \left(\frac{\ell_P}{\ell_M}\right)^{-1} \cdot \frac{p_P}{p_M} \qquad \text{(b)}$$

$$\frac{r_P}{r_M} = \left(\frac{\ell_P}{\ell_M}\right)^{-2} \cdot \frac{p_P}{p_M} \qquad \text{(c)}$$

$$\frac{u_P}{u_M} = \frac{\ell_P}{\ell_M} \qquad \text{(d)}$$

$$\frac{a_P}{a_M} = \frac{\ell_P}{\ell_M} \qquad \text{(e)}$$

$$\frac{\ell_{cP}}{\ell_{cM}} = \frac{\ell_P}{\ell_M} \qquad \text{(f)}$$

$$\frac{E_P}{E_M} = \left(\frac{\ell_P}{\ell_M}\right)^{-2} \frac{p_P}{p_M} \qquad (g)$$

$$\frac{\nu_P}{\nu_M} = 1 \qquad (h)$$

$$\frac{\sigma_{uP}}{\sigma_{uM}} = \left(\frac{\ell_P}{\ell_M}\right)^{-2} \frac{p_P}{p_M} \qquad (i)$$

$$\frac{\gamma_{uP}}{\gamma_{uM}} = 1 \qquad (k)$$

The equations (a) to (i) determine the dimensions, the loads, and material parameters in the model. And from γ_{uM} the unknown γ_{uP} is determined from equation (k).

In practice, however, it is not possible to satisfy all equations (a) to (i) at the same time. If the model is made of the same material as the prototype, then it follows from (g) that

$$\frac{p_P}{p_M} = \left(\frac{\ell_P}{\ell_M}\right)^2 \qquad (5)$$

and all model laws can be satisfied except (f) which says

$$B_M = \frac{\ell_M}{\ell_{cM}} = B_P = \frac{\ell_P}{\ell_{cP}} \qquad (6)$$

i.e. the brittleness modulus shall be the same in the model as in the prototype. This, however, cannot be achieved, because when using the same material in the model and the prototye one has

$$B_M = \frac{\ell_M}{\ell_{cM}} = \frac{\ell_M}{\ell_{cP}}$$

instead of, from (6),

$$B_M = B_P = \frac{\ell_P}{\ell_{cP}}$$

Now, using (k), γ_{uP} can be written

$$\gamma_{uP} = g \cdot \gamma_{uM}$$

where the correction factor g can be found by calculations using the fictitious crack model on the following two models:

Model 1
is identical with the physical model and for this model

$$\ell_{cM}^{(1)} = \ell_{cP}$$

which means

$$B_M^{(1)} = \frac{\ell_M}{\ell_{cM}^{(1)}} = \frac{\ell_P}{\ell_{cP}} \cdot \frac{\ell_M}{\ell_P} = B_P \frac{\ell_M}{\ell_P}$$

and all model laws except (f) are satisfied.

Model 2
is a fictitious model being the same as model 1 except for $\ell_{cM}^{(2)}$ being determined from (f):

$$\ell_{cM}^{(2)} = \ell_{cP} \frac{\ell_M}{\ell_P}$$

which means

$$B_M^{(2)} = \frac{\ell_M}{\ell_{cM}^{(2)}} = \frac{\ell_M}{\ell_{cP}} \cdot \frac{\ell_P}{\ell_M} = B_P$$

As all model laws for model 2 are satisfied, it follows from (k) that

$$\gamma_{uP} = \gamma_{uM}^{(2)} = \frac{\gamma_{uM}^{(2)}}{\gamma_{uM}^{(1)}} \gamma_{uM} = g \cdot \gamma_{uM}$$

$$g = \frac{\gamma_{uM}^{(2)}}{\gamma_{uM}^{(1)}}$$

Defining the scale ratio α by

$$\alpha = \frac{\ell_P}{\ell_M} \tag{7}$$

the following relations are obtained

$$\ell_M = \ell_M^{(1)} = \ell_M^{(2)} = \alpha^{-1} \ell_P$$

$$\ell_{cM}^{(1)} = \ell_{cP}$$

$$G_{FM}^{(1)} = G_{FP}$$

$$B_M^{(1)} = \alpha^{-1} B_P$$

$$\ell_{cM}^{(2)} = \alpha^{-1} \ell_{cP}$$

$$G_{FM}^{(2)} = \alpha^{-1} G_{FP}$$

$$B_M^{(2)} = B_P$$

When calculating $\gamma_{uM}^{(1)}$ and $\gamma_{uM}^{(2)}$ using the fictitious crack method, the only difference between model 1 and model 2 is that $w^{(2)} = \alpha^{-1} w^{(1)}$ which follows from $G_{FM}^{(2)} = \alpha^{-1} G_{FM}^{(1)}$. I.e. the σ-w curve for model 2 is affine with that of model 1.

In order to sketch the function $g = g(\alpha)$, a new parameter, THE BRITTLENESS INDEX α_c is defined as follows

$$\alpha_c = \frac{B_P}{B_c} \tag{8}$$

Hence,

$$\alpha_c = \frac{B_P}{B_c} < 1 \Rightarrow B_P = B_M^{(2)} < B_c$$

i.e. model 2 is ductile for $\alpha_c < 1$ and brittle for $1 < \alpha_c$. Furthermore,

$$\alpha_c = \frac{B_P}{B_c} < \alpha \Rightarrow B_M^{(1)} = \alpha^{-1} B_P < B_c$$

i.e. model 1 is ductile for $\alpha_c < \alpha$ and brittle for $\alpha < \alpha_c$. Here, »ductile» and »brittle» do not mean anything more than

ductile: $B < B_c$

brittle: $B_c < B$

and often B_c cannot be determined in the usual way as explained above. However, using (1) from linear fracture mechanics with $G_c = G_F$, one obtains

$$\sigma_{cM}^{(1)} = \frac{\sqrt{EG_{FM}^{(1)}}}{\theta\sqrt{a_M}} = \frac{\sqrt{EG_{FP}}}{\theta\sqrt{\alpha^{-1} a_P}} = \sqrt{\alpha}\ \sigma_{cP} = \frac{\sqrt{\alpha}}{\sqrt{\alpha_c}} \sigma_u \tag{9}$$

$$\sigma_{cM}^{(2)} = \frac{\sqrt{E G_{FM}^{(2)}}}{\theta\sqrt{a_M}} = \frac{\sqrt{E\alpha^{-1} G_{FM}^{(1)}}}{\theta\sqrt{a_M}} = \frac{1}{\sqrt{\alpha}}\,\sigma_{CM}^{(1)} = \frac{1}{\sqrt{\alpha_c}}\,\sigma_u \quad . \tag{10}$$

Now, consider the two cases $\alpha_c < 1$ and $1 < \alpha_c$, separately.

$\alpha_c < 1$:

Model 2 is ductile and assuming $\alpha > 1$, model 1 is ductile. Hence

$$g = \frac{\gamma_{uM}^{(2)}}{\gamma_{uM}^{(1)}} = \frac{\sigma_u}{\sigma_u} = 1$$

$1 < \alpha_c$:

Model 2 is brittle. For $\alpha_c < \alpha$, model 1 is ductile and (10) gives

$$g = \frac{\gamma_{uM}^{(2)}}{\gamma_{uM}^{(1)}} = \frac{\sigma_{cM}^{(2)}}{\sigma_u} = \frac{1}{\sqrt{\alpha_c}} < 1$$

For $\alpha < \alpha_c$, model 1 is brittle and (9) and (10) give

$$g = \frac{\gamma_{uM}^{(2)}}{\gamma_{uM}^{(1)}} = \frac{\sigma_{cM}^{(2)}}{\sigma_{cM}^{(1)}} = \frac{1}{\sqrt{\alpha}}$$

This result is shown in figure 3.

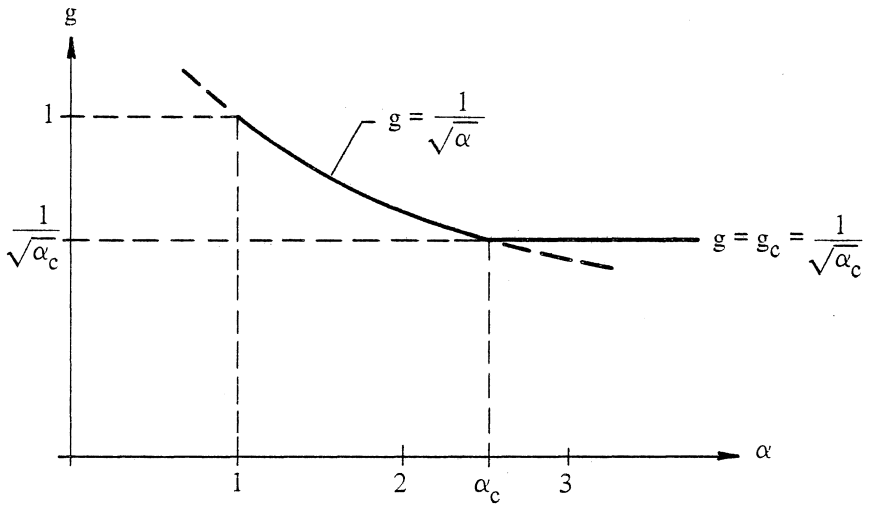

Figure 3.

From figure 3 it is seen that the function $g = g(\alpha)$ in the model law $\gamma_{uP} = g\gamma_{uM}$ is completely determined by the value of the brittleness index α_c.

Although σ_c is the critical value of a stress σ_0 which is often not actually existing it is believed that the result obtained above from (9) and (10) borrowed from the linear fracture mechanics, can be used in the following way: $g = g(\alpha)$, see figure 3, can be determined by calculations using the fictitious crack method. Only a few calculations are necessary because if $g = 1$ for the first trial, then $\alpha_c < 1$ and $g = 1$ for all $1 < \alpha$. Furthermore, if two calculations give the same result $g = g_c < 1$, then from figure 3.

$$\alpha_c = \frac{1}{g_c^2}$$

$$g = \frac{1}{\sqrt{\alpha}} \qquad \text{for } 1 < \alpha \leqslant \alpha_c$$

$$g = g_c = \frac{1}{\sqrt{\alpha_c}} \qquad \text{for } \alpha_c \leqslant \alpha$$

and also the critical brittleness modulus B_c is determined by

$$B_c = \frac{B_P}{\alpha_c} = g_c^2 B_P = g_c^2 \frac{\ell_P}{\ell_{cP}} = g_c^2 \ell_P \frac{\sigma_u^2}{EG_F} \tag{11}$$

AN OPTIMAL LINEAR σ-w RELATION

In order to make a check of the theory g can be calculated for different values of α in the interval $1 < \alpha \leqslant \alpha_c$. Then, provided it is permissible to use (9) and (10) from linear fracture mechanics, the result should be $g = 1/\sqrt{\alpha}$, especially for $\alpha = \alpha_c$ one should obtain $g = 1/\sqrt{\alpha_c}$, and the theory can be checked without making any experiments. Not relying on (9) and (10) the theory can only be checked by making experiments.

If, as an approximation, the σ-w relation is taken to be linear, this relation is determined by the two parameters σ_u and G_F or σ_u and ℓ_c.

σ_u can be determined by a cylinder splitting test and G_F by a 3 point bending test as proposed in [4]. As there are some problems, however, regarding this test [5] it is proposed that the test is made on two similar models with different values of α. The largest model then could be looked upon as the prototype ($\alpha = 1$) and

$$g_1 = \frac{\gamma_u\ (\alpha = 1)}{\gamma_u\ (\alpha > 1)}$$

obtained from the tests could be compared with

$$g_2 = \frac{\gamma_{uM}^{(2)}}{\gamma_{uM}^{(1)}}$$

obtained from calculations.

Then G_F can be adjusted so that the difference between g_1 and g_2 is minimized. In this way no use is made of linear fracture mechanics, only results from dimensional analysis are used to determine G_F.

REFERENCES

[1] Langhaar, H.L., *Dimensional Analysis and Theory of Models,* John Wiley & Sons, 1951.

[2] Hillerborg, A., *A Model of Fracture Analysis,* Division of Building Materials, The Lund Institute of Technology. Report TVBM-3005, 1978.

[3] Hillerborg, A., *Analysis of one single crack.* Chapter 4.1 in Wittman, F.H. (ed.), *Fracture Mechanics of Concrete,* Elsevire, Amsterdam, 1983.

[4] RILEM Draft Recommendation. *Determination of the Fracture Energy of Mortar and Concrete by Means of Three-point Bend Test on Notched Beams.* Materials & Structure, Vol. 18, No. 106, 1985.

[5] Hillerborg, A., *Results of Three Comparative Test Series for Determining the Fracture Energy G_F of Concrete.* Material & Structure, Vol. 18, No. 107, 1985.

[6] Harder, N.A., *Notes on Fracture Mechanics.* Report: R8612 (in Danish). Institute of Building Technology and Structural Engineering, AUC, Aalborg, Denmark, 1986.

TIME-DEPENDENT FRACTURE OF CONCRETE
AN EXPERIMENTAL AND NUMERICAL APPROACH

Einar Aassved Hansen, Norwegian Institute of Technology, Division of Concrete Structures, and SINTEF, Cement and Concrete Research Institute , N-7034 Trondheim-NTH

Matz Modéer, Norwegian Contractors, Holtet 45, N-1320 STABEKK, and Norwegian Institute of Technology, Divison of Concrete Structures, N-7034 Trondheim-NTH

ABSTRACT

The necessity of time-dependent fracture mechanics analyses of concrete failure is pointed out. A proposed numerical method simulating a visco-elastic fracture behaviour is summarized together with future plans. The aim and content of an experimental program regarding the time-dependent behaviour of concrete are given.

INTRODUCTION

Application of fracture mechanics to failure analyses of concrete has led to a better understanding of the concrete failure mechanisms. Mathematical models, which in a more realistic manner simulate the observed behaviour of concrete during failure, have been developed. However, it is not until recently that the influence of time has been incorporated in the models. As the mechanical behaviour of concrete is strongly time-dependent, the fracture process being no exception, this is a major improvement.

In the work presented in this paper the concept of the fictitious crack model (FCM), originally proposed by Hillerborg, Modéer and Petersson /1/, is used. The time-dependent behaviour is taken into account by using visco-elastic crack elements, rather than purely elastic ones. A summary of the numerical method is given together with a description of the experimental work in progress.

NUMERICAL TECHNIQUE

Numerical calculations are needed when failure analyses based on the FCM are carried out. Different solution techniques have been proposed, as the line crack approach and the smeared crack approach (the latter is the crack band theory by Bazant & Oh /2/). Common to both is the use of the finite element method (FEM). In this work the line crack approach is used.

The line crack approach

The fracture of concrete is characterized by strain softening. This is due to micro cracking in advance of the progress of a major crack. In the line crack approach this behaviour is simulated by uniaxial truss elements in the micro cracked zone in front of the major crack. The elements have a negative stiffness (below they are called FCM elements) to account for the decreasing stress transfer with increased deformation. They are introduced in nodes where the tensile strength is reached.

Visco-elastic behaviour

The FCM element behaves like a spring with negative stiffness i.e. it describes an elastic time-independent stress-strain relation. But the concept of the FCM can also be used to describe a time-dependent fracture prosess. This is achieved by letting a visco-elastic equation govern the stress-strain relation in the truss element. In mechanical terms, this is the same as combining springs with dashpots as in rheological models.

Rheological models are used to give a phenomenological description of the actual nature of creep. The creep deformation may consist of a partly reversible visco-elastic movement and possibly also a plastic movement /3/. The visco-elastic movement consists of a purely elastic phase and a purely viscous phase. A viscous deformation is in the same way as a plastic deformation never recovered at unloading. It is always time-dependent and there is always proportionality between the rate of viscous strain and the applied stress at a given time.

Visco-elastic element

A time dependent behaviour can be simulated numerically by prescribing a visco-elastic constitutive equation to a FCM element, on general form written as:

$$u = g(\dot{u}, p, \dot{p}) \qquad (1)$$

where u is the deformation and p the corresponding load in the element, and $\dot{u}$ and $\dot{p}$ their time-derivates.

To test the validity of visco-elastic FCM elements, most existing FEM software have to be modified. In this paper a short review of a numerical solution technique reported by Sönnerlind and Eriksson is given /4/.

In /4/ the following presumptions are made:

- the microcracked zone behaves visco-elastic
- material outside the microcracked zone behaves purely elastic
- the crack path is known in advance
- the crack path follows the element boundaries
- the non-linear crack formation is simulated by uniaxial load and deformation

A substructure technique is used, by which the problem only contains the degrees of freedom that either have external forces or are located along the crack path.

In the FEM model, double nodes are placed along the crack path as if a crack already existed. The model is then analysed with a number of load cases equal to the number of double nodes plus the number of external loads. Each load case is either a unit load in one of the nodes with external force or a pair of unit loads in the two corresponding crack nodes, see Fig 1. This is in accordance with the technique used by Petersson /5/.

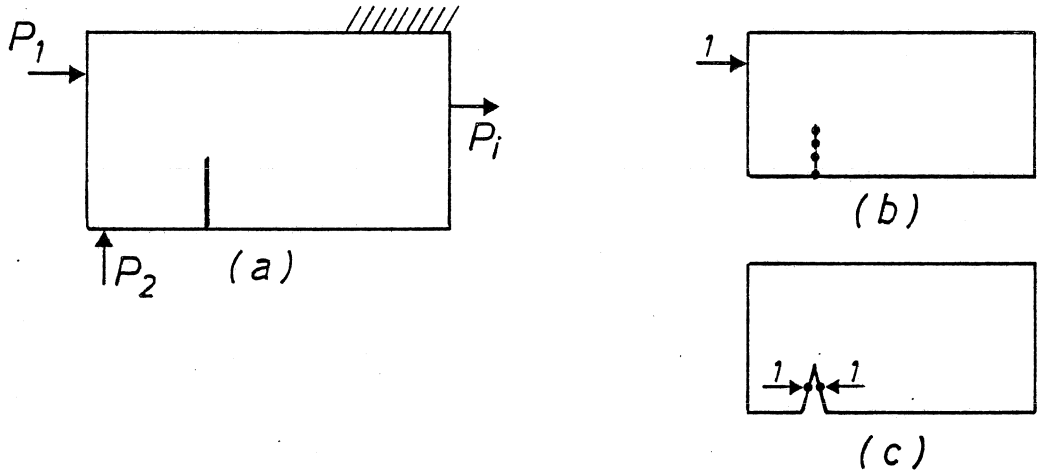

Fig 1. Structure with external forces (a) and examples of load-cases; an unit load in a node with an external force (b) and a pair of unit loads in two corresponding crack nodes (c).

As a result of the analysis with unit loads, it is possible to establish the following relations:

$$\begin{Bmatrix} u_p \\ u_s \end{Bmatrix} = \begin{Bmatrix} A_{pp} & A_{ps} \\ A_{sp} & A_{ss} \end{Bmatrix} \begin{Bmatrix} p_p \\ p_s \end{Bmatrix} \qquad (2)$$

where u_p - displacement in nodes with external forces

u_s - relative displacement between corresponding crack nodes

p_p - external forces

p_s - pair of forces between corresponding crack nodes

and where the content of matrix **A** is the calculated displacements from an analysis with unit loads.

During a complete failure analysis the crack opening will initially be zero. When the tensile strength is reached in one node, it starts separating in two corresponding nodes according to some constitutive visco-elastic equation. If a limiting crack width is reached, no stress will be transferred, and the two corresponding crack nodes behave independently. According to this it is possible to divide $\mathbf{u}_s$ into three different categories and write:

$$\mathbf{u}_s = \begin{Bmatrix} \mathbf{u}_c \\ \mathbf{u}_a \\ \mathbf{u}_o \end{Bmatrix} \begin{matrix} \text{- type 1: "closed"} \\ \text{- type 2: "active"} \\ \text{- type 3: "open"} \end{matrix}$$

If this is introduced into eq (2) and **p** is separated in the same way, **A** can be written as a matrix of 4 x 4 submatrices. Two conditions must be fulfilled i.e. $\mathbf{u}_c = \mathbf{o}$, and the forces corresponding to $\mathbf{u}_o$ equal zero, i.e. $\mathbf{p}_o = \mathbf{o}$. Together with a constitutive equation coupling each element in $\mathbf{u}_a$ and $\mathbf{p}_a$, the problem can then be solved. The analysis is carried out in an iteration loop, and the components in $\mathbf{u}_s$ may change from $\mathbf{u}_c$ through $\mathbf{u}_a$ to $\mathbf{u}_o$ during the iteration.

Visco-elastic concrete element

Results from the test analyses, on a three point bend specimen with five different constitutive equations, showed that the solution technique works without any numerical problems. Therefore, it remains to find a constitutive equation that describes the actual time-dependency of concrete. With such an equation the numerical method can be applied to concrete materials.

EXPERIMENTAL PROGRAM

To get some insight to the time-dependence an experimental program has been started. The results from this progressing work will give input to a first proposal to a visco-elastic equation

governing time-dependent fracture of concrete. The FEM program can then be used to compare analysis with experimental results to further improve the constitutive equation.

The direct scope of the experimental work is to examine the time-dependence of fracture energy and to measure the crack formation rate under constant load. The crack formation will be observed by use of a TV-based holographic technique. As the experimental work is still in progress the results will be presented in a later paper.

Test program

The same concrete mix was used for all specimens. It contains no admixtures, Standard Portland cement (SP4A), crushed aggregate 8/16 mm, and natural sand 0/5 mm. The water-cement ratio is 0.48. The compressive strength at 28 days is approx. 65 MPa.

To produce the desired number of specimens six batches were made. From each of the first three batches, two plates (100 mm x 600 mm x 1200 mm) were cast in a horizontal position. From each of the last three batches, ten beams (100 mm x 100 mm x 1200 mm) were cast in moulds. In addition, from each batch, nine cubes (100 mm x 100 mm x 100 mm) were cast.

The specimens were covered with wet burlaps and a thin polymer folium until demoulding, that took place after about 24 hours. Then the specimens were cured in water at 20°C until the time of testing. At the age of 14 days, five beams (100 mm x 100 mm x 1200 mm) were cut from each of the six plates, as shown in Fig 2.

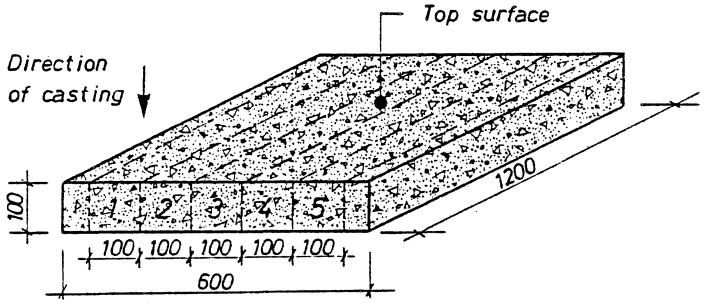

Fig 2. From each plate five beams were cut. Dimensions in mm.

The specimens are going to be tested, according to the test program given in Fig 3. Half the number of them will be tested at the age of 28 days, and the other half at the age of 90 days.

Type of specimen	Number of specimens	Purpose
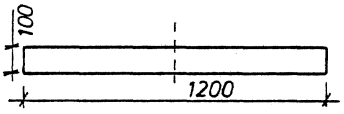	30	Dynamic E-modulus
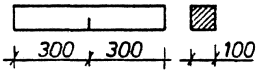	42	Fracture energy Crack width
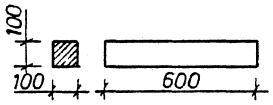	18	Tensile strength and E-modulus
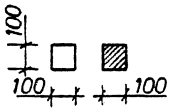	18	Compressive strength

Fig 3. Test program to be carried out on 28 and 90 days old concrete.

First the dynamic E-modulus of the beams is measured. Then the beams are cut in two equally long parts. These shorter beams are used either for determining the tensile strength and the tensile E-modulus, or for fracture energy tests. In the fracture energy specimens a notch, 50 mm deep and 2 mm wide, is sawn in the middle of the 600 mm long beam.

The fracture energy tests are performed in a specially designed fracture energy set-up that does not introduce any gravitational effects on the test results and which has well defined boundary conditions. On some specimens the fracture energy is determined according to normal practice, i.e. at a constant rate of deformation. In this way the maximum load is reached in 1.5-2 minutes. On other specimens the deformation is stopped at a level corresponding to a load below maximum. At this load level

cracks will continue to grow. In order to keep the load constant, the deformation in the direction of the load must be increased. With the test machine used, it is initially possible by control of deformation to keep the load constant within at least 0.1 %. But after a while the damage in the fracture zone is so extensive, that it is no longer possible to maintain a constant load. The test is then continued in a normal manner, i.e. the load will decrease in a stable manner with increased deformation. In this way a fracture energy time-dependence is found. The deformation at the notch mouth, at the notch tip, and 25 mm ahead of the notch tip (in the crack path direction) is measured. This is done in order to see how the fracture zone grows under constant load.

The tensile test is carried out in a set-up for direct tensile strength measurements on prismatic specimens.

CONCLUSIONS

A numerical method, based on the fictitious crack model, is developed. The method makes possible time-dependent failure analyses of an arbitrary material. Crack formation is simulated by visco-elastic crack elements.

The preliminary tests of the FEM program with visco-elastic FCM elements have been successful. It remains to establish a visco-elastic equation, that describes the behaviour of concrete.

REFERENCES

/1/ Hillerborg, A., Modéer, M., Petersson, P.-E., "Analysis of crack growth in concrete by means of fracture mechanics and finite elements", Cement and Concrete Research, Vol 6, 1976, pp 773-782.

/2/ Bazant, Z. P., Oh, B. H., "Crack band theory for fracture of concrete", RILEM, Materiaux et Constructions, Vol 16, No 93, 1983, pp 155-177.

/3/ Neville, A. M., "Properties of concrete", third edition, the Pitman Press, Great Britain, 1981.

/4/ Sönnerlind, H., Eriksson, L., "A method for simulating crack element with arbitrary constitutive properties", restricted report (in Swedish) Stockholm, Sweden, 1986.

/5/ Petersson, P.-E., "Crack growth and development of fracture zones in plain concrete and similar materials", report TVBM-1006, University of Lund, Div. of building materials, Sweden, 1981.

APPLICATION OF FRACTURE MECHANICS IN COMPUTER CALCULATIONS OF MINIMUM REINFORCEMENT IN CONCRETE STRUCTURES SUBJECTED TO RESTRAINED SHRINKAGE

Miroslaw Grzybowski, MSc

Department of Structural Engineering
Royal Institute of Technology
Stockholm
SWEDEN

1. INTRODUCTION

The minima of reinforcement specified in different codes of practice were calculated quite a long time ago, using simple theories. Comparisons between reinforcement minima according to different building codes are made in this paper. Common application of computers and development of numerical methods, particularly Finite Element Method, and the latest achievements in application of Fracture Mechanics to concrete give the possibility of testing those old, not very exact formulas.

In order to specify the minimum reinforcement in the case of a wall subjected to restrained shrinkage computer calculations have been performed. This paper describes these calculations and the theory used in the finite element analysis. The results are discussed.

2. MINIMUM REINFORCEMENT ACCORDING TO DIFFERENT BUILDING CODES AND RESEARCH WORKS

2.1 CODE MODÈLE CEB-FIP 1978 /1/

The conditions for determining the minimum reinforcement area in all cases of loading are proposed in § 15 of CODE MODÈLE. The stress in reinforcement during cracking in concrete should be lower than the yield strength of reinforcement - f_{yk}.
This means that:

$$\rho_{min} = \frac{A_s}{A_{c,ef}} = \frac{f_{ctm}}{f_{yk}} \qquad \text{.....(1)}$$

in which $A_{c,ef}$ is an effective (reduced) area of concrete:

$$A_{c,ef} = A_g \left(\frac{P_{cr}}{P} \right)^3 + n \cdot A_s \cdot \left[1 - \left(\frac{P_{cr}}{P} \right)^3 \right] \qquad \text{.....(2)}$$

f_{ctm} is the mean tensile strength of concrete defined as a function of the compressive strength f_{ck}.

2.2 NORME SIA 162 1983 (SWITZERLAND) /2/

$$\rho_{min} = \frac{A_s}{A_c} = \frac{f_{ct}}{0.7\ f_{yk}} \quad \text{.....(3)}$$

According to this formula, proposed in the Swiss building code, stress in reinforcement is reduced to 70 % of yield strength. This gives greater reinforcement. In cases of massive constructions the cross-sectional area should be reduced to max 200 mm from each surface of the structure.

2.3 BBK 79 (SWEDEN) /3/

$$\rho_{min} = \frac{A_s}{A_{ef}} = \frac{f_{cth}}{f_{st}} \quad \text{.....(4)}$$

in which A_{ef} is an effective area of concrete, Fig. 1.

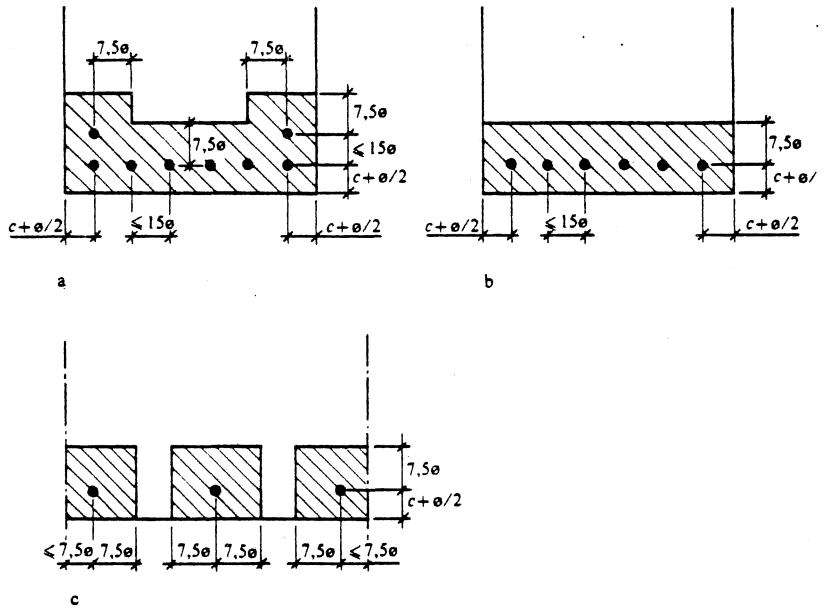

Fig. 1 An effective area of concrete according to the Swedish building code BBK 79.

f_{cth} is defined as 1.5 x f_{ctk}.

2.4 The research report "ARMATURE MINIMALE POUR LE CONTROLE DE LA FISSURATION" - J-P JACCOUD, H CHARIF. LAUSANNE 1985 /4/

$$\rho_{min} = \frac{A_s}{A_{ct}} = \frac{f_{ct,ef}}{f_{yk}/\gamma} = \frac{\eta \cdot f_{ctm}}{f_{yk}/\gamma} \quad \ldots\ldots (5)$$

in which:

A_{ct} - the total area of the cross section

γ - the safety factor, proposed to be 1.2

η - a factor reducing the concrete tensile strength. Schiessl /5/ proposes η between 0.4 and 0.8 depending on the thickness of concrete element, Fig. 2.

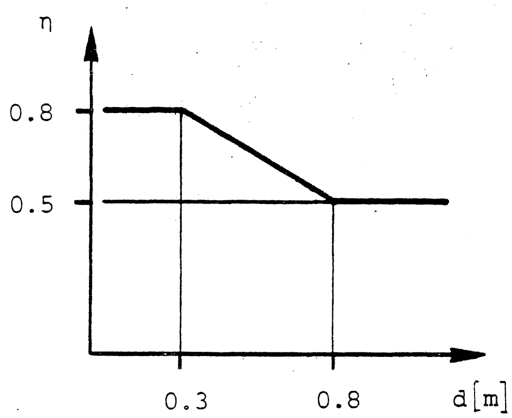

Fig. 2 Factor η reducing the concrete tensile strength.

3. THE MECHANISM OF SHRINKAGE - INDUCED CRACK PROPAGATION IN A CONCRETE WALL

All above mentioned proposals give similar results in cases of not very thick concrete walls, plates and other types of structures. The degree of reinforcement designed in accordance with these methods seems to be too high. Many tests have been done which prove the fact that concrete has lower tensile strength during the forming of the first crack ($f_{ct,o}$), than its usual tensile strength (f_{ctm}). According to the results from the direct tensile tests presented in /4/ and /6/ $f_{ct,o}$ is about 30% lower than f_{ctm}.

Lower concrete tensile strength gives a lower value of the ratio f_{ct}/f_{yk} and an equal relative decrease in the minimum reinforcement area.

There is also anoter factor contributing to decrease of ρ_{min}. The tensile strength is never reached at the whole cross-section of the concrete structure at the same moment. In order to explain this, let's consider our particular structure. This is a very long wall (we assume that it is infinitely long) which stands on a very stiff base e g rock. The wall is drying. Since the length is infinite the shrinkage induced by drying is restrained, which causes tensile stress. As the process of drying continues tensile stresses increase. The stresses are greatest at the surface of the wall and drop to a minimum in the middle. After the peak tensile stress is reached a crack is formed. According to the Fictitious Crack Model (FCM) introduced by Hillerborg in /7/ the tensile stress in concrete doesn't drop to zero. The fictitious crack forms, while it is still able to carry some load, Fig. 3.

As the load (restrained shrinkage) increases the fictitious crack increases in length and width. When the width reaches a limiting value, the stresses drop to zero, and a real crack forms.

Following the process of drying and crack propagation there are different stress distributions through the wall at different times, Fig. 4.

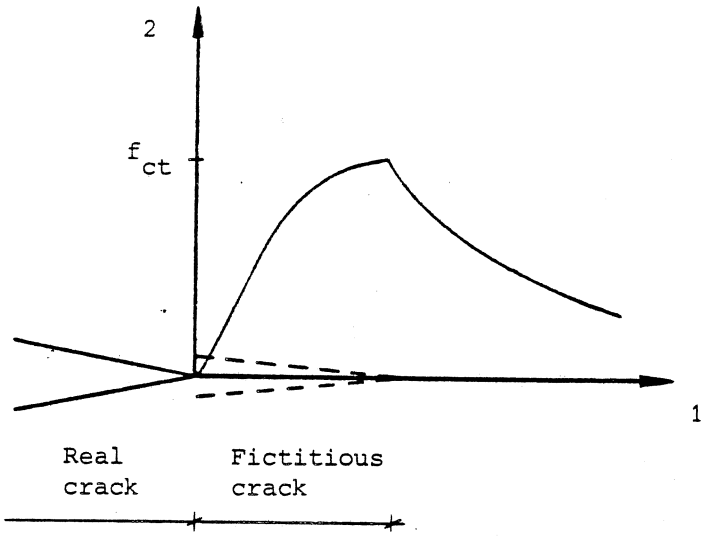

Fig. 3 Stress distribution according to the Fictitious Crack Model.

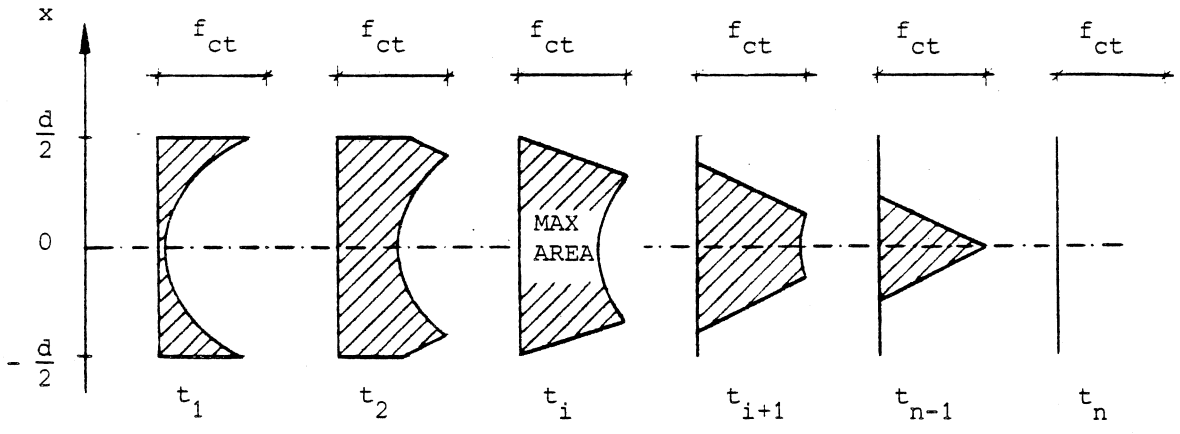

Fig. 4 Stress distribution through the wall at different times, caused by restrained shrinkage and crack propagation.

At a certain time t_i the force

$$F_{ti} = s \cdot \int_{-d/2}^{d/2} \sigma_{ti}(x)\, dx \quad \ldots\ldots (6)$$

in which d is the thickness of the wall, s - the distance between the rebars, reaches its maximum value. This is the maximum force which should be carried by one rebar. The value of this force is lower than the value usually used for counting the minimum reinforcement $F = f_{ct} \cdot A_c$.

The aim of these calculations was to investigate this force using a numerical approach, and describing concrete and its properties as exactly as possible.

4. THEORY USED IN CALCULATIONS

4.1 Drying of concrete

A differential equation describing diffusion in one direction in concrete was proposed by Bazant in /8/

$$\frac{\partial}{\partial x}\left(k_h \frac{\partial h}{\partial x}\right) + \frac{\partial h_h}{\partial t} + k \cdot \frac{\partial T}{\partial t} = \frac{\partial h}{\partial t} \quad \ldots\ldots (7)$$

in which:

h - humidity
x - space coordinate
t - time
T - temperature
k_h - nonlinear humidity coefficient

Fig. 5 shows the result of the calculation of the humidity at various times $t' = t - t_o$ after the beginning of the process of drying. In the calculation the following values were used:
$d = 0.16$ m, $t_o = 7$ days.

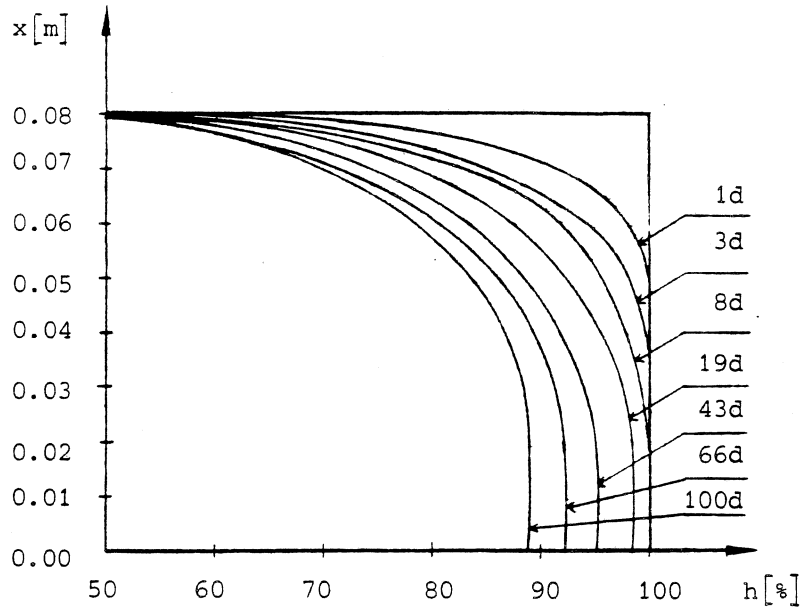

Fig. 5 Humidity distribution in the wall at various times.

4.2 The shrinkage of concrete

The formula proposed by Bazant and Panula in /9/ was used.

$$\varepsilon_{sh}(t', t_o) = \varepsilon_{sh\infty} (1-h^3)\ S(t') \quad \text{.....(8)}$$

4.3 Constitutive relations for concrete

An analytical constitutive relation of concrete under a general three dimensional stress state was used. The concrete is assumed to be a continuous, isotropic and elastic - plastic material.

The constitutive relations for concrete proposed by A.C.T Chen and W-F Chen /10/were adopted in FEM-calculations.

The failure function, the initial discontinuous function and the loading functions are functions of J_1 (the first invariant of the stress state tensor σ_{ij}) and J_2 (the second invariant of the deviatoric stress tensor S_{ij}).

The proposed functions have the following forms:

The failure function (plus in the third term to describe the compression region, minus for the tension - compression region):

$$f_u(\sigma_{ij}) = \frac{K^2}{3} J_2 - \frac{K^2}{36} J_1^2 \pm \frac{1}{12} J_1^2 + \frac{1}{3} A_u J_1 = \tau_u^2 \quad \ldots\ldots\ldots\ldots\ldots\ldots (9)$$

The initial discontinuous function:

$$f_o(\sigma_{ij}) = \frac{K^2}{3} J_2 - \frac{K^2}{36} J_1^2 \pm \frac{1}{12} J_1^2 + \frac{1}{3} A_o J_1 = \tau_o^2 \quad \ldots\ldots\ldots\ldots\ldots\ldots (10)$$

The loading function:

$$f(\sigma_{ij}) = \frac{\frac{K^2}{3} J_2 - \frac{K^2}{36} J_1^2 \pm \frac{1}{12} J_1^2 + \frac{\beta}{3} J_1}{1 - \frac{\alpha}{3} J_1} = \tau^2 \quad \ldots\ldots\ldots\ldots\ldots\ldots (11)$$

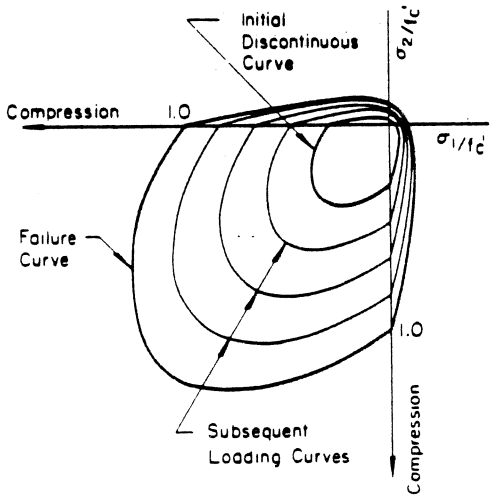

Fig. 6 Initial Discontinuos, Loading and Failure Curves in Biaxial Principle Stress Space /10/.

The incremental elastic - plastic strain-stress relationship used in the FEM-program:

$$d\varepsilon_{ij} = \left[H_{ijkl} + \frac{\frac{\partial f}{\partial \sigma_{ij}} \frac{\partial f}{\partial \sigma_{kl}}}{H \sqrt{\frac{\partial f}{\partial \sigma_{rs}} \frac{\partial f}{\partial \sigma_{sr}}}} \right] d\sigma_{kl} \qquad \text{.....(12)}$$

in which H_{ijkl} is the elastic compliance matrix and H is the strain hardening rate function.

4.4 The Fracture Mechanics approach

The Fictitious Crack Model (FCM) was used in the analysis. Fig. 7 shows two stress - deformation relations proposed by Pettersson /11/, which were adopted in the calculations. The value of the fracture energy G_F was chosen to be 60 N/m and the tensile strength of concrete 3 MPa.

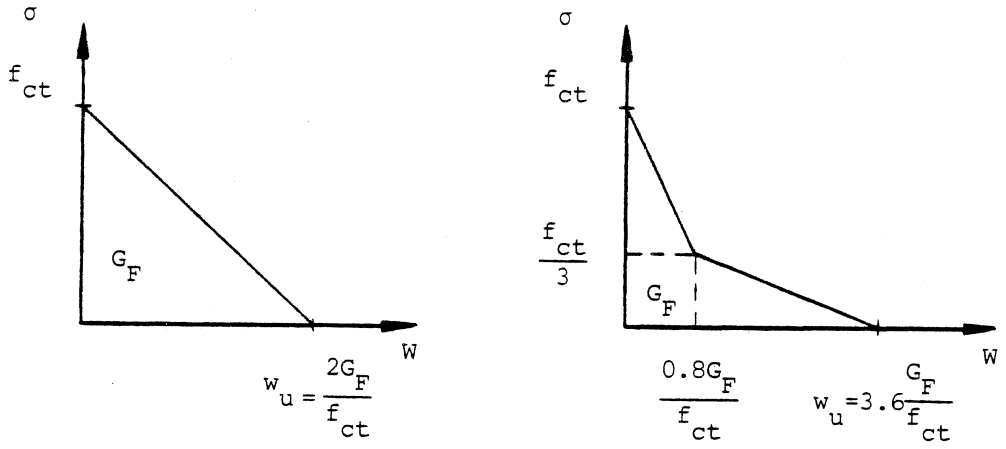

Fig. 7 The σ-w curves used in the analysis.

5. FEM - ANALYSIS

A two-dimensional finite element analysis of the wall subjected to drying shrinkage was performed. The mesh for this analysis is shown in Fig. 8.

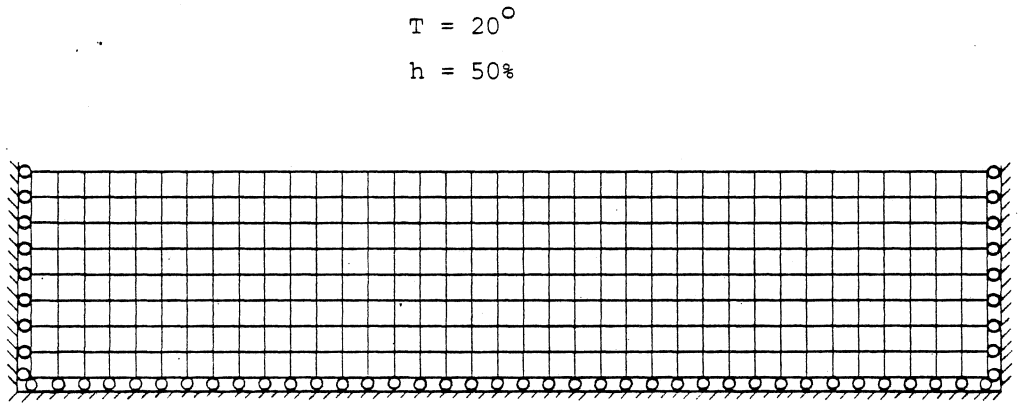

Fig. 8 Finite element model.

This mesh idealizes a representative horisontal cross section through the wall. Since the drying conditions - temperature and humidity at both sides of the wall are the same, the drying process proceeds symmetrically. So, only half of the thickness of the wall was analysed. The degree of freedom in the x-direction at both ends is restrained (this is to imitate the wall of infinite length). The mesh is composed of 8 rows x 37 element. Totally 296 four - node square elements. The parameters of the environment in which the wall is drying were chosen: temperature T = 20°C, humidity h = 50%.

The first crack was initiated in the middle of the length of the model by the time the load was equivalent to two days of drying. The crack was propagated through the whole thickness of the wall when a load equivalent to 66 days of drying was reached.

6. CONCLUSIONS

A finite element approach has been taken to analyse the crack propagation in drying concrete. The long concrete wall subjected to restrained shrinkage has been calculated using The Fictitious Crack Model.

Based on the results of the calculations the following major conclusions may be stated for the concrete structures in which the restrained shrinkage occurs.

I Shrinkage - induced cracking begins at very early age - a few days after the drying process has started (in this calculation, 2 days).

II Cracking through the whole thickness of the structure occurs after 2-3 months, depending on the thickness of the wall. For the 0.16 m thick wall this period was calculated to be 66 days.

III The total maximum tensile force (defined earlier in this paper) which should be carried by one rebar was found to be 70% of the value of the force usually used in calculations of minimum reinforcement ($F = f_{ct} \cdot A_c$).
This leads to the very important conclusion that in concrete structures subjected only to restrained shrinkage the minimum reinforcement area may be reduced to 70% of the minima specified in codes of practice.

REFERENCES

/1/ Comité Euro-International du Béton, "Code Modèle CEB-FIP pour les Structures en Béton", Bulletin d'Information No 124/125F, 1978.

/2/ Société Suisse des Ingénieurs et des Architectes, "Nouvelle Norme SIA 162 pour les Ouvrages en Béton, Béton Armé et Béton Precontraint", Zurich 1983.

/3/ Statens Betongkommitté, "Bestämmelser för Betongkonstruktioner", BBK 79. Stockholm 1979.

/4/ Jaccoud, J-P., Charif, H., "Armature Minimale pour le Contrôle de la Fissuration". Publikation IBAP no 109, Ecole Polytechnique Federale de Lausanne, 1985.

/5/ Schiessl, P., "Mindestbewehrung zur Vermeidung klaffenden Risse", Institut für Betongstahl und Stahlbetonbau, Bericht 284, Munich 1985.

/6/ Falkner, H., "Zur Frage der Rissbildung durch Eigen - und Zwängspannungen infolge Temperatur in Stahlbetonbauteilen", Deutscher Ausschuss für Stahlbeton, Heft 208. Berlin 1969.

/7/ Hillerborg, A., "A Model for Fracture Analysis", Report TVBM-3005, Division of Building Materials, University of Lund, Sweden 1978.

/8/ Bazant, Z.P. Najjar, L.J, "Nonlinear Water Diffusion in Nonsaturated Concrete", Materials and Structures (RILEM), Vol. 5, 1972.

/9/ Bazant, Z.P., Panula, L., "Practical Prediction of Time - Dependent Deformations of Concrete - Part 1: Shrinkage", Materials and Structures (RILEM), Vol. 11, 1978.

/10/ Chen, A.C.I., Chen, W-F., "Constitutive Relations for Concrete", Journal of the Engineering Mechanics Division, ASCE, EM4, August, 1975.

/11/ Pettersson, P-E., "Crack Growth and Development of Fracture Zones in Plain Concrete and Similar Materials", Report TVBM-1006, Division of Building Materials, University of Lund, Sweden 1981.

NOTATION

A_c, $A_{c,ef}$, A_{ct} = area of concrete, effective area of concrete, total area of concrete;

A_g = gross area of section;

A_s = area of tension reinforcement;

A_o, A_u, τ_o, τ_u = material constants;

d = thickness;

E_c = concrete modulus of elasticity

F = force;

f_{ck}, f_{ctm} = compressive strengths of concrete

f_{ct} = tensile strength of concrete;

f_{cth} = raised value of concrete tensile strength;

f_{yk} = yield strength of reinforcement;

$f(\sigma_{ij})$, $f_o(\sigma_{ij})$, $f_u(\sigma_{ij})$ = loading function, initial discontinuous function, failure function;

H = strain hardening rate function;

H_{ijkl} = elastic compliance matrix;

h = humidity;

J_1 = first invariant of the stress tensor
$= \sigma_1+\sigma_2+\sigma_3$;

J_2 = second invariant of the stress tensor
$= \frac{1}{6}\ (\sigma_1-\sigma_2)^2+(\sigma_2-\sigma_3)^2+(\sigma_3-\sigma_1)^2$;

k_h = nonlinear humidity factor;

P = axial load;

P_{cr} = axial load at which cracking occurs;

S_{ij} = deviatoric stress tensor
$= \sigma_{ij} - \frac{1}{3}\sigma_{ii}\ \delta_{ij}$;

S = distance between rebars;

$S(t')$ = square - root hyperbolic law in time;

T = temperature;

t, t_o, t' = total time, time at which drying process starts, $t-t_o$;

w = crack width;

x = space coordinate;

α, β, K^2 = parameters;

γ = safety factor;

ε_{ij}, $d\varepsilon_{ij}$ = strain tensor, incremental strain tensor;

ε_{sh}, $\varepsilon_{sh\infty}$ = shrinkage strain, shrinkage strain after the infinite time;

σ_{ij}, $d\sigma_{ij}$ = stress tensor, incremental stress tensor;

σ_i = principal normal stress in direction i;

η = coefficient;

ρ_{min} = minimum reinforcement;

δ_{ij} = Kronecker delta, $\delta_{ij}=1$ when $i=j$; $\delta_{ij}=0$ when $i\neq j$;

MODELLING OF HOOK ANCHORS

Lennart Elfgren and Ulf Ohlsson
Division of Structural Engineering
Luleå University of Technology,
S-951 87 LULEÅ, Sweden

Paper presented at a Nordic Seminar on "Fracture Mechanics of Concrete Structures" at Lund Institute of Technology, Lund, Sweden, on November 6, 1986.

1. GENERAL

The anchorage in concrete of inserts and fixings can be classified into three groups depending on the way the load is transferred into the concrete, see Fig. 1 [1]:

- The load is transferred by concrete compressive stresses (hook anchors)
- The load is transferred by adhesion (adhesive anchors)
- The load is transferred by friction (expansion anchors)

In this paper hook anchors are analysed with the fictitious crack model [2]-[5]. Modelling of adhesive anchors by the same method is discussed in [6]-[8].

2. HOOK ANCHOR

This kind of anchor i often placed in the structure before the concrete is cast. However, there are also anchors which are placed in a hole drilled into the structure.

The propagation of a crack from the edge of the "hook" can be studied by a discrete crack approach [2]. In Fig. 2 an example is given of such a study [3], [4].

As can be seen from Fig. 2, the fictitious (dashed line) and the real cracks (full line) grow as the load is increased. The cracks form a cone and the crack tip has to penetrate a larger area the more it grows. This implies that the crack is very stable also for fatigue loads. As soon as the crack tip penetrates a small distance, the stress in the zone around the crack tip will decrease and thus the crack propagation will be halted. For this reason there is usually no fatigue problems for the concrete, for a bolt which is loaded at a level reasonably below its static failure load.

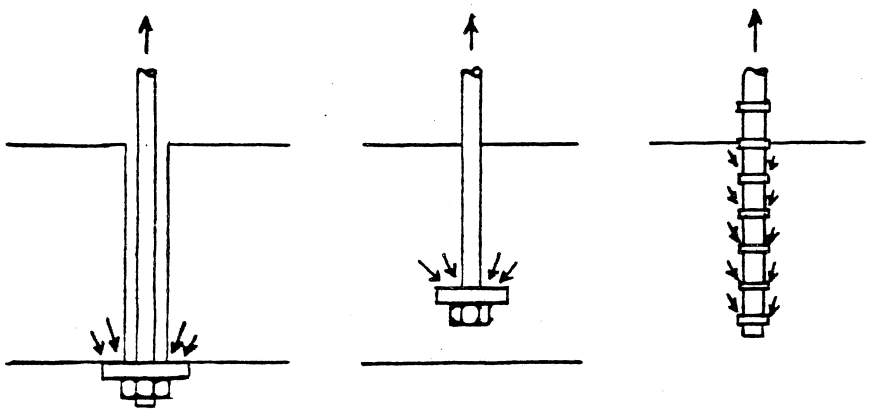

(a)

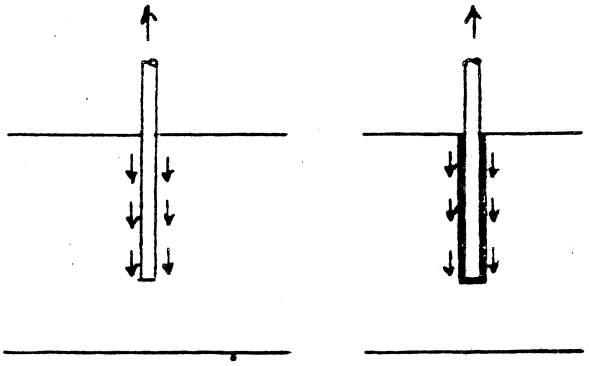

(b)

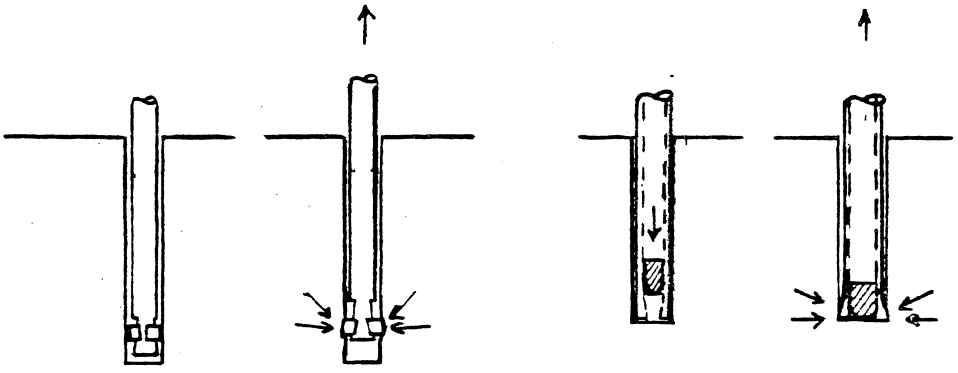

(c)

Fig. 1 Different ways of load transfer from an anchor to concrete [1]
(a) Compressive stresses - hook anchors
(b) Adhesive stresses - adhesive anchors
(c) Friction stresses - expansion anchors

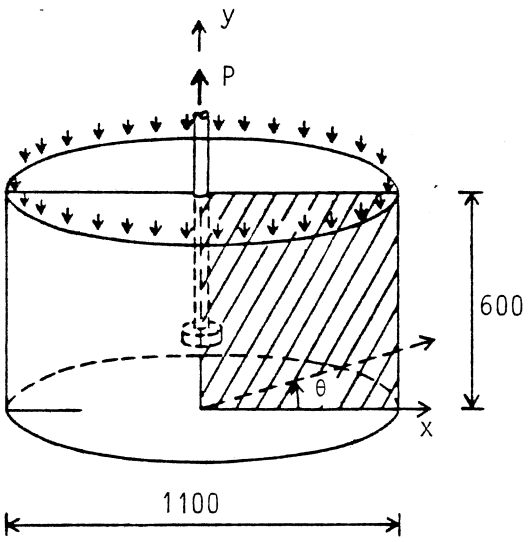
y
P
600
θ
x
1100

(a)

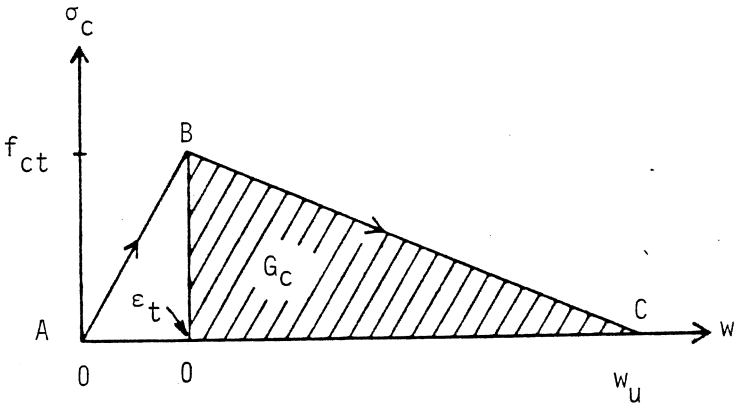
σc
fct
B
Gc
εt
A
C
w
0
0
wu

(b)

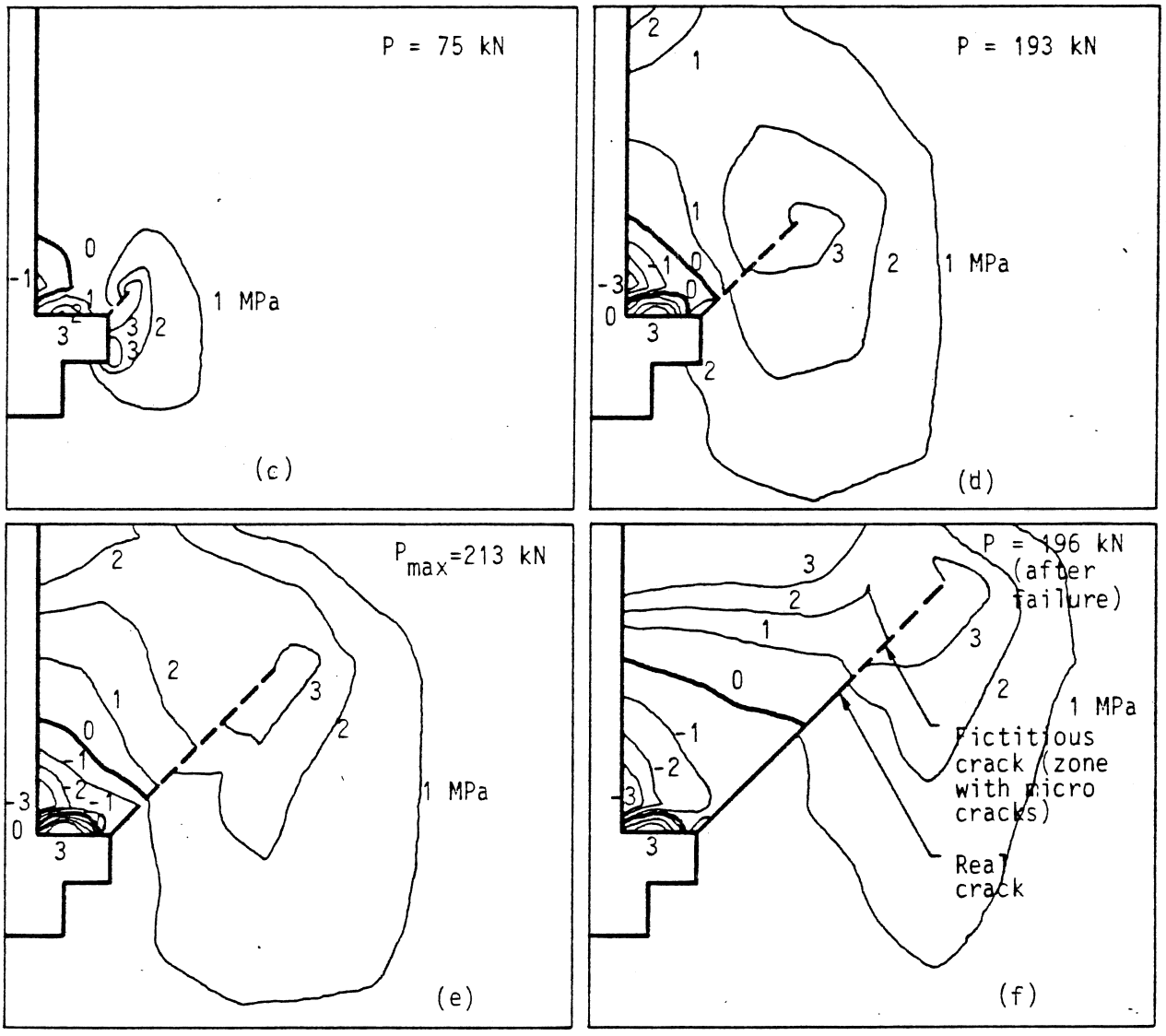
P = 75 kN
1 MPa
(c)
P = 193 kN
1 MPa
(d)
Pmax=213 kN
1 MPa
(e)
P = 196 kN
(after
failure)
1 MPa
Fictitious
crack (zone
with micro
cracks)
Real
crack
(f)

Fig. 2 Fracture mechanics model used for study of crack propagation [3], [4]. (a) Dimension of finite element model (96 axisymmetric elements + 10 linear crack elements). (b) Material model for loading (AB) and unlaoding (BC) of crack element; ε_t = tensile strain, w = crack width. The following material properties were used for steel and concrete: E_s = 210 GPa, ν_s = 0.3, ϱ_s = 7 800 kg/m^3, E_c = 30 GPa, f_{ct} = 3.0 GPa, ν_c = 0.2, ϱ_c = 2 400 kg/m^3, G_c = 60 N/m (fracture energy) and $w_u = 40 \times 10^{-6}$ m (maximum fictitious crack width. No shear capacity was assumed. (c)-(f) Isostress lines for maximum tensile stress for different load levels. A micro crack (fictitious crack) is marked with a dashed line and a real crack is marked with a full line. (c) P = 75 kN, (d) P = 193 kN, (e) P = 213 kN, maximum load, (f) P = 196 kN, after maximum load. The figure illustrates a test, where the anchor head deflection is the steering parameter.

The influence of material properties and crack path have been studied in [5] and some examples are given in Figs. 3 to 8.

In Fig. 3 the geometry of a bolt and a crack is given. The crack propagation has here approximately been choosen to be in the direction of the maximum tensile stress at the crack tip. Material properties are given in Fig. 4 and some results from finite element calculations are given in Figs. 5 to 8.

In Fig. 5 load-deformation diagrams are given for a straight crack with an inclination of 45^o. Three different fracture energies are compared to each other, one lower (50 N/m) and one higher (150 N/m) than the standard value (100 N/m) shown in Fig. 4. It can be seen from Fig. 5 that a higher fracture energy gives a higher load-carrying capacity.

In Fig. 6 a load-deformation diagram is given for the curved crack according Fig. 3. In Fig. 7 the deformed geometry of the same bolt is shown close to the maximum load.

In Fig. 8 the stresses and deformations in three crack elements are illustrated for different load levels. The load levels are also indicated in Fig. 6. In element 1 the shear stress first reaches a maximum value. This leads to a modification of the tensile stress - deformation diagram, see Appendix A. In elements 5 and 9 the tensile stresses first reach maximum values. This leads to modification of the shear stress - deformation diagrams, see Appendix A.

3. DISCUSSION

Comparisons of analytical results with test results [5] show that the fictitious crack in general gives a plausible description of what happens when a hook anchor is loaded.

Further studies should be directed at

- the interaction between the tensile and the shear stress-strain diagrams
- the values of the material properties
- other forms of crack patterns.

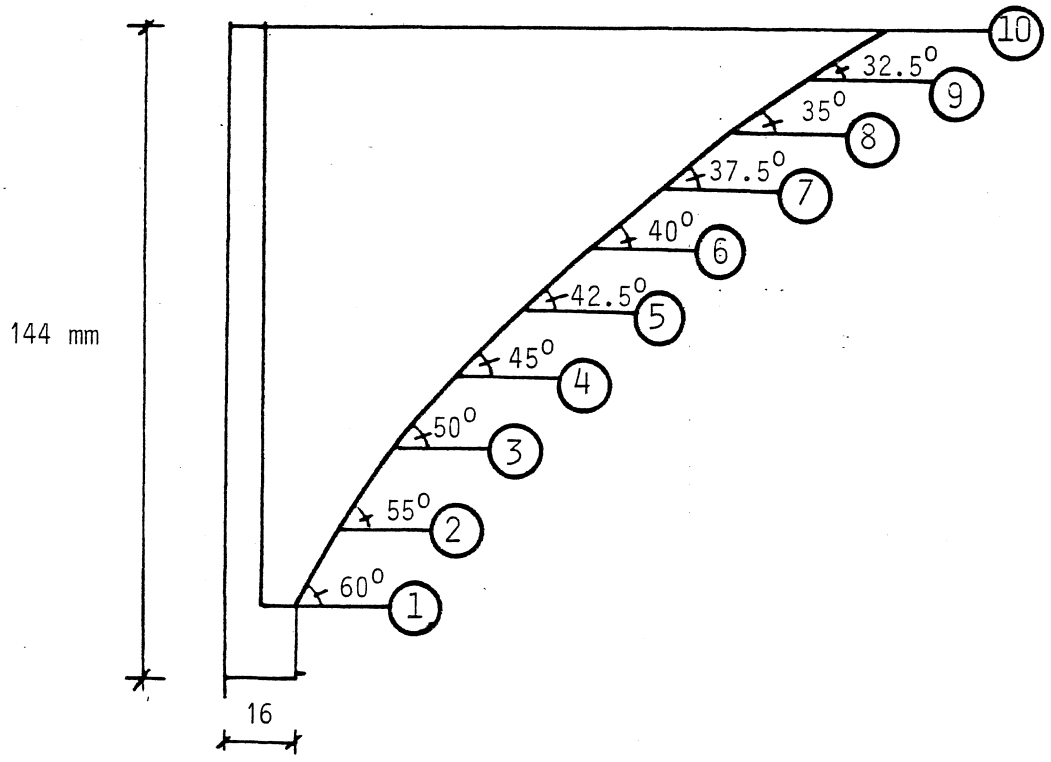

Fig. 3 Anchor with inclined crack embedded in a cylindrical concrete foundation with a diameter of 2.8 m and a height of 0.8 m [5]

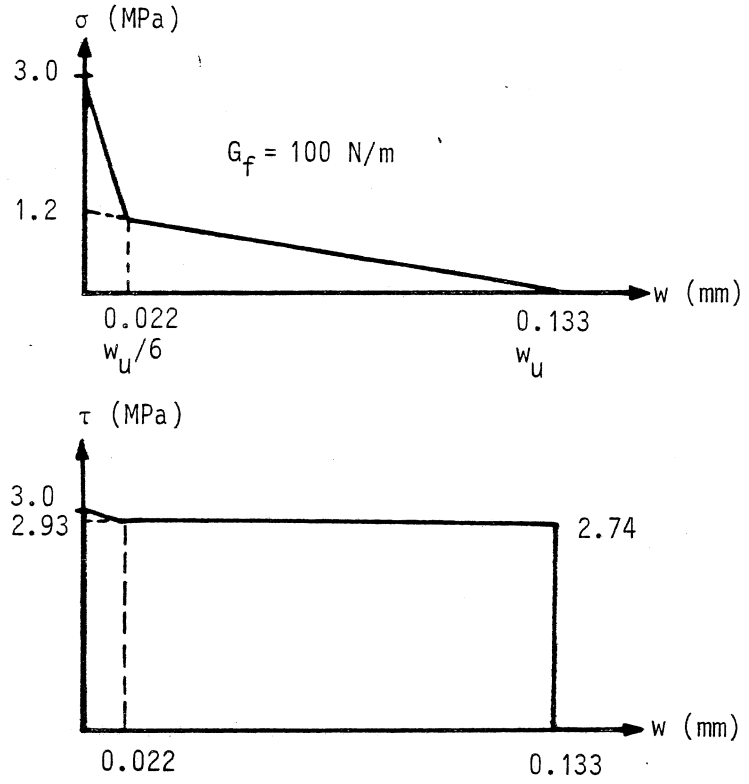

Fig. 4 Material properties used in finite element modelling of crack in Fig. 3 [5]

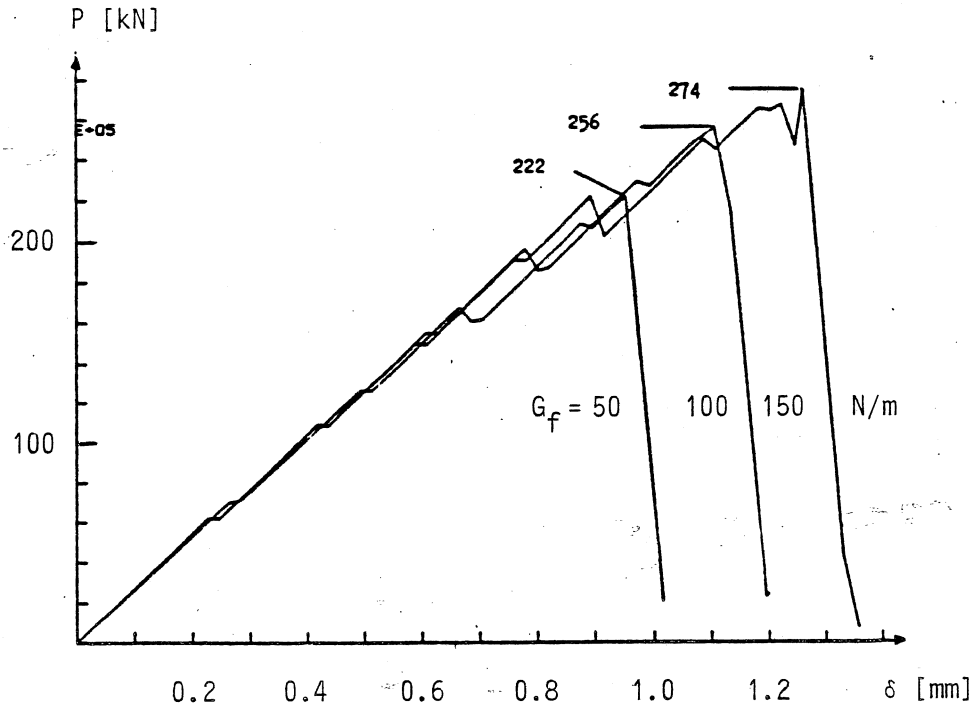

Fig. 5 Load-deflection diagrams for an anchor with the same general dimensions as the anchor in Fig. 3. However, a straight crack is studied with an inclination of 45^{o} and three different fracture energies are compared, 50, 100 and 150 N/m. Material properties according to Fig. 4 with different values of w_u (0.5 x 0.133, 0.133 and 1.5 x 0.133 mm) [5]

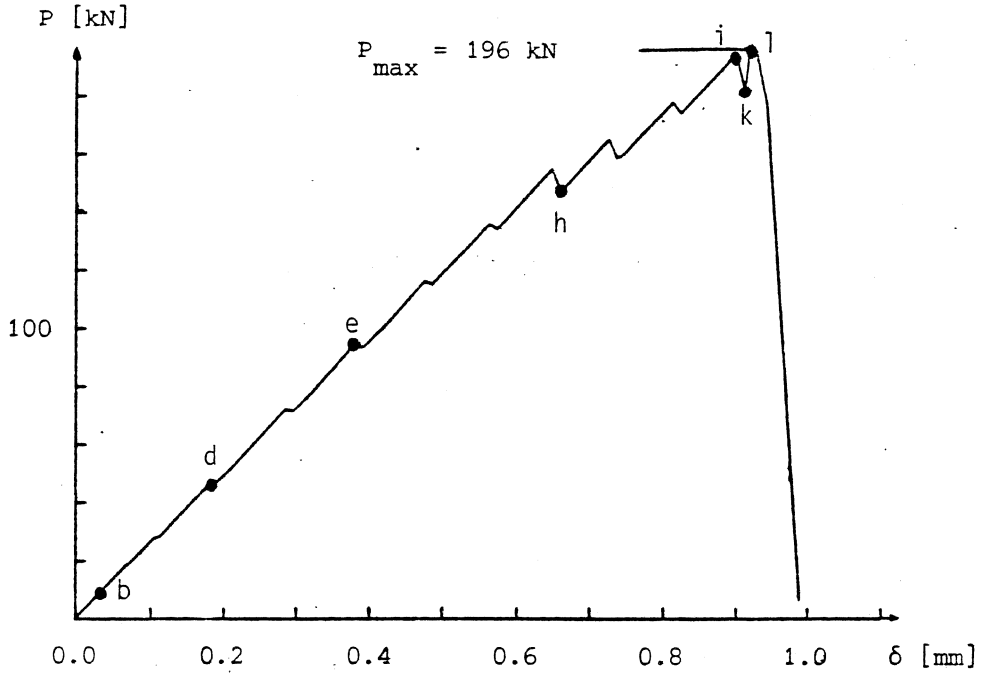

Fig. 6 Load-deflection diagram for anchor in Figs. 3 and 4 [5]. Load levels indicated by letters refer to Fig. 8

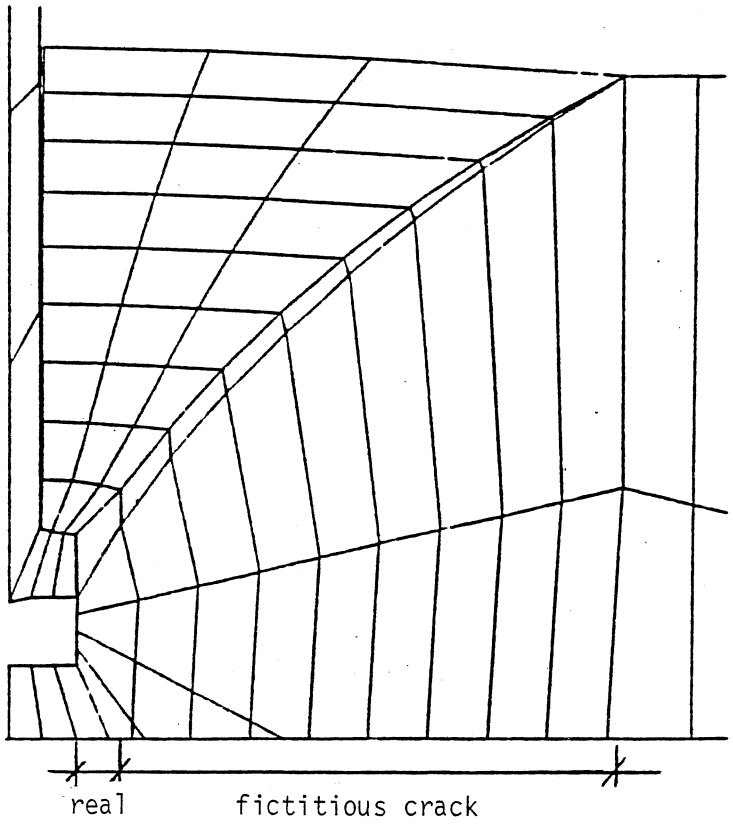

Fig. 7 Deformation at 95 % of P_{max} for anchor in Fig. 3 [5]

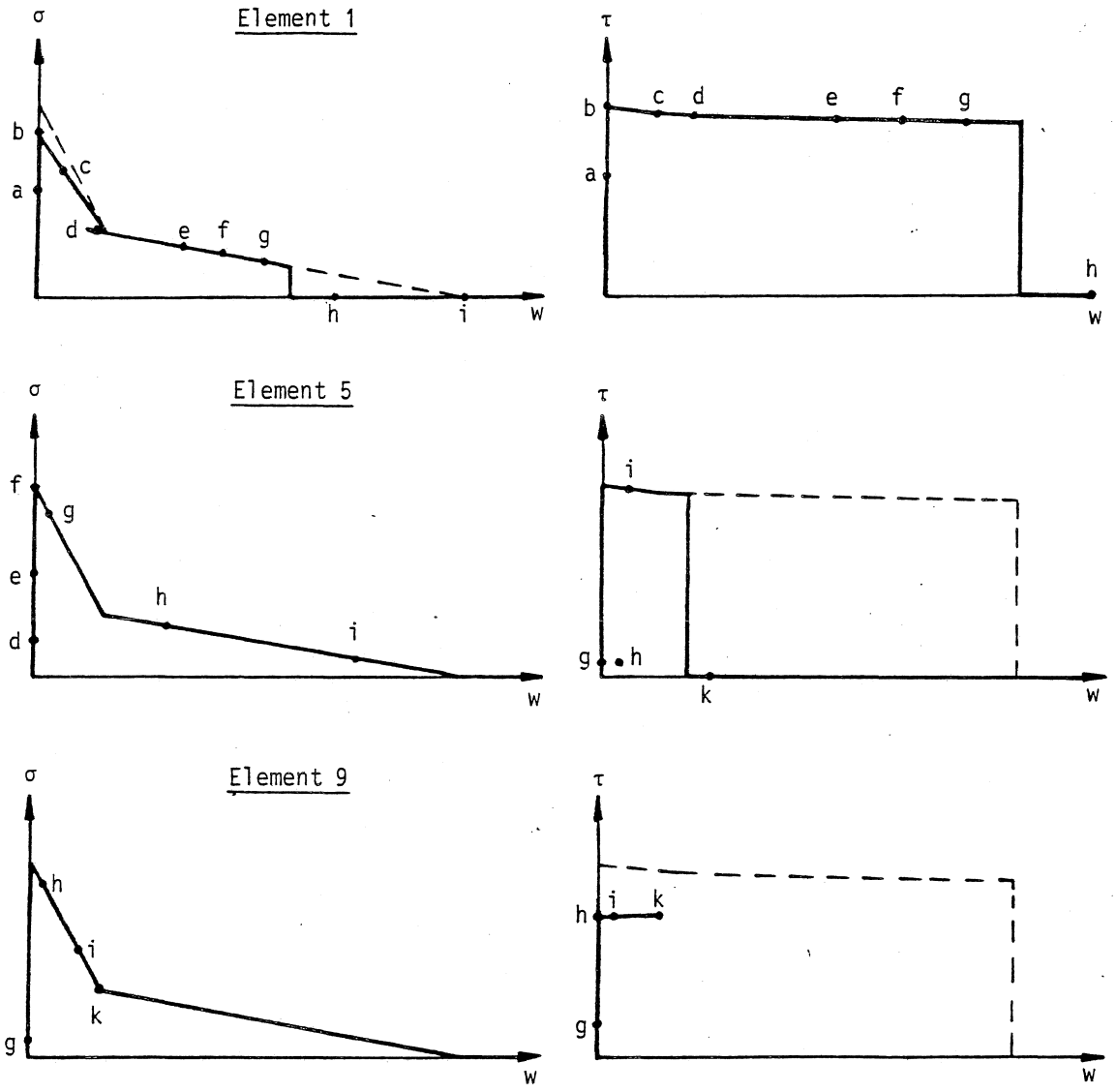

Load levels		Load level	Elements that pass fracture line 1	2	3
a	5.2 kN	a-b	1s		
b	10.4 kN	b-c	2s		
c	36.1 kN	c-d		1s	
d	46.8 kN	d-e	3s		
e	98.0 kN	e-f	4-5t	2s	
f	133.2 kN	f-g	6t	3s, 4-5t	
g	144.3 kN	g-h	7-9t, 10s		1
h	146.9 kN	h-i		6-8t	
i	194.4 kN	i-k		9t	2-3, 5
k	181.1 kN	k-l			
l	196.3 kN	l-		10s	4, 6-9

(s = shear mode dominating, t = tension mode dominating; cf. Fig. A2)

Fracture lines

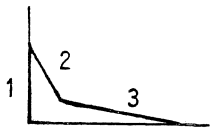

Fig. 8 Stresses and deformations in elements 1, 5 and 9 for different load levels for the anchor in Figs. 3, 4, 6 and 7.

APPENDIX A

CONSTITUTIVE MODELLING OF LINKAGE ELEMENTS [9]

General

The fracture mechanics of bonding discussed here concerns the contact zone between two materials: steel and concrete. Both sliding effects and tensioning effects are considered, because fracture occurs in two directions simultaneously. The failure can be characterized as a fracture zone, a crack, which arises in the contact surface between the steel and the concrete. The model is in principle the same as Gylltoft has presented in [9] for the bond between steel and concrete.

Constitutive modelling

The two materials steel and concrete are modelled separately as isotropic and linear elastic materials, characterized by Young's modulus of elasticity E and Poisson's ratio ν. The contact zone between the the steel and the concrete, the fracture zone, is modelled as a non-linear material. Here both normal stresses σ (normal to the contact surface) and shear stresses τ (within the contact surface) are considered. In this study, only one shear direction is considered.

Stresses in the shear direction often exceed the stresses in the normal direction. The shear capacity consists not only of pure shear strength but also of frictional forces, which will play an important role.

These two types of contribution are difficult to separate, so only the sum of them is considered. The dominating part played by the shear stresses and the relatively constant nature of the frictional resistance produced by the frictional forces even with large variations in deformation make it possible to obtain a rough estimate of the constitutive relations in the shear direction from direct experimental measurement, at least when loading is monotonic. Such a relationship is sketched in Fig. A1a.

Path OABE in Fig. A1a usually has a good correlation with experimental results. In this case, path OABCD is used as a simplification.

The constitutive relationship in the direction normal to the contact surface, path OABC in Fig. A1b has the same principal configuration as for concrete in tension.

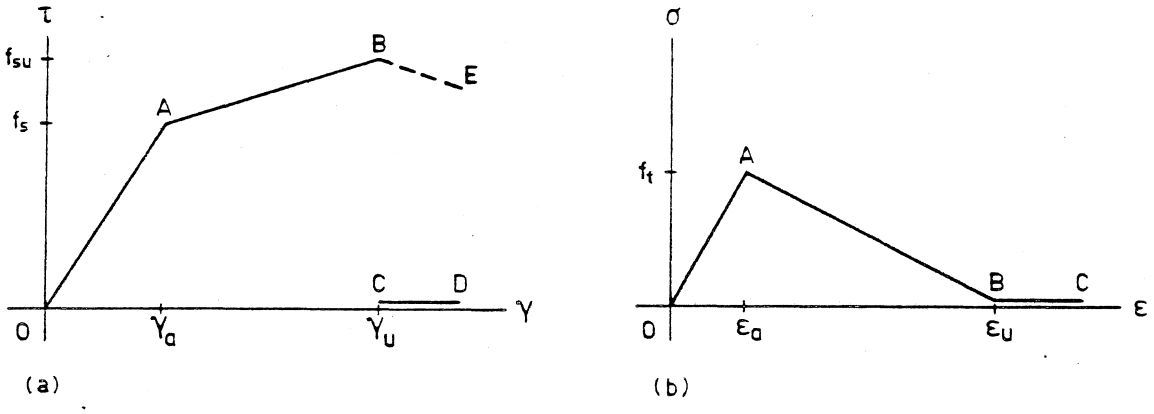

Fig. A1 Constitutive relations for the fracture zone under monotonic loading
(a) Shear direction
(b) Direction normal to the contact surface

Fracture criterion

All the lines in Fig. A1 are upper limits for a stiffer performance during cyclic loading, here called "elastic" performance. When the lines are reached, some sort of "fracturing" occurs. The lines are therefore called "fracture stress lines".

When fracture occurs in one direction, this must also influence the behaviour in the other direction. The assumptions used here are shown in Fig. A2. The different stages of the fracture process, corresponding to one fracture stress line each, are marked 1, 2 and 3 in Fig. A2. The principle applied here is that each fracture stage should be reached in the two directions at the same time.

Fracture stress line 1 is automatically reached in the two directions simultaneously, since the lines in both directions pass through the origin of coordinates.

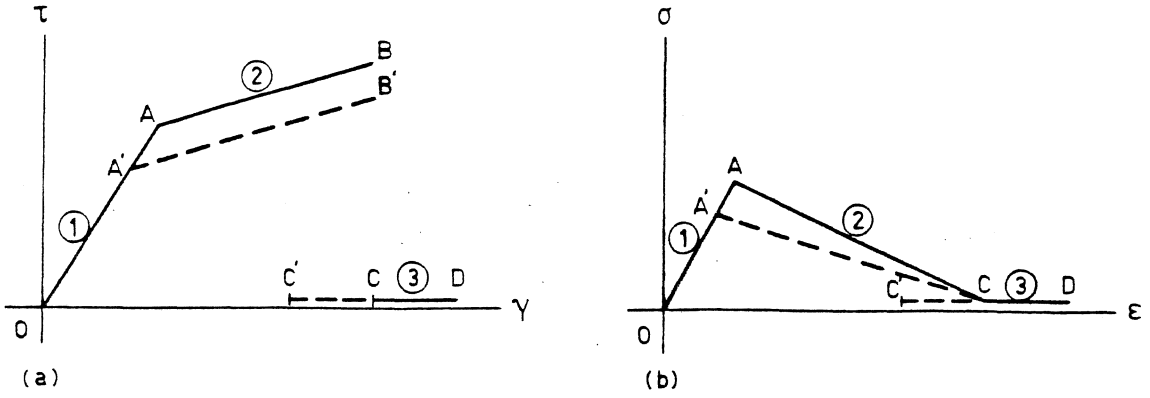

Fig. A2 Interaction between the constitutive relations in the two directions (τ-γ) and (σ-ε) [9]

If fracture stress line 2 is first reached in shear, point A in Fig. A2a, line AC in Fig. A2b will be rotated around point C to position A'C until fracture stage 2 is also reached in tension. On the other hand, if fracture stress line 2 is first reached in tension, point A in Fig. A2b, line AB in Fig. A2a will be lowered to position A'B' until fracture stage 2 is also reached in shear. The fracture stress line parameters are changed in such a way, that the point common with the subsequent fracture stress line (indicated by a higher number) is kept unchanged. When local unloading takes place in a crack element the stresses in that element will decrease. This may explain why some points in Fig. 8 are not situated on any fracture line.

"Ultimate fracture", fracture stress line 3, will also be reached in the two directions at the same time. This means that when point C is reached in one of the two directions, line CD in the other direction will be changed to position C'D, so that the stress is reduced to zero in that direction also.

The onset of each fracture stage occurs when either the shear stress τ or the tensile stress σ first reaches its corresponding fracture stress line, independent of the stress magnitude in the other direction. This may be called a "maximum stress criterion".

References

[1] Elfgren, Lennart: Förankringar i betongkonstruktioner. Anförande vid Byggnadsteknikdag vid Statens Provningsanstalt i Borås den 10 oktober 1984 (Fixings in concrete structures. Paper presented at a Building Technology Day at the National Swedish Testing Institute, Borås, October 10, 1984. In Swedish). Division of Structural Engineering, Luleå University of Technology, Paper 84:08, Luleå 1984, 12 pp.

[2] Hillerborg, Arne: Analysis of one single crack. Chapter 4.1 in Wittman, Folker "Fracture mechanics of concrete", Elsevier, Amsterdam 1983, pp 223-249 (ISBN 0-444-42198-8)

[3] Elfgren, Lennart; Cederwall, Krister; Gylltoft, Kent; and Broms, Carl Erik: Fatigue of anchor bolts in reinforced concrete foundations. IABSE Colloquium "Fatigue of steel and concrete structures". Lausanne March 1982, Proceedings, IABSE Reports, Vol. 37, Zürich 1982, pp. 463-470

[4] Håkansson, Mats; Nilsson, Roger: Förankringar i betongfundament. Beräkningar med finit elementmetod. Försök med statiska och dynamiska laster. (Anchor bolts in reinforced concrete foundations. Calculations with finite element methods. Tests with static and dynamic loadings. In Swedish with English summary). Division of Structural Engineering, Luleå University of Technology, Diploma work 1981:011E, Luleå 1981, 71 pp.

[5] Lundin, Barbro; Svensson, Lars: Datormodellering av hakförankrad infästning. En studie av icke-linjär brottmekanik för betongkonstruktioner. (Computer modelling of anchor bolts. A study of nonlinear fracture mechanics applied to concrete structures. In-Swedish). Division of Structural Engineering, Luleå University of Technology, Diploma work 1986:23E, Luleå 1986, 48 pp.

[6] Helgevold jr, Hakån and Kirknes, Svein: Klebeankare i betong. Samband mellan laster og deformasjoner for forskjellige innlimingslengder. (Adhesive anchors in concrete structures. Load-deformation relationships for various bond lengths. In Norwegian). Division of Structural Engineering, Luleå University of Technology, Diploma work 1984:17E, Luleå 1984, 74 pp.

[7] Granlund, Stig-Ola: Kemankare. En finit elementmodellering av last-deformationsegenskaper vid cyklisk belastning. (Adhesive anchors. Finite element modelling of load-deformation relationships for cyclic loading. In Swedish). Division of Structural Engineering, Luleå University of Technology, Paper 85:15, Luleå 1986, 21 pp.

[8] Granlund, Stig-Ola; Gylltoft, Kent and Elfgren, Lennart: A fracture mechanics model for adhesive anchors. Presented at a Nordic seminar on "Bond and anchorage in concrete" at Chalmers University of Technology, Göteborg October 23, 1985. Division of Structural Engineering, Luleå University of Technology, Paper 86:03, Luleå 1986, 19 pp.

[9] Gylltoft, Kent: Fracture mechanics models for fatigue in concrete structures. Division of Structural Engineering, Luleå University of Technology, Doctoral thesis 1983:25D, Luleå 1983, 210 pp.

[10] Nilsson, Larsgunnar and Oldenburg, Mats: FEMP. An interactive graphic finite element program for small and large computer systems. Division of Structural Engineering, Luleå University of Technology, Technical Report 1983:07T, Luleå 1983, 116 pp.

MODELLING OF MULTIPLE CRACK FORMATION IN REINFORCED CONCRETE STRUCTURES. ANALYSIS OF BEAM WITH LONGITUDINAL REINFORCEMENT.

Bjørn Bergan
Norwegian Institute of Technology, Trondheim
Division of Concrete Structures

INTRODUCTION

Nature of the problem

Consider the severely cracked beam shown in Fig. 1. The figure illustrates two important problems in analyses of reinforced concrete:

- the large number of cracks developed before failure
- when the ultimate load is reached, the final crack propagates diagonally from a point near the support instead of penetrating where the moment has its maximum

These phenomena are, of course, related to the mechanical properties of concrete, and to interaction between reinforcement and concrete.

Aim and scope

The ultimate goal is to simulate the process of multiple cracking and its effect on the interaction between steel and concrete.

The aim of this study was to investigate the obstacles in applying an incremental method as suggested by Modéer /1/ to multiple crack problems.

METHOD OF ANALYSIS

Fracture criteria

Fracture in concrete

A major principal stress criterion is utilized to govern fracture within concrete. As the maximum principal stress exceeds the tensile strength, a fracture zone is created. With a few reservations, this condition renders reasonably good correlation with concrete fracture. It is also easy to compute the load at which fracture occurs. A more general criterion would be a modified major principal stress criterion with a cut-off on the tension/compression side. However, this requires a more complicated algorithm for computing fracture load.

Stresses parallel to cracks are neglected that is,all fracture within concrete is assumed to be tensile.

Bond stress

A shear stress criterion is used between steel and concrete (Fig. 2). The selected curve is based on experiments performed by Nilson /2/, and a multi-linear curve is approximated. This is a commonly used approach to modell bond stress variations. /2/, /4/, /5/. In most cases, it yields fairly good results. Stresses normal to the bond zone are not accounted for. As shown by Robins and Standish /3/, a pure shear stress criterion renders too low fracture limits when compressive forces are applied normal to the direction of the reinforcement. Such loading conditions are present near the support of the beam. A Mohr-Coulomb fracture condition would give even better results. Modéer /1/ suggests an angle of friction of 39^0.

Fracture in steel

As for concrete a major principal stress criterion is applied to the reinforcement.

Adapting the fracture criteria to FEM analysis

Membrane elements are chosen for concrete and reinforcement. Truss elements are utilized for representing bond.

Fracture of concrete

Since all fracture is assumed to be tensile, simple truss elements are sufficient to simulate the microcracked zone. The negative modulus of elasticity is determined based on a linear σ-w approximation (Fig. 3). The area of the microcracked concrete (MCC) element is calculated as the fraction of the total cross sectional area represented by the node.

These definitions secure that the strain energy rate consumed in the fracture zone is of the right order of magnitude. The MCC element is eliminated as the accumulated stress in the node reaches zero.

Bond stress

Truss elements are utilized in the zone between concrete and reinforcement. In addition, the vertical displacements of the corresponding concrete and steel nodes are coupled. This is done in order to obtain a non-singular global system. Moduli of elasticity are calculated from the multi-linear approximation in Fig. 2. The cross sectional area is determined as the surface area of the reinforcement which is represented by the node.

Computational method

The method utilized in this study is based on a series of FE calculations on slightly different element meshes. For each run, another node reaches its fracture criterion, and the element structure is modified according to the foregoing paragraphs. A load of unity is applied during FE computation, and the load and stresses are then multiplied with a factor so that the accumulated stress in one node equals its fracture condition. A more detailed description is presented in Appendix E, /1/.

Crack arrest

As two or more cracks are developed close to each other, the release of elastic strain energy close to the microcracked area will lead to complicated stress distributions. Local compression zones between cracks are created, and this effect is commonly known as "crack arrest".

Crack arrest must be specifically dealt with in the analysis. Because of the special properties of the MCC elements, artificial tensile forces are induced during the closing of cracks.

The problem is overcome by changing the modulus of elasticity of the MCC elements back to the original E_c (Fig. 5) as soon as a negative displacement is detected in a fracture zone. The global system is kept numerically stable by coupling the degrees of freedom normal to the truss axis. An average cross sectional area is used for these crack arrest elements. This yields a stiffness divergence of maximum 37% from the exact value.

This action is based on the assumption that the modulus of elasticity of concrete in compression is not seriously affected by transverse cracks.

SIMULATION PROGRAM

Test specimen

General

The selected specimen is a beam with longitudinal reinforcement only. It is included in the comprehensive study of shear strength in reinforced concrete beams by Bresler and Scordelis /6/.

Geometry and Material Data

Fig. 4 illustrates the geometry of the tested beam.
A table of material data used in this analysis if given in Fig. 5.

Choice of Element Types and Mesh Size

The original element mesh is shown in Fig. 6. Isoparametric quadrilateral constant strain elements are selected for their reasonably good accuracy and low cost. Ström /7/ concludes that quadrilateral four-node elements subjected to bending yield reasonably accurate results in linear elastic analyses. Cook /8/ concludes that quadrilateral elements "tend to stiffen and loose accuracy if their form become a general quadrilateral rather than a rectangle".

The mesh refinement is based mainly on the distance between the cracks. Secondary measures have been expedient element shapes and economy.

Computational resources

The analysis is carried out on a computer with a 64 bit representation. The linear elastic finite element program used executes all calculations in single precision variables. A Gauss type equation solver was applied to handle the negative diagonal elements of the stiffness matrix.

PRESENTATION OF RESULTS

Numerical condition of the system

The equation solver failed to carry out decomposition when a load of 35% of the expected fracture load was reached.

Open cracks were not created, but 30 microcracked concrete elements were introduced in the element mesh. Neither bond failure nor yielding in the reinforcement were present at this stage.

An explanation for the abrupt termination has not yet been fully established, but it is believed that the difference in stiffness of adjacent elements is too big.

This singularity problem may be remedied in several ways. The author suggests one of two measures to be taken:

1. Utilizing an FE program which calculates in double precision variables, or

2. Applying forces instead of elements in the fracture zones to represent dissipation of fracture energy.

Stress distributions during load history

Fig. 7 shows the bond stress distribution of the lower reinforcement bar at 6 different load levels. The increasing fluctuations are assumed to be due to crack arrest. In Fig. 8, the concrete stresses close to the reinforcement are presented at the same load levels as above. In Fig. 8, the concrete stresses close to the reinforcement is presented at the same load levels as above. The increasing fluctuations in bond stress are assumed to be due to crack arrest. This is confirmed by the stresses in the corresponding concrete elements. Concrete stresses at 3 vertical projections are shown in Fig. 9.

Reinforcement stresses are plotted at 3 stages of load history in Fig. 10.

The load-deflection curve is presented in Fig. 11.

Accuracy of the analysis

The correlation between the crack pattern of the actual experiment and the analysis is poor. Several cracks are formed at a level of 44.8 kN in the experiment, while at a load of 54 kN in the analysis, no cracks are initiated yet. This discrepancy is probably caused during estimation of material parameters. Tensile strengh, f_t, and characteristic length, l_{ch}, are determined from experimental results of modulus of elasticity and modulus of rupture. The relationship between tensile strength and modulus of rupture was approximated based on beam experiments by Modéer /1/. The experiments in /6/ was performed after 13 days curing, and this was not accounted for in the estimation.

As accuracy was of secondary importance in this investigation, material data were not altered to match the experimental values.

CONCLUSIONS

Two problems concerning multiple crack analyses were revealed in the present study.

1. Singularity.
   The choice of numeric representation of the reinforced concrete beam caused computational problems. Different approaches to overcome these difficulties are suggested.

2. Crack arrest.
   Release of elastic strain energy from two or more microcracked zones, causes artificial increase in stresses at nodes subjected to crack arrest.

Furthermore, the study indicates that a multiple crack approach may yield a greater understanding of the structural behaviour of reinforced concrete.

REFERENCES

1. Modéer, M.:
"A Fracture Mechanics Approach to Failure Analyses of Concrete Materials", report TVBM-1001, Div. of Building Materials, University of Lund, Sweden, 1979.

2. Nilson, A.H.:
"Nonlinear Analysis of Reinforced Concrete by the Finite Element Method", ACI Journal, Proceedings, v.65, no. 9, USA, September 1968, pp 757-766.

3. Robins, P.J., Standish, I.G.:
"Effect of Lateral Pressure on Bond of Reinforcing Bars in Concrete", Proceedings of the International Conference on Bond in Concrete, Paisley, Scotland, June 1982, Applied Science. Publishers LTD, London 1982, pp. 262-272.

4. Ngo, D., Franklin, H.A., Scordelis, A.C.:
"Finite Element Study of Reinforced Concrete Beams with Diagonal Tension Cracks", report no. UC SESM-70-19, Structures and Materials Research, University of California, Berkeley, USA, 1970.

5. Gustafsson, P.J.:
"Fracture Mechanics Studies of Non-yielding Materials like Concrete", report TVBM-1007, Division of Building Materials, University of Lund, Sweden, 1985.

6. Bresler, B., Scordelis, A.C.:
"Shear Strength of Reinforced Concrete Beams,--Series II", report no. 64-2, Institute of Engineering Research, University of California, Berkeley, USA, 1964.

7. Ström, O.:
"Nonlinear Analysis of Reinforced Concrete Structures using Beam and Membrane Elements", Division of Structural Mechanics, The Norwegian Institute of Technology, Trondheim, Norway, 1986.

8. Cook, R.D.:
"Concepts and Applications of Finite Element Analysis", 2nd Ed., John Wiley & Sons, New York, USA, 1981.

9. Gerstle, K., Ingraffea, A.R., Murray, D., Nilson, A.H., Mirza, M.S.:
"Modeling of Reinforcement and Representation of Bond", State-of-the Art Report on Finite Element Analysis of Reinforced Concrete, ASCE, New York, USA, 1982.

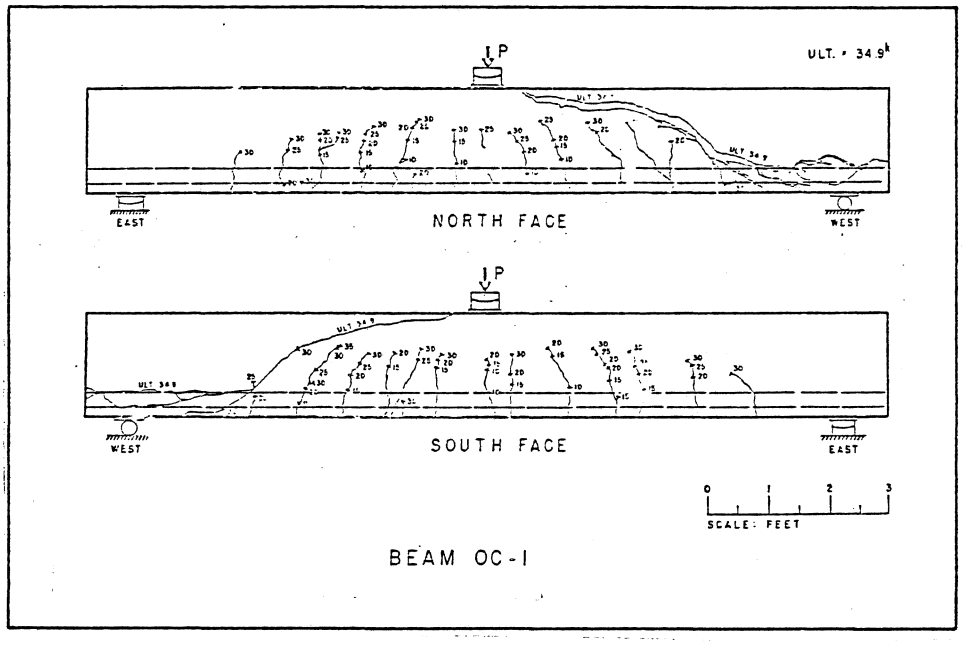

Figure 1.
Crack patterns of the beam analysed; OC-1, /6/.

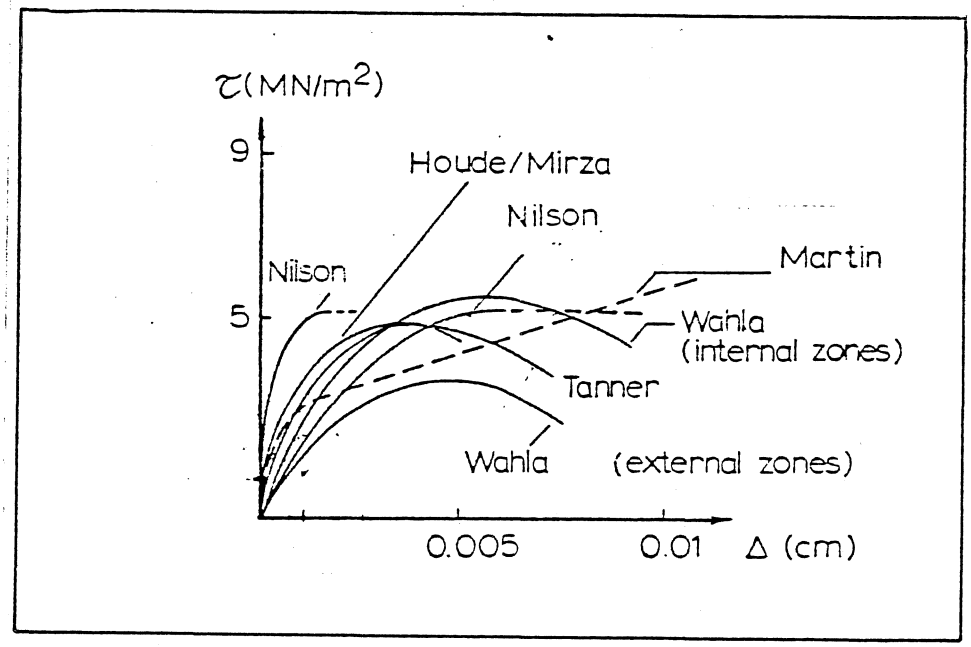

Figure 2a.
Comparison of mean bond stress-slip relationships. /9/

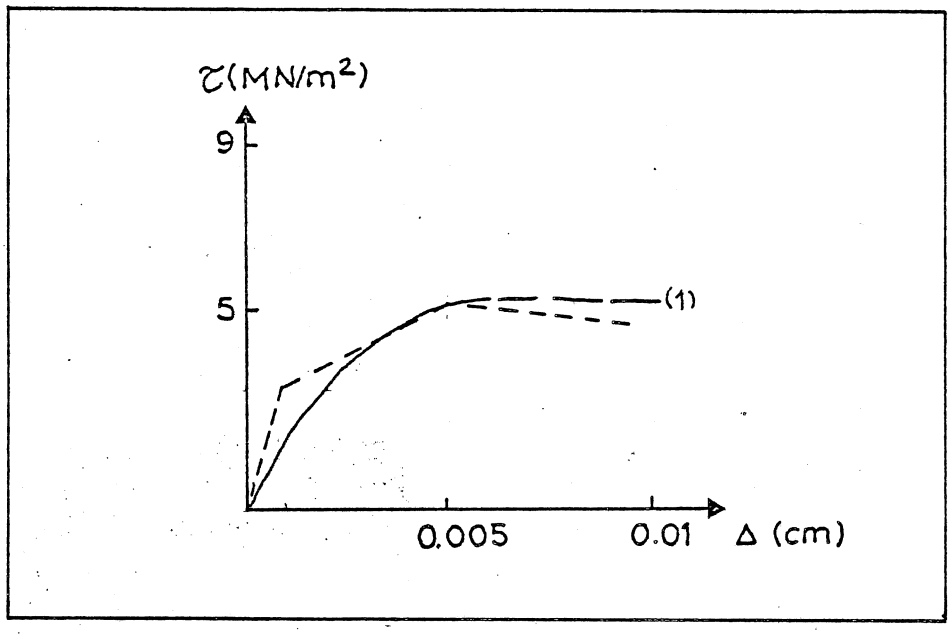

Figure 2b.
Selected curve (1) and linear approximation.

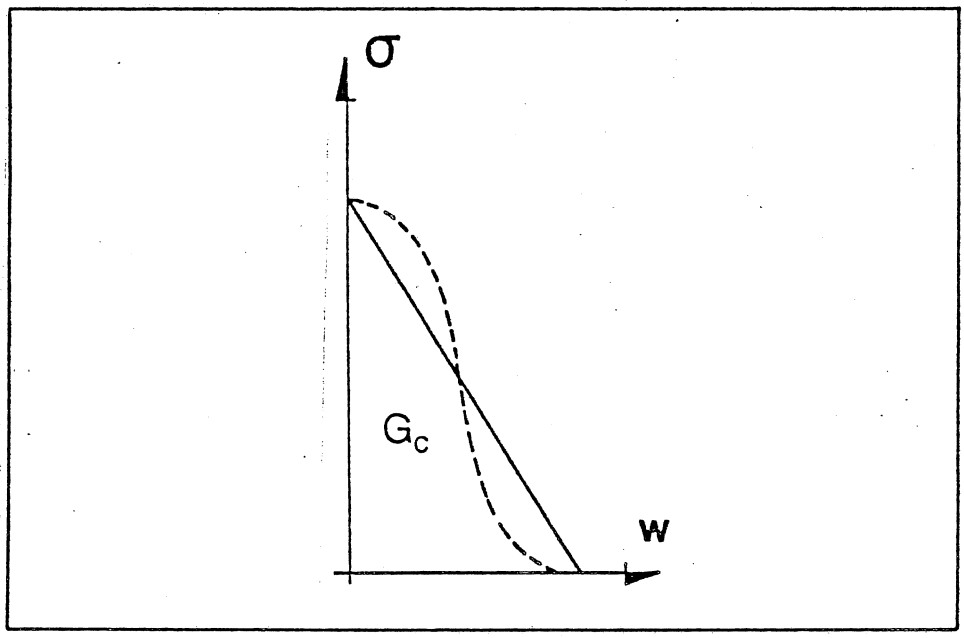

Figure 3.
Approximation of stress-displacement relationship for microcracked concrete. /1/

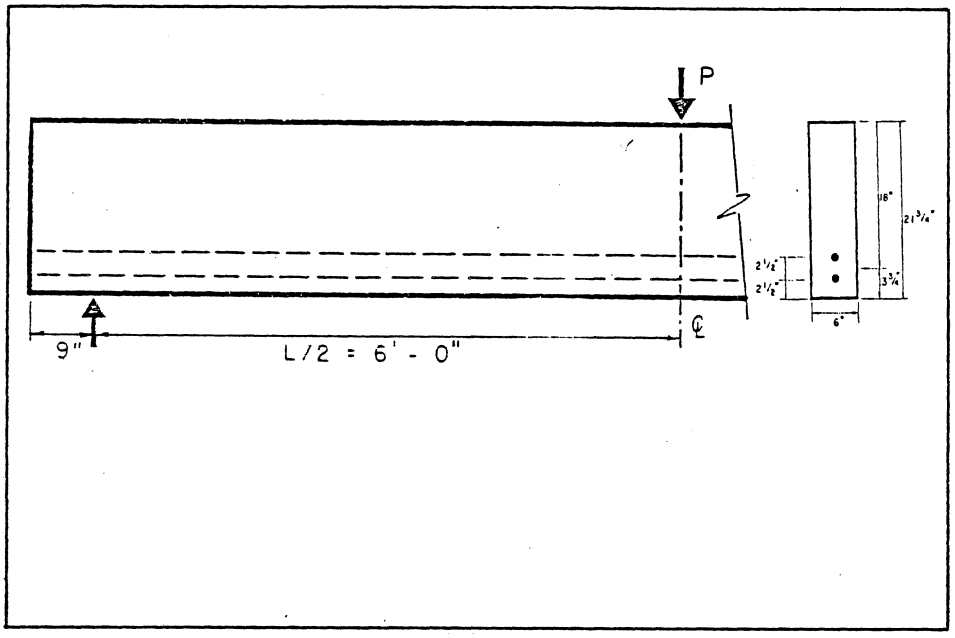

Figure 4.
Geometry of the analysed beam.

ELEMENT	E [N/mm^2]	ν [-]	σ_{max} [N/mm^2]
Concrete	28300	0.2	2.7
Reinforcement	191500	0.3	655
Bond link	3		3.0/5.0
Microcracked Concrete, tension	-0.30		0
Microcracked Concrete, compression	28300		

Fracture mechanics parameters.

l_{ch} = 470 mm
G_F = 120 N/m

Figure 5.
Material data applied in the analysis.

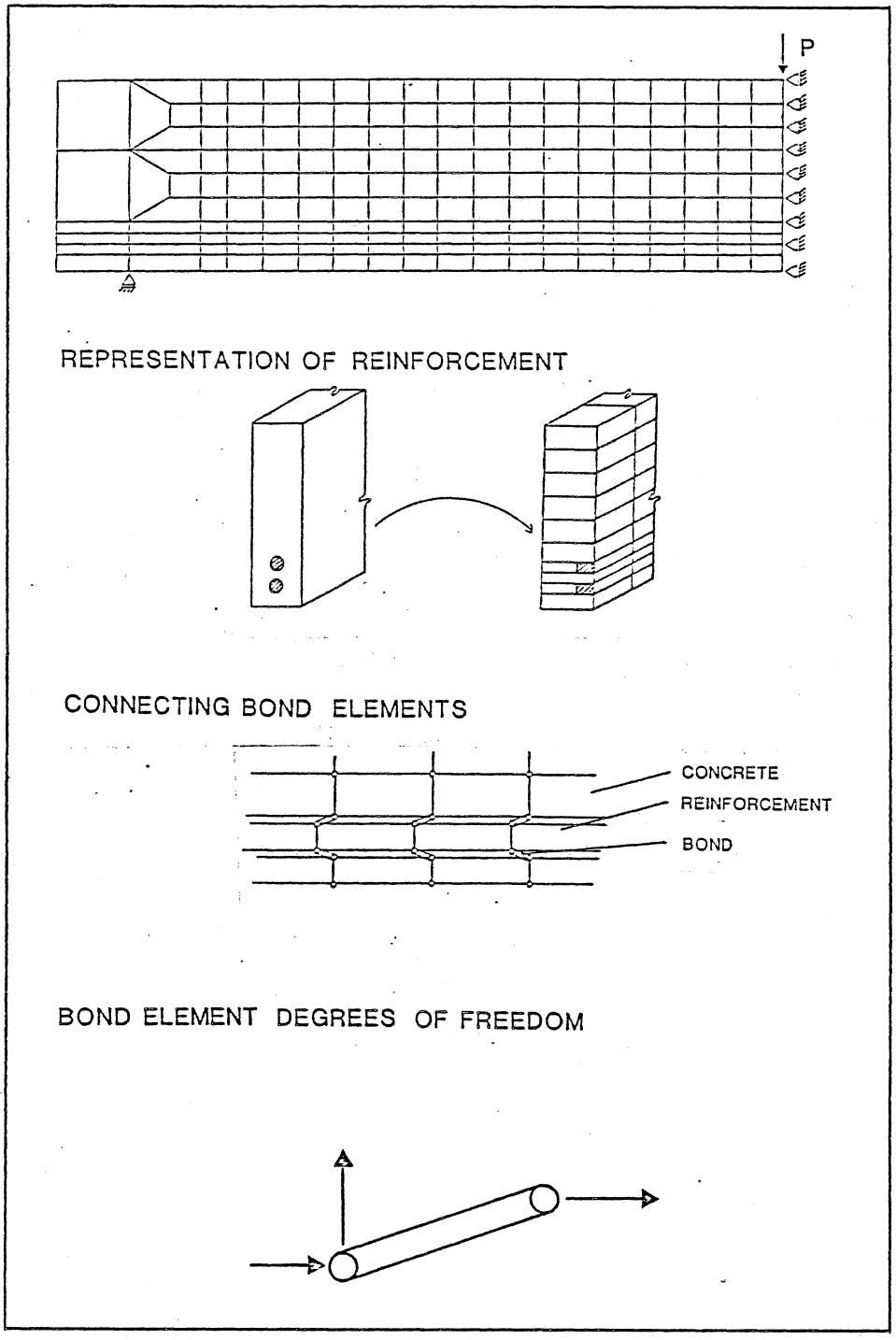

Figure 6.
Element mesh of the unfractured beam, details of bond and reinforcement representation.

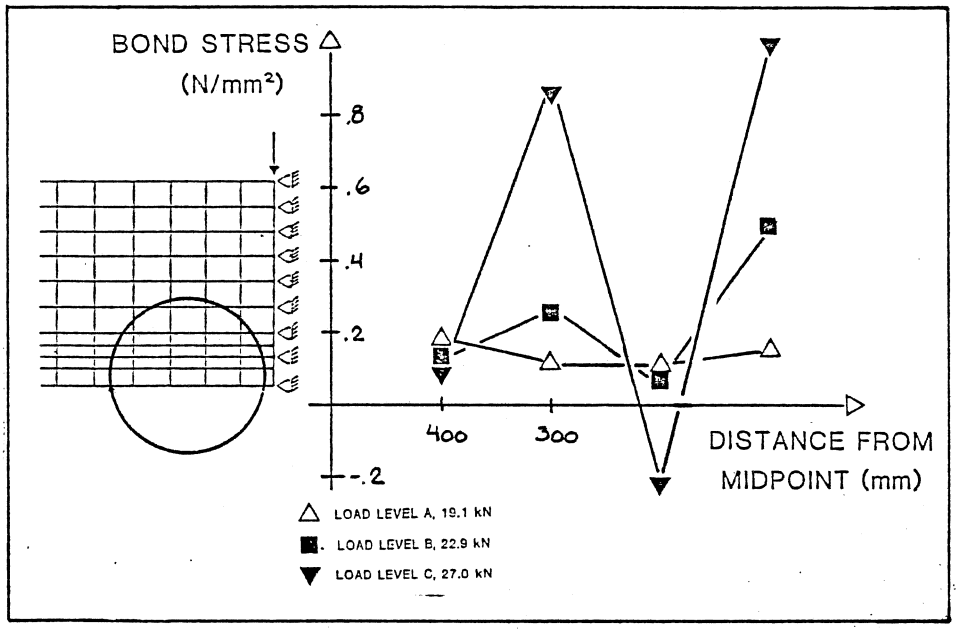

Figure 7.
Bond stress along middle section of the lower reinforcement bar.

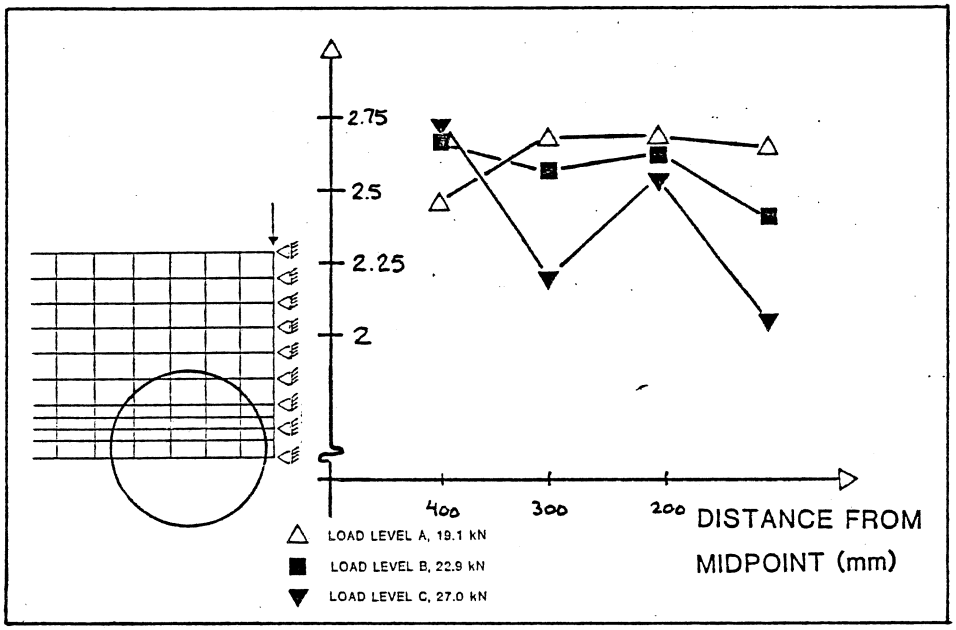

Figure 8.
Horizontal stresses in concrete just below the lower reinforcement bar.

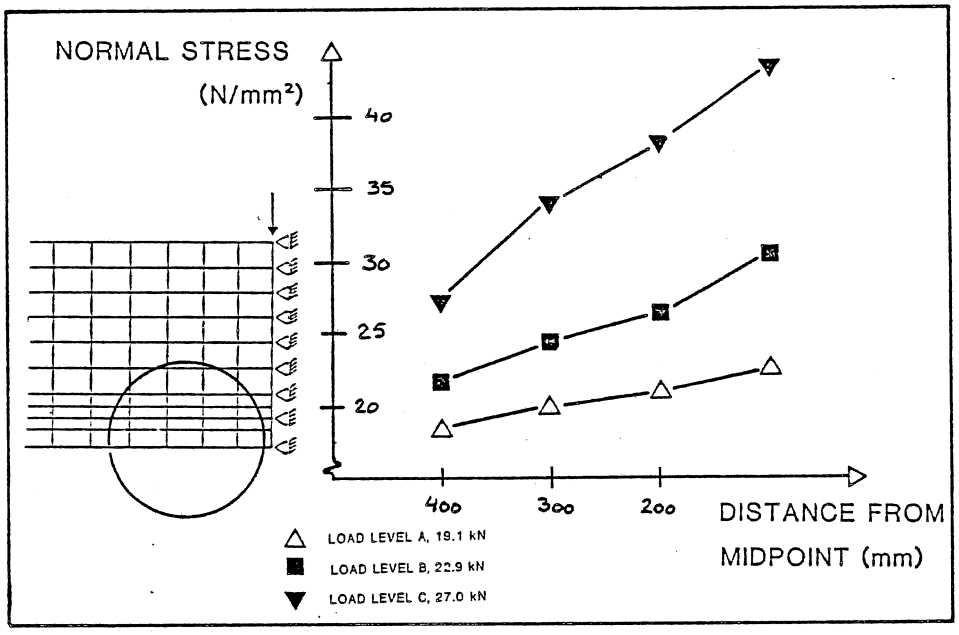

Figure 10.
Horizontal stresses in reinforcement at the middle section of the beam.

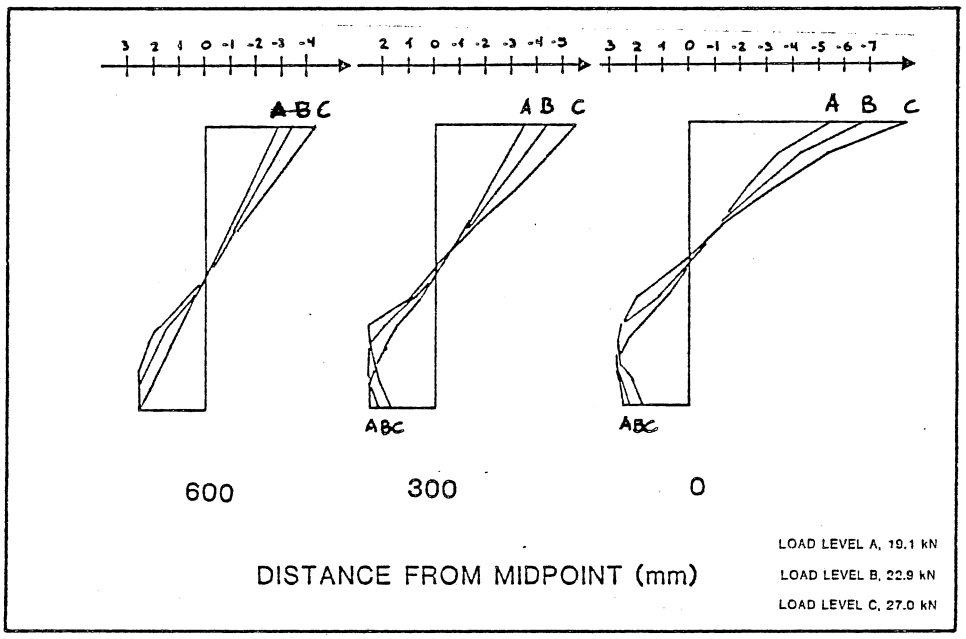

Figure 9.
Horizontal stresses in concrete at 3 vertical projections as indicated.

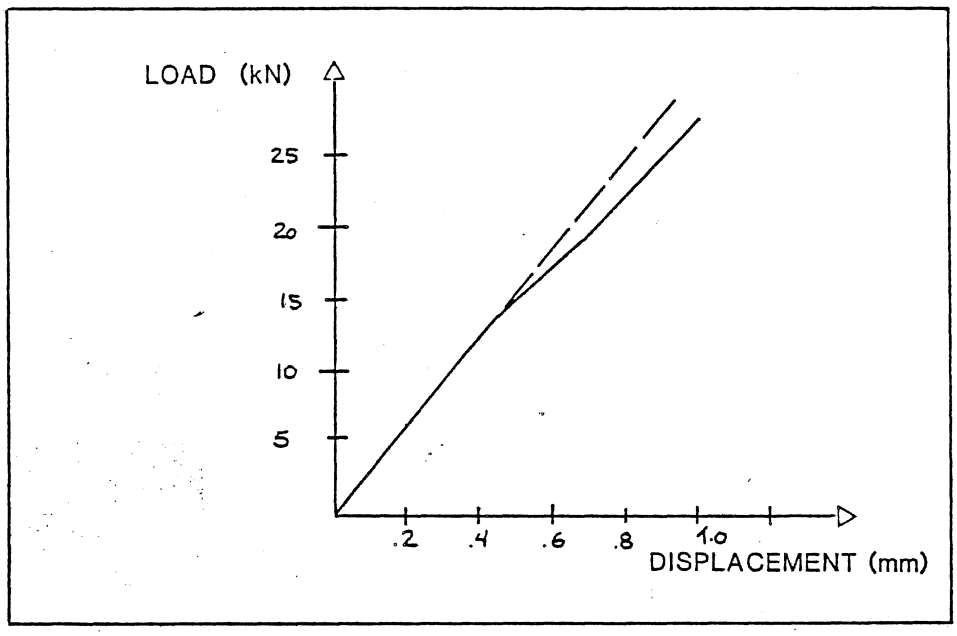

Figure 11.
Load-deflection curve of the analysis.

Betongens brottmekanik
Nordiskt miniseminarium
Lund 86.11.06

Prediction of shear force and shear displacement for construction joints and cracks in concrete.

Jan Norberg
Inst. f. brobyggnad
KTH
S-10044 Stockholm

Introduction

In the case of damaged concrete construction or in the case of prefabricated concrete combined with cast in place concrete the transfer of forces between the old and new concrete has great importance for the construction. A description of the transfer of bond forces is very complicated and the design recommendations are empirical. The microplanemodel proposed by Bazant and Gambarova /1/ gives the possibility to calculate the stress in cracks and construction joints in concrete from the elastic stadium over to the cracked stadium.

The stresses in the material are the sum of stress in planes of various directions. Each plane is assumed to represent microcracks parallell to the plane. In an isotrop material planes of all directions will be equally frequent.

The strain in the planes is the transformed global strain tensor. In each plane the stress depends on the strain in the same plane. Only the normal strain and the normal stress in each plane are considered in this paper. The sum of planes is able to transfer shear stress even if the shear stress in the planes is neglected.

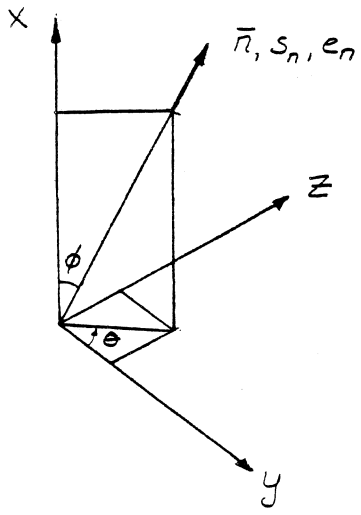

Fig 1 Definition of directions

The normal strain in any plane , e_n , is the strain vector of the plane projected on to the direction of the normal of the plane.

$$e_n = n_i n_j e_{ij} \tag{1}$$

Where e_{ij} is the global strain tensorn and n_i cosinus for the angle between the normal of the plane and the global direction of coordinates i.

The normal stress , s_n , depends on the normal strain in the same plane, e_n .

$$s_n = F(e_n) \tag{2}$$

If the virtual work in the volume of an unit sphere is equal to the virtual work done by forces on the surface of an unit sphere we get.

$$\delta W = \frac{4}{3}\pi\, s_{ij}\delta e_{ij} = \int_S s_n \delta e_n dS \tag{3}$$

where S and $4\pi/3$ are the area and the volume of an unit sphere, and on the surface of an unit sphere the displacement is related to the strains by: $\delta u = r\delta e_n = \delta e_n$

Substituting Eq 1 into Eq 3 we get

$$\frac{4}{3}\pi\, s_{ij}\delta e_{ij} = \int_S s_n n_i n_j \delta e_{ij} dS \tag{4}$$

As (4) holds for every δe_{ij} the global stress tensor can be calculated.

$$s_{ij} = \frac{3}{4\pi}\int_S s_n n_i n_j dS \tag{5}$$

According to (1) and (2) the incremental stress in the planes is

$$ds_n = (ds_n/de_n) n_k n_l de_{kl}$$

Differentiation of (5) will give the incremental stiffness.

$$ds_{ij} = \frac{3}{4\pi}\int_S \frac{ds}{de}_n n_i n_j n_k n_l dS\ de_{kl} \tag{6}$$

$$D_{ijkl} = \frac{3}{4\pi}\int_S \frac{ds}{de}_n n_i n_j n_k n_l dS \tag{7}$$

Where D_{ijkl} are the components of the incremental stiffness matrix. The integrals of (5) and (6) have to be evaluated numerically by approximation as a finite sum. If the sum is evaluated on a grid in the ϕ-θ plane the stress and the incremental stiffness can be calculated by Eq 8 and Eq 9.

$$s_{ij} = \frac{3\pi}{2N}\sum_{\alpha=1}^{N}\left[n_i n_j \sin\phi\ s_n \right]_\alpha \tag{8}$$

$$D_{ijkl} = \frac{3\pi}{2N}\sum_{\alpha=1}^{N}\left[n_i n_j n_k n_l \sin\phi\ \frac{ds}{de}_n \right]_\alpha \tag{9}$$

Where N is the number of points on the surface of a sphere which contribute to the sum and α is the point where the contribution to the sum is calculated. The strain and hereby the stress will be equal on diametrically opposite points on the surface of the sphere. The sum can be calculated on one half of the surface of the sphere. In the case of plane strain due to symmetry the sum can be done over only one fourth of the sphere.

A constitutive relation for the planes.

In each plane the normal stress is related to the normal strain according to fig 2.

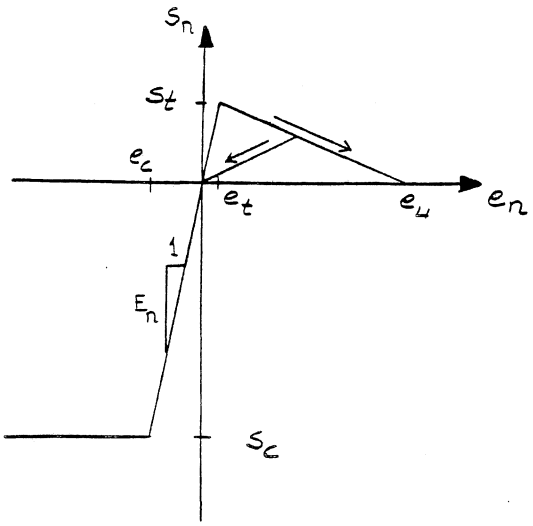

Fig 2 normal stress versus normal strain

Elastic stadium

The elastic modulus of the planes is two times Young's modulus of the material. The elastic properties of an isotropic material with Young's modulus , E , will hereby be obtained. The Poisson ratio will be constant in the elastic stadium , $\nu = 0.25$.

Compression

The maximal compression stress in the planes is set to the uniaxial compression stress of the material. An ideal plastic relation is assumed in the planes. Even if a straight line relation is used in the planes the sum of planes becomes gradually softer with increasing strain. The assumption of maximal compression stress in the planes will have great importance for the shear stress in the crack. With the conditions that are used in the following calculations, the stress in a crack the maximal compression stress normal to the plane of the crack will be equal to the maximal compression stress in the planes.

Tension

The relation between stress and strain is approximated with straight lines. An elastic relation is assumed up to the maximal tension stress in the planes. With increasing strain a linear decreasing relation between strain and stress is assumed. The relation between strain and crack width is expressed by the equivalent length. The equivalent length is equal to the length of the side of four-node rectanglar finite element in finite element calculations. In the case of unloading in the planes the stress is assumed to unload toward origo. In the sum of planes this assumption will lead to an unloading in a straight line towards origo for unloading in uniaxial tension. Depending on the value equivalent length used in the calculations the maximal tension stress in the planes will be exceeded at different crack widths. The maximal tension stress in the sum of planes will hence depend on the equivalent length.

Fracture energy

Accordind to these relations in the planes between strain and stress, the value of fracture energy will be constant for different values of the equivalent length.

$$G_F = \underbrace{2\,E\,e_t}_{s_t}\ \underbrace{e_u l}_{w_u}^{\frac{3}{2}} \qquad (10)$$

Fig 3 shows the relation between normal stress and crack width for different values of equivalent length. The calculated maximal tension stress decreases with increasing equivalent length.

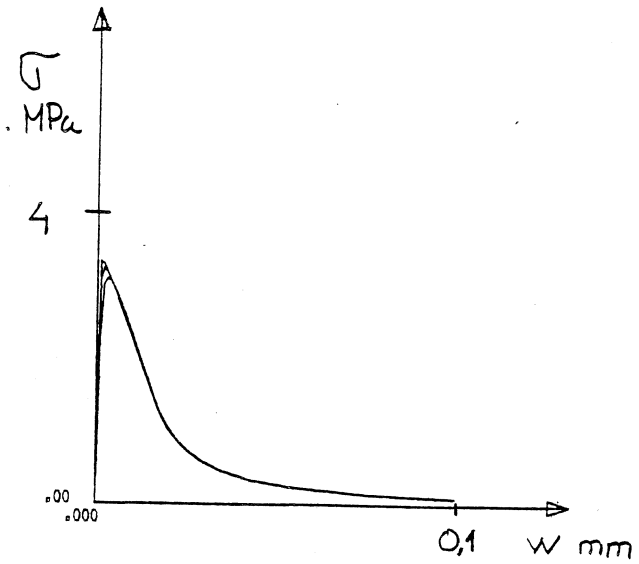

Fig 3 normal stress versus crack width
calculated values for different equivalent lengths, l=4-16 mm

A computer program is developed to determine the stress in a construction joint or a crack. The crack width and the shear displacement in the crach are assumed to be constant along the whole crack.
From the strain in the crack band the stress is calculated. The maximal strain in every plane must be stored if unloading in the planes are taken into account.

The following data are used in the calculations:

s_c = -30 MPa
e_t = $6*10^{-5}$
G_F = 86.4 N/m
E = 30000 MPa
l = 4, 8 och 16 mm
For different values of the equivalent length the following can be calculated.

l	e_u	s_t	f_t
mm		MPa	MPa
4	$4*10^{-3}$	3.60	3.35
8	$2*10^{-3}$	3.60	3.26
16	$1*10^{-3}$	3.60	3.12

The maximal tension stress , f_t , is the value for the case of uniaxal strain.

In the calculations the crack width, w , first is increased to a certain value without shear displacement, Δ . The shear displacement is then increased with a constant crack width. The following relations between strain and displacement are used in the crack band.

$e_x = w/l$

$\gamma_{xy} = \Delta/l$

$e_y = e_z = \gamma_{xz} = \gamma_{yz} = 0$

With increasing shear displacement the stiffness both normal to the crack plane and in it decreases. With increasing shear displacement the normal stress changes from tension to compression. The calculations are carried out up to a shear displacement value of twice the crack width.

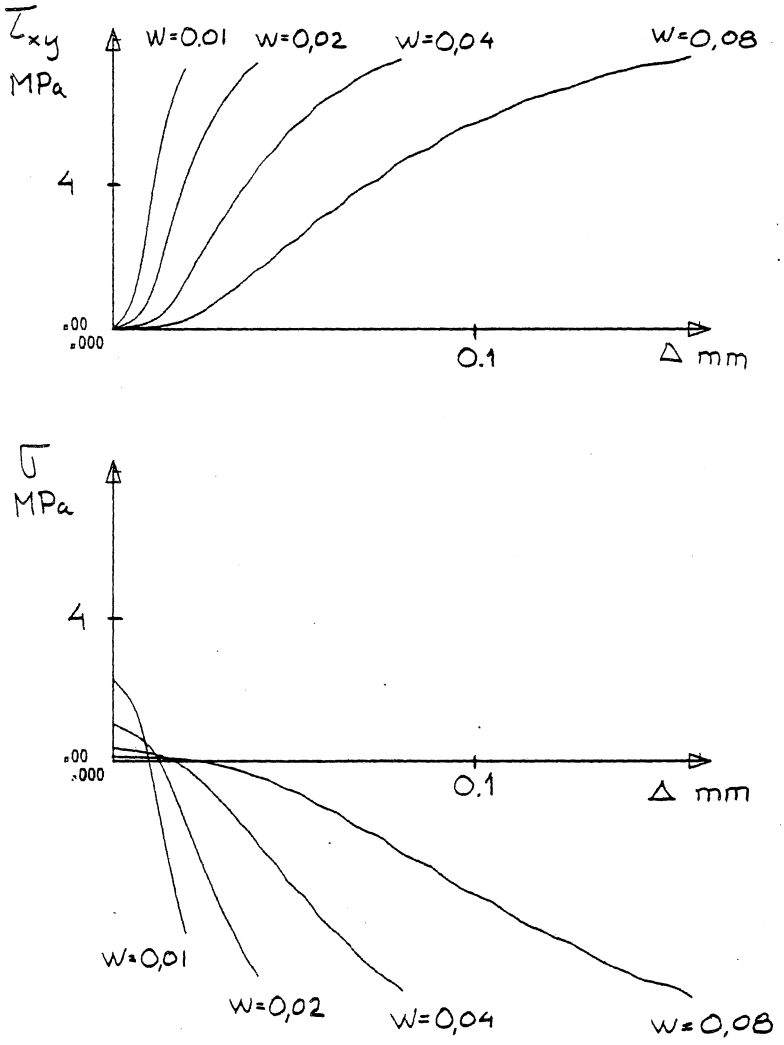

Fig 4 Calculated values of shear and normal stress in a crack band with constant crack width and increasing shear displacement.
l = 4 mm

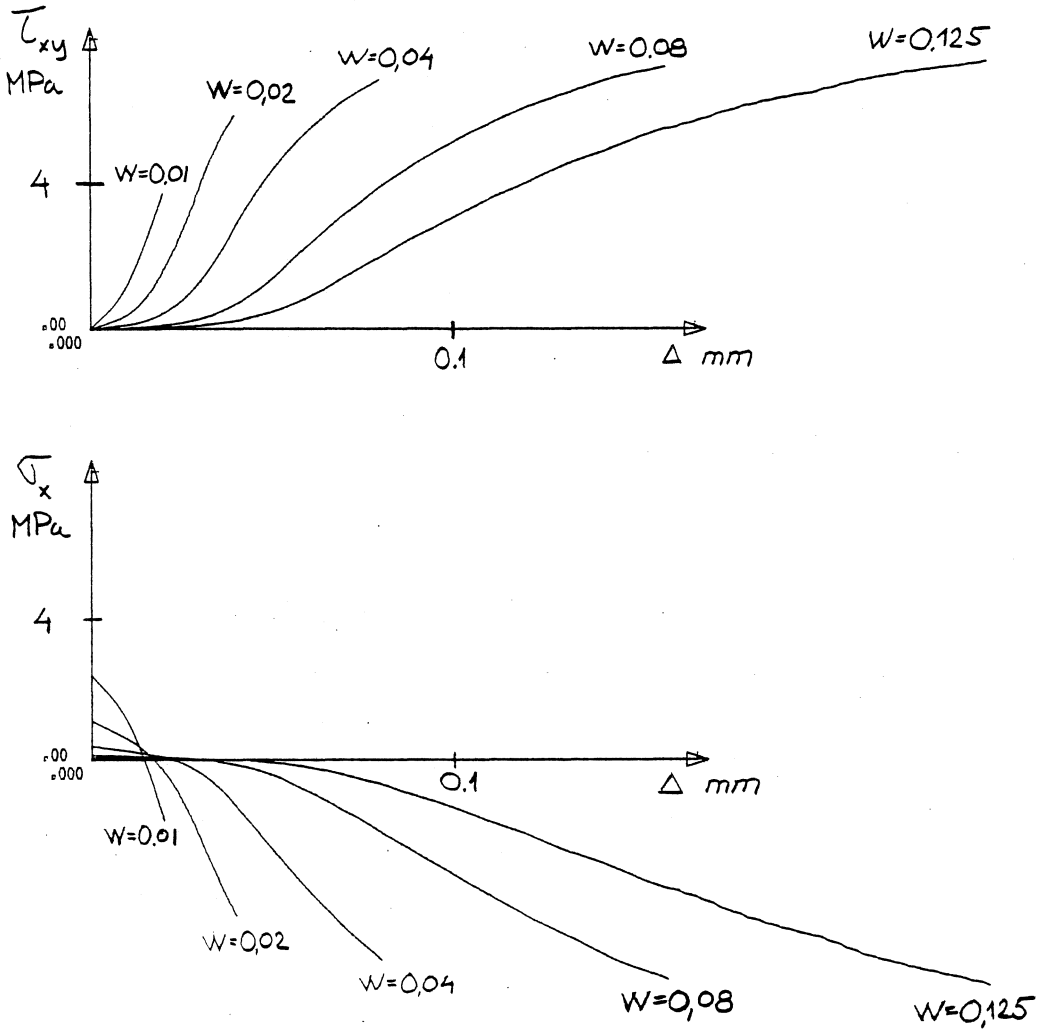

Fig 5 Calculated values of shear and normal stress in a crack band with constant crack width and increasing shear displacement.
l = 16 mm

In the calculations the contribution from planes in compression and the contribution from planes in tension can be separated (fig 6). At large deformations most of the stress transfer in a crack band is done by compression in the planes.

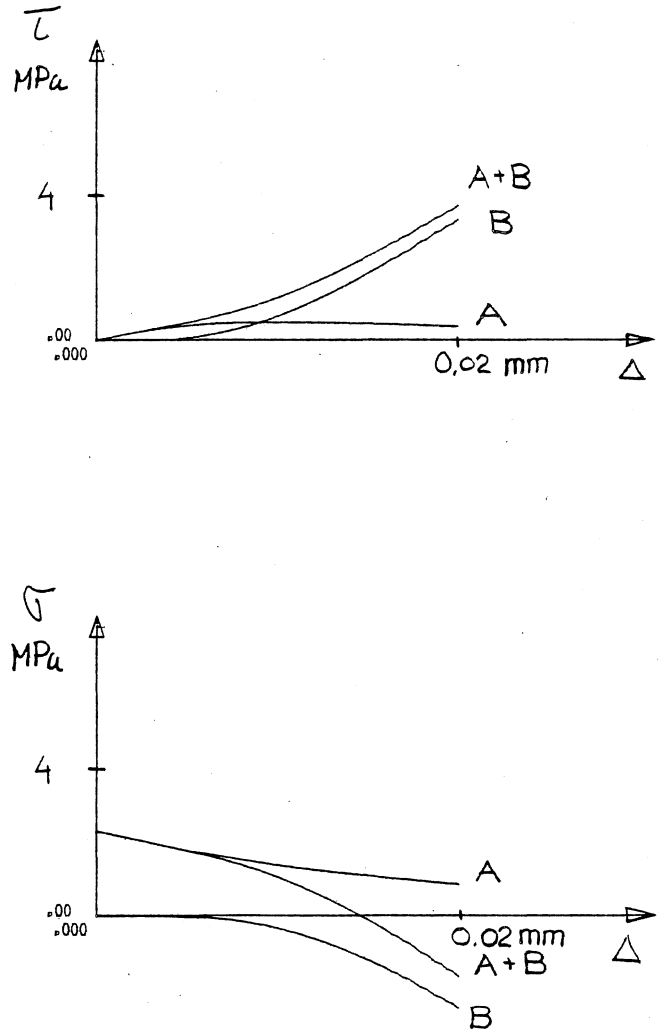

Fig 6 Calculated values of shear and normal stress in a crack band with constant crack width and increasing shear displacement.

l = 16 mm

A = stress from planes in tension

B = stress from planes in compression.

Fig 7 shows stress and strain in planes with the normal in the xy-plane. Strain and stress are showed in the right size in radial direction. First the crack width is increased at zero shear displacement. The shear displacement is then increased at constant crack width. Planes in certain directions will now have a decreasing strain and in planes in other directions the strain will increase. This unloading in certain directions will create a path dependence in the stress on how a certain strain condition is reached.

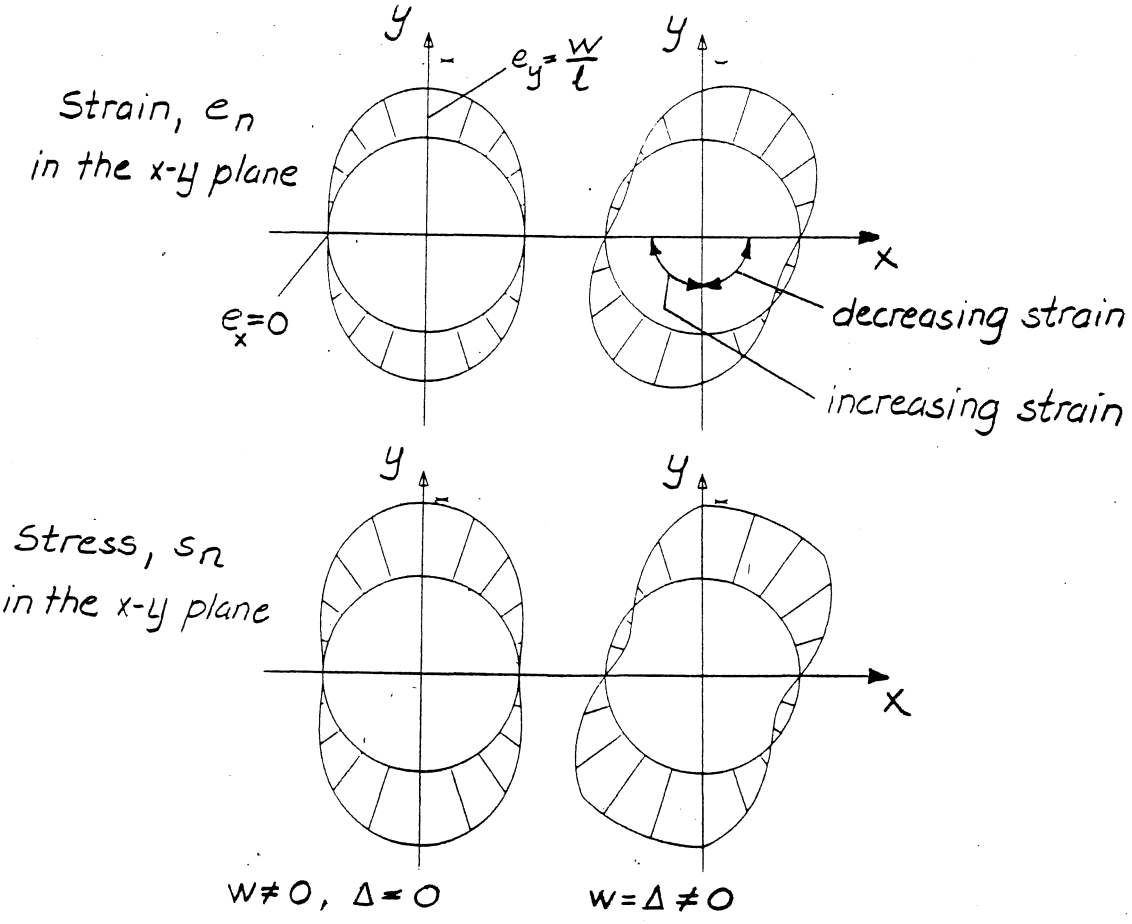

Fig 7 Stress - strain in the xy-plane

The transfer of shear forces in cracks and contruction joints in concrete has been experimentally studied by a number of investigators.

A recent investigation has been made by Walraven /2/. The transfer of shear stress in a crack with compressive normal stress can be expressed by a friction coeffecient.

$$\tau_{xy} = \mu \sigma_x \qquad (11)$$

Fig 8 shows calculated values with the multiplane model compared with experiments done by Walraven. The cube strength of concrete is used as the compressive strength in the planes. Perfectly plastic behavior is assumed in the planes both in compression and tension, the result is hereby uneffected by the equivalent length. The respons of the crack band is calculated for zero tension strength in the planes and for a tension strength of 1/10 of the cube strength. Walraven's results lie between these two extremes.

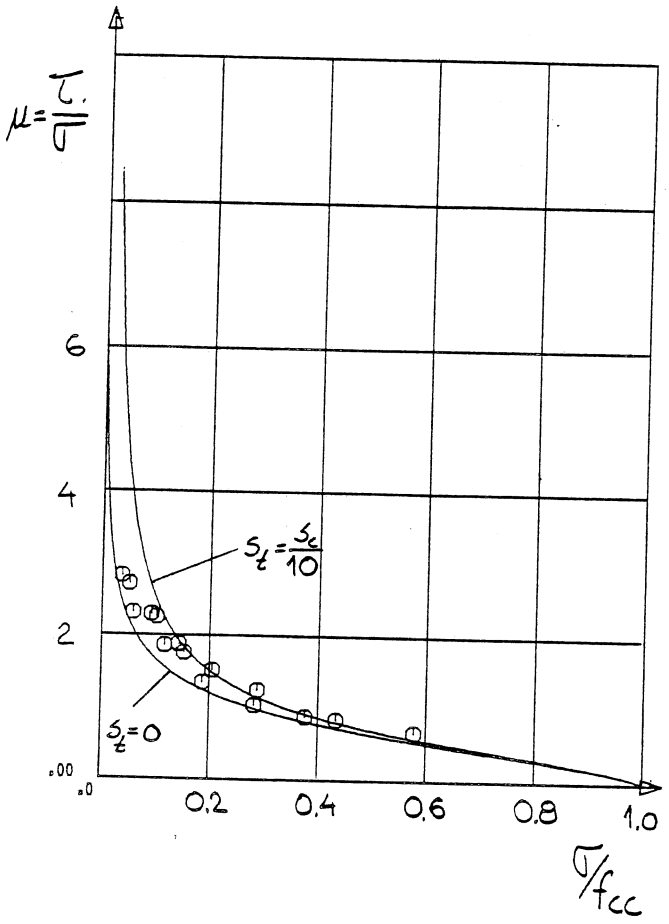

Fig 8 Friction coefficient versus normal stress in a crack.

References:

/1/ Bazant, Z. P. and Gambarova, P. G. Crack shear in concrete: Crack band microplane model. Journal of Structural Engineering. Vol 110, No 9, September, 1984

/2/ Reinhardt, H. W. and Walraven, J. C. Cracks in concrete subject to shear. Journal of the Structural Division, Proceedings of the American Society of Civil Engineers, Vol 108, No ST1, January, 1982.

The following symbols are used in this paper:

e_n	=	normal strain in the planes
e_t	=	strain at maximal tension stress in the planes
e_u	=	strain at zero tension stress in the planes
e_c	=	strain at maximal compression stress in the planes
s_n	=	normal stress in the planes
s_t	=	maximal tension stress in the planes
s_c	=	maximal compression stress in the planes
E_n	=	elastic modulus of the planes
E	=	Young's modulus for the material
w	=	crack width
Δ	=	shear displacement in a crack
l	=	equivalent length
n_i	=	cosine for the angle between the normal of a plane and the global direction i
e_{ij}	=	global strain tensor
s_{ij}	=	global stress tensor
f_t	=	maximal tension stess in the material
f_c	=	maximal compression stess in the material
G_F	=	Fracture energy
D_{ijkl}	=	Stiffness matrix
N	=	Number of integration points
ϕ	=	angle between the normal of a plane and the global x-direction
θ	=	angle between the normal of a plane and the global y-direction
S	=	surface area of a unit sphere
σ_x	=	normal stress in a crack
τ_{xy}	=	shear stress in a crack
μ	=	friction coefficient at compressive normal stress in a crack
ν	=	Poisson ratio

ICE-ABRASION OF CONCRETE

Lanu Matti Pekka
Research Scientist
Technical Research Centre of Finland (VTT),
Kemistintie 3,
SF-02150 Espoo,
Finland

1. INTRODUCTION

VTT has entered upon a new research project concerning concrete technology in arctic offshore structures. This is a continuation research to a previous project in the same research area.

The purpose of this study is to find a way of handling the abrasion resistance of concrete in offshore structures under artic conditions. The factors that usually cause abrasion are the repeating freezing and thawing of concrete as well as the forces produced by moving ice being smashed against the structure. As a final result we hope to obtain more knowledge of new mixes and structures that can bear arctic conditions.

The project is composed of several sub-tasks; these are presented in a form of a list below:

The inspection of existing sea structures

In this part an attempt is made to find out to what extent certain structures have been damaged. Some lighthouses on the Finnish coast have already been investigated.

The fracture theory of concrete

The principal task is to develop a theory that can explain the failure mechanism of concrete in the case of restraint forces and external forces. The method will be used with the aid of FEM analysis in a computer program. Some tests are included in this part of study.

The factors of resistance

In this part, the factors that cause chemical and physical corrosion of concrete are studied. The effect of time on resistance is also examined.

The design values of concrete used in offshore structures

The cube strength of concrete in offshore structures is usually higher than 60 MPa and the air content is about 7 %. The Finnish Standards lack the design values for these kinds of concrete.

Functional requirements for concrete in arctic conditions

A summary of different factors that contribute to the resistance of concrete.

An abrasion testing method

An abrasion testing machine and suitable analytical methods are developed in this study.

High-strength concrete

The basic concept of high-strength concretes 60...120 MPa.

2. ENVIRONMENTAL EFFECTS ON OFFSHORE STRUCTURES

Good resistance of concrete is necessary to arctic offshore structures. In arctic conditions the continuous freezing and thawing in sea water causes microcracking in the transition regions between aggregate particles and cement mortar. Subsequent to cracking the bond effect between mortar and aggregate is damaged and so the abrasion process can be very quick. Fig. 1 shows test results of the freezing-and-thawing tests.

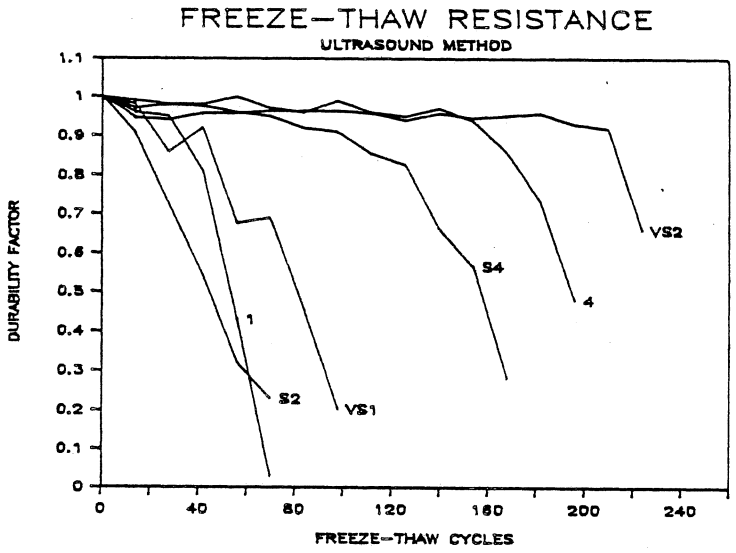

air content
3 and 7 %

1.4 blast furnace

S2, S4 silica

VS1, VS2 blended cement

Fig. 1. Strength of test specimens measured after freezing-and-thawing cycles.

Loads caused by moving ice crushing against the structure are also rather considerable. The fact that these loads are dynamic and cyclic has to be taken into account. The magnitude of force depends on the age and temperature as well as on the dimensions and velocities of ice.

Chemical corrosion may also cause a loss of strength.

All these factors can cause visible damage to offshore structures as shown in Fig. 2.

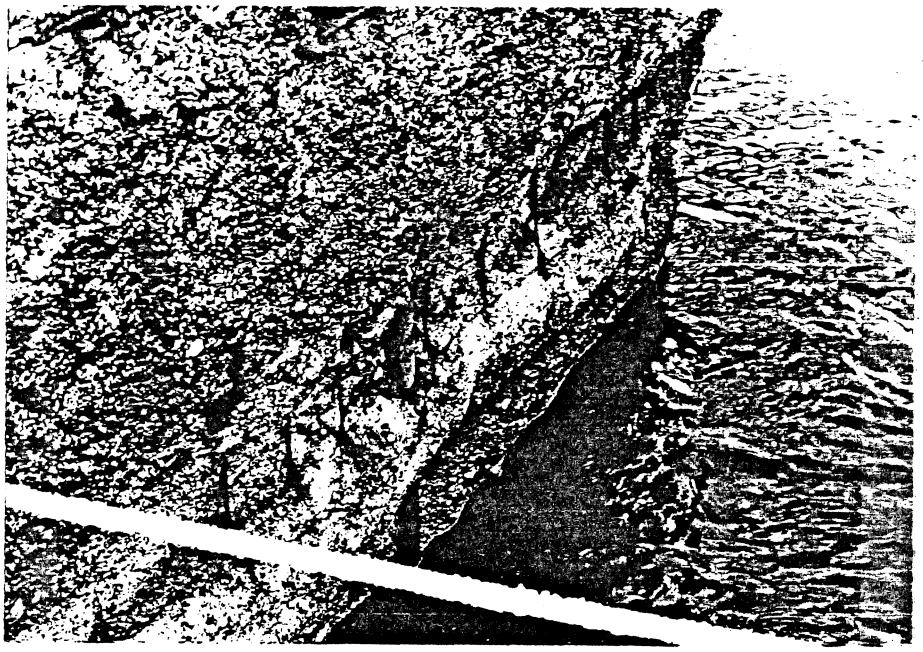

Fig. 2. Damage to the surface of a lighthouse.

3. TESTS

In order to discuss the effect of different loading types we need to know certain material properties and how these properties change during the time that loading conditions are changing. In this connection the stress-strain relationship of concrete is of primary importance. The effect of microcracking and fatique as well as chemical corrosion has to be included in this relationship and therefore we have to perform tests in which these factors are taken into account. Previous studies indicate that freezing-and-thawing tests in which test specimens are placed in salt water is a reliable manner to model the effects of cyclic freezing. Different mix proportions are chosen and the specimens (cylinders and cubes) made with these mixes undergo first freezing-and-thawing tests each having certain amount of cycles. Subsequently the compressive strength and fatique strength of specimens are obtained, as shown in Fig. 3. The crack patterns in the failure areas are also examined.

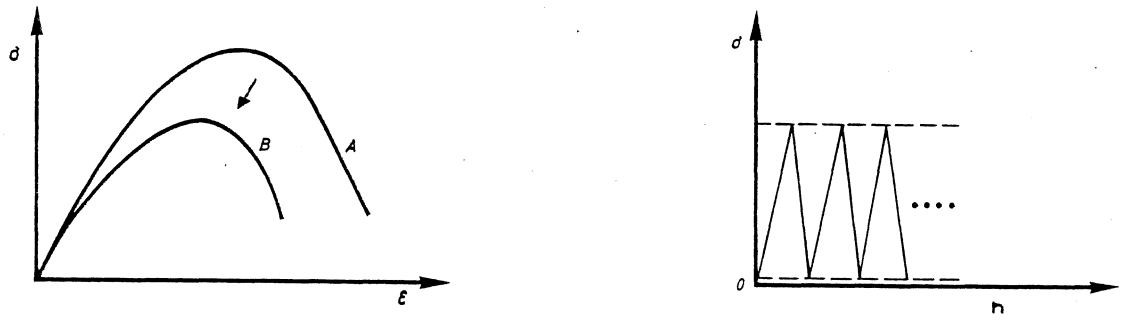

Fig. 3. Material properties after freezing-and-thawing tests.

Test specimens are made with different mix proportions. In addition to Portland cement, blastfurnace cement and Portland cement with silica fume are also used. Some of the specimens are made using lightweight aggregate. The cube strength varies from 40 MPa to 60 MPa and air content from 3 % to 7 %.

Studies concerning the ice force that is acting upon a small aggregate particle visible on the surface of a specimen are of special interest.

The bond strength of the transition region between cement paste and particles should also be studied, for which reason the following tests are carried out. A particle (ø = 35 mm) embedded in concrete as shown in Fig. 4 is pulled out from the concrete simultaneously with the determination of the force needed. The same mix proportions are used for the specimens as in determining the stress-strain relation, except that the maximum particle size of aggregate is here 8 mm. The specimens undergo a freezing-and-thawing test prior to the pull-out test in order for these results to be compatible with stress-strain relation.

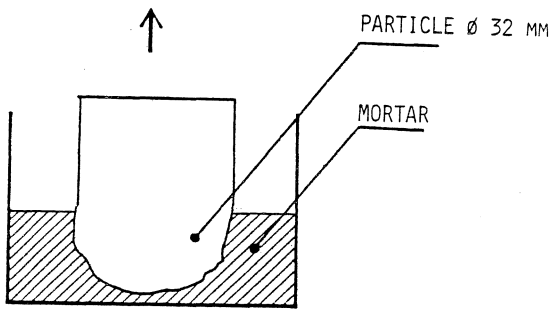

Fig. 4. Test specimens for determination of bond strength.

4. APPLICATION OF FRACTURE THEORY

The constitutive models of concrete need to be adjusted to fit experimental data. However, the data needed in calibration is not complicated. Here are some examples:

Cedolin: the compressive strength f_c, the initial values of the Young's modulus E_0, and the Poisson's ratio ν_0 /1/.

Kotsovos: the uniaxial cylinder compressive strength f_c /1/.

Ottosen: the initial Young's modulus E_0, the initial Poisson's ratio ν_0, the uniaxial compressive and tensile strength f_c and f_t, strain corresponding to compressive strength ε_c and the post-failure parameter D describing strain softening /1/.

In this study attempts are made to apply our experimental data to the different constitutive models of concrete. The input data is determined in such a way that the ice-abrasion, freeze-thaw effect, etc. are taken into account. This means that the material properties depend not only

on current stresses or strains but on the strain rates and long-term attacks such as corrosion and repeated freezing.

A way of adding these constitutive models and failure criteria to a computer program, called ADINA, is studied. It is a practical, allpurpose FEM program and its program code is easy to modify.

The loads brought about by moving ice have to be modelled truthfully. However, forces are cyclic and dynamic and in calculations these effects have to be treated in a simple way. Loading can be converted into static load by the Wöhler diagram. The method can be calibrated with test results of abrasion tests.

5. CONCLUSIONS

A lack of information leads to difficulties. The effect of chemical corrosion and microcracking in the transition region is not distinct. The modelling of ice forces also needs some studying.

This project has now reached its middle stage. Aims and plans are made and fixed, and tests are about to begin. The final results are to be expected at the end of the year 1987.

REFERENCES

1. Concrete under multiaxial states of stress; constitutive equations for practical design. Paris 1983. Comité Euro-International du Beton, Bulletin d'information 156.